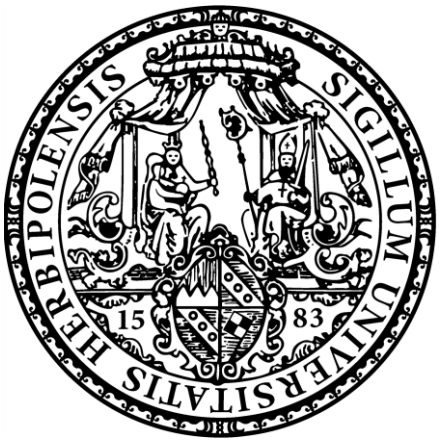

Identifying the role of Myb-MuvB in gene expression and proliferation of lung cancer cells

Identifizierung der Rolle des Myb-MuvB in der Genexpression und der Proliferation von Lungenkrebszellen

Doctoral thesis for a doctoral degree
at the Graduate School of Life Sciences,
Julius-Maximilians-Universität Würzburg,
Section Biomedicine

submitted by

Katja Simon

from

Prüm

Würzburg, 2017

Submitted on: ……..……..

Office stamp

Members of the *Promotionskomitee*:

Chairperson: Prof. Dr. Utz Fischer

Primary Supervisor: Prof. Dr. Stefan Gaubatz

Supervisor (Second): Dr. Peter Gallant

Supervisor (Third): Prof. Dr. Svenja Meierjohann

Supervisor (Fourth): ……..
(If applicable)

Date of Public Defence: ……..……

Date of Receipt of Certificates: ……..

Substantial parts of this thesis were published in the following article:

Iltzsche F.*, Simon K.*, Stopp S*., Pattschull G.*, Francke S., Wolter P., Hauser S., Murphy DJ., Garcia P., Rosenwald A., Gaubatz S. (2017) „**An important role for Myb-MuvB and its target gene KIF23 in a mouse model of lung adenocarcinoma**"; Oncogene; 36(1):110-121

*These authors contributed equally to this work

Table of Content

1. Introduction 1
1.1 The mammalian cell cycle and its regulation 1
1.1.1 The mammalian cell cycle 1
1.1.2 Regulation and control of eukaryotic cell cycle 2
1.1.3 The pRB/E2F pathway 4
1.2 The DREAM/ MMB complex 5
1.3 MYBL2 (B-Myb) 8
1.3.1 Physiological Role of B-Myb 8
1.3.2 B-Myb in cancer 9
1.4 DREAM/MMB as potential target for cancer therapy 10
1.5 Lung cancer 12
1.6 Aim of thesis 13
2. Materials and Methods 14
2.1 Materials 14
2.1.1 Chemical stocks and reagents 14
2.1.2 Antibiotics 17
2.1.3 Enzymes 17
2.1.4 Buffers and solutions 18
2.1.4.1 General buffers 18
2.1.4.2 Buffers for whole-cell lysates 19
2.1.4.3 Buffers for immunoblotting 20
2.1.4.4 Buffers for flow cytometry (FACS) 21
2.1.4.5 Buffers for immunostaining 21
2.1.4.6 Buffers for immunohistochemistry 21
2.1.4.7 Buffers for genomic DNA extraction (HotSHOT) 21
2.1.5 Transfection reagents 22
2.1.6 Antibodies 22
2.1.6.1 Primary antibodies 22
2.1.6.2 Secondary antibodies 23
2.1.7 Plasmids 23
2.1.8 Primer sequences 24
2.1.8.1 Murine primer for quantitative real-time PCR 24
2.1.8.2 Human primer for quantitative real-time PCR 24
2.1.8.3 Primer for cloning 24

2.1.8.4 Primer for sequencing 25
2.1.8.5 Primers for genotyping 25
2.1.9 siRNA sequences 25
2.1.10 Lentiviral shRNA sequences 26
2.1.11 Cell lines 26
2.1.11.1 Murine cell lines 26
2.1.11.2 Human cell lines 27
2.1.12 Media and additives 27
2.1.12.1 Media for cell culture 27
2.1.12.2 Additives 27
2.1.12.3 Media for bacterial cell culture 27
2.1.13 Bacterial strains 28
2.1.14 Mouse strains 28
2.1.15 Markers 29
2.1.16 Kits 29
2.1.17 Devices 29
2.2 Methods 30
2.2.1 Cell culture 30
2.2.1.1 Passaging of cells 30
2.2.1.2 Cryopreservation and Resuscitation of frozen cell lines 30
2.2.1.3 Counting cells 31
2.2.1.4 Cell treatment with different reagents 31
2.2.1.5 Establishing of tumor cell lines 31
2.2.1.6 Transient transfection 32
2.2.1.6.1 Plasmid transfection with calcium phosphate 32
2.2.1.6.2 Liposomal transfection 34
2.2.1.7 Cell infection 35
2.2.1.7.1 Retroviral infection of murine tumor cell lines 35
2.2.1.7.2 Lentviral infection of pINDUCER-shRNAs 35
2.2.1.8 Concentration of Lenti-Cre virus 36
2.2.1.9 Lenti-Cre virus titer determination with NIH3T3 zeG reporter cell line 36
2.2.1.10 Cell proliferation assay with crystal violet staining (Growth curves) 37
2.2.1.11 Flow cytometry analysis using the intercalating dye Propidium Iodide 38
2.2.2 Molecular biological methods 39
2.2.2.1 RNA isolation 39
2.2.2.2 Reverse transcription (RT-PCR) 39
2.2.2.3 Quantitative real-time PCR (qRT-PCR) 40
2.2.2.4 Isolation of plasmid DNA from bacteria 42

2.2.2.4.1 Mini preparation 43
2.2.2.4.2 Midi/Maxi preparation 43
2.2.2.5 Isolation of plasmid DNA fragments from agarose gels 43
2.2.2.6 Isolation of genomic DNA from tumor slides 43
2.2.2.7 Extraction of genomic DNA (HotSHOT) 44
2.2.2.8 Genomic DNA PCR 44
2.2.2.9 Cloning of lentiviral shRNAs (miR30 shRNAs for the pINDUCER vector system) 46
2.2.2.10 Agarose gel electrophoresis 46
2.2.2.11 Restriction digestion 47
2.2.2.12 Ligation 47
2.2.2.13 Transformation 48
2.2.2.14 Sequencing 49
2.2.3 Biochemical methods 50
2.2.3.1 Whole cell lysates 50
2.2.3.2 Bradford assay 50
2.2.3.3 SDS polyacrylamide gel electrophoresis (SDS-PAGE) 51
2.2.3.4 Immunoblotting 52
2.2.3.5 Immunofluorescence 53
2.2.4 Immunohistochemical methods 54
2.2.4.1 Preparation of paraffin sections 54
2.2.4.2 H&E staining 55
2.2.4.3 Antibody staining of tissue sections 55
2.2.5 Mouse husbandry 56
2.2.5.1 Mouse facility 57
2.2.5.2 Anaesthesia of mice 57
2.2.5.3 Infection of mice with Lenti-Cre 57
2.2.6 Statistical analysis 58
3. Results 59
3.1 Role of MMB in lung tumorigenesis *in vivo* 59
3.1.1 NSCLC mouse model with conditional alleles of B-Myb 59
3.1.2 Tumor burden is reduced when B-Myb is depleted 61
3.1.3 Mitotic genes are targets of MMB in lung cancer *in vivo* 63
3.1.4 Reduced expression of p-Erk and Ki-67 in tumors after loss of B-Myb 66
3.1.5 Incomplete recombination of B-Myb after lentiviral Cre-infection *in vivo* 68
3.1.6 Incomplete recombination of B-Myb alleles in tumor cell lines 69
3.1.7 Characterisation of B-Myb cell lines 71
3.1.8 Proliferation is impaired in BC2 cell line after deletion of B-Myb 73

3.1.9 Loss of B-Myb results in a higher frequency of cellular abnormalities and an abnormal cell cycle profile 73

3.2 ShRNA mediated depletion of B-Myb in human lung cancer cell lines 75

3.2.1 Lentiviral system is not efficient enough for downregulation of MMB targets 75

3.2.2 SiRNA mediated depletion of B-Myb in human lung tumor cells 84

4. Discussion 87

5. Summary 95

6. Zusammenfassung 96

7. References 97

8. Appendix 116

8.1 List of figures 116

8.2 Abbreviations 117

8.3 Own publications and conference contributions 120

8.4 Curriculum vitae 121

8.5 Acknowledgements 122

8.6 Affidativ 123

1. Introduction

1.1 The mammalian cell cycle and its regulation

1.1.1 The mammalian cell cycle

The cell cycle is a universal process by which cells reproduce through division into daughter cells and duplication of DNA (DNA replication) (Nurse, 2000). It is strictly controlled by a regulatory network which is - at least in parts - highly conserved from yeast to human (Morgan, 2007). The most important role of the cell cycle is to determine the cell's decision to either proliferate or to withdraw from the cycle and enter the quiescent state (Lania et al., 1999). Precise cell cycle events ensure the survival of living organisms; loss of this precision would cause genomic instability, which is associated with cancer formation (Nurse, 2000).

The cell cycle of most eukaryotic cells comprises four discrete phases: The Gap-phases G1 and G2, the synthesis phase (S-phase) and mitosis (M-phase). M-phase involves two distinct division-related processes: mitosis and cytokinesis. The entirety of G1-, G2- and S-phase is termed interphase. The activation of each phase is reliant on the adequate progression and completion of the previous one, which can be monitored by cell cycle checkpoints (Li and Wang, 2014). Cells which have stopped dividing, temporarily or reversibly, enter a state of quiescence (G0 phase).

The G0 phase is a resting period in the cell cycle in which cells have left the cycle and stopped proliferation (Lodish, 2000). Prior to cell division, cells acquire nutrients. This preparation phase is called interphase. Upon external growth stimuli and intrinsic signals, cells enter the cell cycle in early G1 and accumulate nutrients accompanied by cell growth in preparation for subsequent cell cycle events (Cooper, 2000). During G1, also referred to as Growth 1/Gap 1 phase, the cell is metabolically active and continuously grows and increases its protein supply. G1 is followed by S-phase (synthesis) in this part of the cell cycle DNA replication takes place (Schafer, 1998). After DNA replication G2 phase (gap 2) occurs, in which cell growth continues and proteins are synthesized in preparation for mitosis (Harrison, 2011, Alberts et al., 2000). During M-phase, which comprises the nuclear (mitosis) and cellular division (cytokinesis), the sister chromatids are separated and distributed into two daughter cells (Morgan, 2007). During the five phases of mitosis, the pairs of chromosomes condense and attach to fibers that pull the sister chromatids to opposites poles of the cell (Maton et al., 1997). These phases are called prophase, prometaphase, metaphase, anaphase and telophase (Mitchison and Salmon, 2001). Mitosis is followed by cytokinesis, in which the division of the cytoplasm into two daughter cells takes place (Paweletz, 2001).

1.1.2 Regulation and control of eukaryotic cell cycle

Many proteins are involved in cell cycle control; however, cyclins and cyclin-dependent kinases (CDKs) are the most important ones. This class of regulatory molecules is highly conserved among all eukaryotes and was first identified in yeast (Lee and Nurse, 1987). Cyclins form the regulatory subunits whereas CDKs serve as the catalytic subunits of an activated heterodimer. CDKs belong to a family of multifunctional enzymes whose task is to modify various protein substrates involved in cell cycle progression (Malumbres, 2014; Morgan, 2007). However, cyclins have no catalytic activity but are necessary for CDK activation by binding to them. After activation by cyclins, CDKs phosphorylate their substrates to progress in the cell cycle. All eukaryotes possess multiple cyclins, each of which act during a specific stage of the cell cycle (Nebreda, 2006). Most of them are classified as G1 cyclins or mitotic cyclins named after the stage of the cell cycle in which they function. However, in S phase there are also some cyclins required. In eukaryotes, D-type cyclins are the key regulators of G1 progression. D-type cyclins and CDK4 or CDK6 regulate events in early G1 phase, whereas cyclin E-CDK2 triggers the S-phase (Satyanarayana and Kaldis, 2009). Cyclin A-CDK2 and cyclin A-CDK1 complexes complete S phase and CDK1-cyclin B is responsible for mitosis (Nigg, 1995; Hochegger, Takeda and Hunt, 2008; Santamaria et al., 2007; Malumbres et al., 2004). In general, every cyclin-CDK complex modifies a specific group of protein substrates. (Hochegger, Takeda and Hunt, 2008). Progression through the cell cycle is regulated by several CDKs whose activities are in return constricted by CDK inhibitors (CKIs). Based on their structure and CDK targets, two families of CKIs have been identified to manage these events. The first class is the cip/kip (CDK interacting protein/ Kinase inhibitory protein) family, which includes genes like p21 (Sherr and Roberts, 1999). P21 is activated by tumor suppressor p53, which is triggered due to DNA damage (El-Deiry et al., 1993). The inhibitory effect of the cip/kip family is based on the binding and inactivating of cyclin-CDK complexes, leading to cell cycle arrest in G1 phase (Nigg, 1995; Morgan, 1997). The second class of CKIs is the INK/ARF family, which contain genes like p14ARF and p16INK4a. p16INK4a binds to CDK4, which leads to a cell cycle arrest in G1 (Sherr and Roberts, 1999).

Cell cycle checkpoints are mechanisms that control the order and timing of cell cycle transitions to ensure that critical events like DNA replication and chromosome segregation are completed accurately. Furthermore, checkpoints prevent cell cycle progression after the recognition of DNA damage to provide time for repair (Murray, 1992; Hartwell and Kastan, 1994). There are three main checkpoints distributed over the cell cycle: G1/S (restriction) checkpoint, G2/M (G2-M DNA damage) checkpoint and metaphase (spindle assembly) checkpoint. At the G1/S checkpoint it will be decided if a cell delay the cell cycle, enter a resting phase or progress and complete the cycle (Robbins and Cotran, 2004). When DNA damage occurs, the kinases ATM

and ATR, which act as sensors, are initiated and start the signalling cascade, in which p53 is phosphorylated and thereby stabilized. P53 activates several target genes, including p21. Through this mechanism, G1 CDKs are inhibited and DNA damage is repaired prior to DNA replication (Barnum and O'Conell, 2014; Musacchio and Salmon, 2007; Harper and Elledge, 2007). The second checkpoint is the G2/M checkpoint, which prevents cells from entering mitosis when DNA damage occurs. This process provides an opportunity for repairing and stopping the proliferation of damaged cells and thus for maintaining genomic stability (Löbrich and Jeggo, 2007). When genomic DNA is damaged, the sensory DNA-PK/ATM/ATR kinases are activated, which leads to the initiation of two parallel cascades that inactivate the Cdc2-cyclin B complex (Kastan and Bartek, 2004). The spindle assembly checkpoint (SAC) prevents the start of the anaphase and the segregation of chromosomes until these processes have been properly completed (Elledge, 1996; Lara-Gonzalez et al., 2012; Hauf, 2013). Checkpoint proteins enrich at unattached kinetochores, which leads to the initiation of a signalling cascade that ultimately blocks the APC/C (anaphase-promoting complex/cyclosome) and a multi-subunit E3 ubiquitin ligase. Thus, the checkpoint delays the anaphase until a proper attachment of all chromosomes is sensed. (Musacchio and Salmon, 2007; Musacchio, 2011).

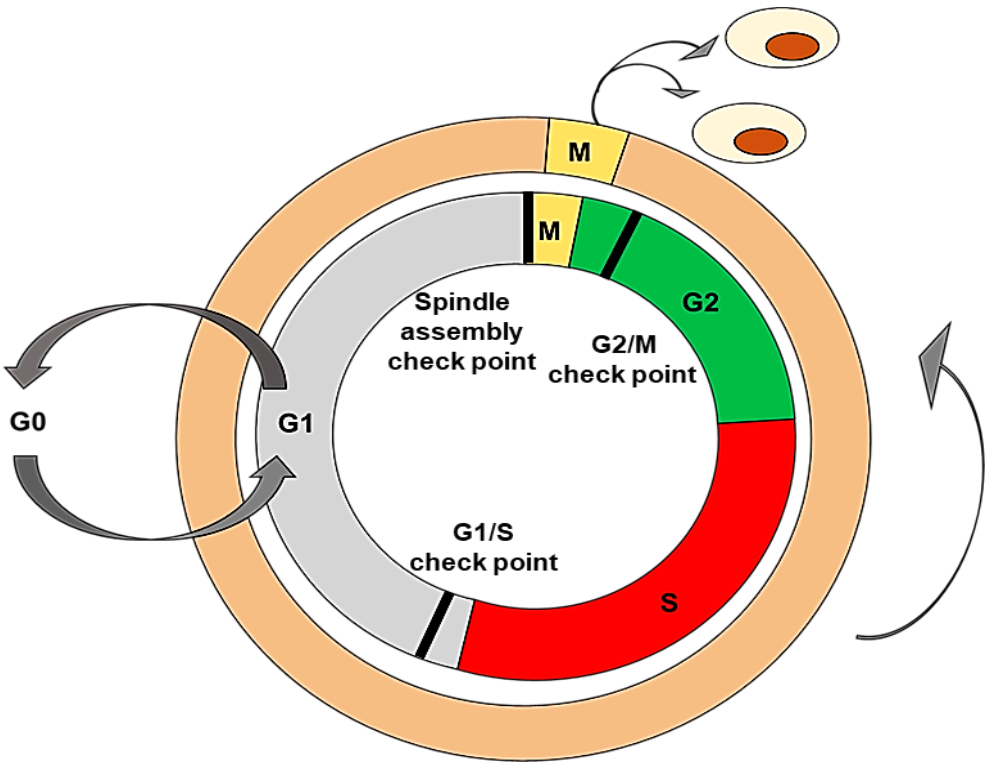

Figure 1: Simplified representation of the mammalian cell cycle
The cell cycle comprises four major phases (S, M, G1, G2) and coordinates DNA duplication and segregation of replicated genomic material to emerging daughter cells. Checkpoints within the cell cycle are crucial instruments to monitor the correct progression. Cells that are no longer dividing withdraw from the cell cycle and enter into a non-proliferative state (G0).

1.1.3 The pRB/E2F pathway

To ensure proper progression during the cell cycle, proteins that are involved in its regulation are expressed at certain times. The progression of the cell cycle is associated with a defined set of genes, which are regulated at the transcriptional level through transcription activators and repressors (Weinberg, 1995; Paggi et al., 1996). It is well known that the product of the retinoblastoma tumor suppressor (pRB) inhibits cell growth by preventing the transcription of growth-regulatory genes (Lania et al., 1999). pRB function is reliant, at least in part, on interactions with the E2F family of DNA-binding transcription factors (E2F) (Chellappan et al., 1991). E2F sites are present in many gene promoters that are essential for cell cycle progression. In this context, pRB occurs to repress the transcription of these genes through its interaction with E2F (Blake and Azizkhan, 1989; Thalmeier et al., 1989). In mammalian cells, pRB and the two pRB-related proteins p107 and p130, referred to as the pocket protein family, play a crucial role in cell cycle progression, especially in G1 to S transition (Dimova and Dyson, 2005). Based on the family name pRB, p107 and p130 share a high homology in a central motif known as the pocket region. This pocket region consists of two highly conserved domains (box A and B) separated by a nonconserved spacer that differ in length (Lania et al., 1999; Harbour and Dean, 2000). DNA tumor viruses that express oncoproteins, such as adenovirus E1A, SV40 large tumor antigen and human papillomavirus (HPV) E7, can bind to the conserved pocket domain of pRB members, which leads to an inactivation of pRB followed by a transformation of cells (DeCaprio et al., 1988; Whyte et al., 1988; Dyson et al., 1998). The E2 factor (E2F) family of DNA- binding transcription factors, which are downstream effectors of the retinoblastoma (RB) protein pathway, play an important role in cell division control in higher eukaryotes. Three E2F family members, known as E2F1, E2F2 and E2F3a, act as transcriptional activators whereas six members termed E2F3b and E2F4-8 act as suppressors (Aslanian et al., 2004). The E2F proteins contain several conserved domains including a DNA binding domain, a dimerization domain, a transactivation domain and a tumor suppressor protein association domain (Dyson et al., 1998; Trimarchi and Lees, 2002). Structurally, E2F1-6 harbour a highly conserved DNA binding and dimerization domain enabling the binding of DNA target sequences as heterodimers with DP1 and DP2 (differentiation-regulated transcription factor-1 and 2) (Gaubatz et al., 1998; Morkel et al., 1997; Cartwright et al.,1998). In contrast, E2F7 has a duplicated conserved E2F-like binding domain but no DP-dimerization domain (Di Stefano et al, 2003; Ren et al., 2002). In addition, E2F6 and 7 lack the transactivation and pocket protein binding domains at the C-terminus in contrast to the rest of the family (Ren et al., 2002). As mentioned before, E2Fs have been categorized according to their structure and function into activators and repressors. E2F1, E2F2 and E2F3a contain an additional cyclin binding domain and predominantly interact with pRb in a cell cycle dependent manner, which leads to transcriptional activation. During the G1-S transition, cyclin D-CDK4/6

and cyclin E-CDK2 phosphorylate pRB, resulting in the release of E2F, which leads to the transcription of E2F target genes (Maiti, 2005; Harbour and Dean 2000). In contrast, E2F3b and E2F4-8 inhibit gene expression. E2F3b, E2F4 and E2F5 are expressed and associated with E2F binding elements and E2F target promotors during G0 (Ogawa et al., 2002). E2F3b represses specific E2F target genes. E2F4-5 act as repressors in two ways: first, they associate with p107 and p130 and bind to E2F regulated promoters, which leads to inaccessibility for activators and secondly, they recruit histone deacetylases (HDAC) to promoters, thereby enabling the silencing of gene transcription (Beijersbergen et al., 1994; Ginsberg et al., 1994; Hijmans et al., 1995; Moberg et al., 1996). E2F6 mediates repression, when Polycomb group of proteins or large multimeric complexes containing Max and Mga proteins are recruited (Ogawa et al., 2002; Trimarchi et al., 2001). The least studied E2F family members, E2F7-8, function independently of DP interaction by forming homo- and heterodimers with each other (Moon and Dyson, 2008; Li et al., 2008).

1.2 The DREAM/ MMB complex

In 2004, two biochemical studies on Drosophila melanogaster described the identification of an E2F/pRB repressor complex. A native multi-subunit complex that contained pRB homologues RBf1 and RBf2, transcription factor E2F2 and MYB, DP, Myb interacting proteins (Mip40, Mip120, Mip130) and chromatin assembly factor 1 (CAF1), a homologue to RB binding protein 4 was identified (Korenjak et al., 2014). This complex includes several homologues of proteins encoded by the synMuvB genes, which have been described to be controlled by a pathway in Caenorhabditis elegans (Ferguson, Sternberg and Horvitz, 1987). According to the model organism and the composition of the complex, it was termed dREAM (Drosophila Rbf, E2F2 and Mip) (Korenjak et al., 2014). In the Botchan group, a highly related complex was identified including Myb, Mips and Caf1 and termed Myb–MuvB (MMB) in relation to the synMuvB genes in worm (Beall et al., 2007). Furthermore, additional MuvB complexes have been discovered over the years in Drosophila melanogaster. One in Drosophila glands and a testis-specific paralog called tMAC (testis-specific Meiotic Arrest Complex). Due to the biochemical studies in Drosophila melanogaster, a similar complex related to dREAM and MMB was found in worm. This complex includes different LIN proteins and DPL1. Only MYB was absent, therefore the complex was named DRM (DP, RB and MuvB) (Harrison et al., 2006). Orthologs of LIN9, LIN54, E2F and MYB are also found in plants (Arabidopsis thaliana) (Fischer et al., 2015; Kobayashi et al., 2015).

In 2007, a mammalian DREAM/MMB complex was discovered and was named DREAM/LINC (Litovchick et al., 2007; Schmit et al., 2007; Pilkinton et al., 2007). The composition of the

mammalian complex is cell cycle dependent: The five-protein core (MuvB core) module of LIN proteins (LIN9, LIN37, LIN52, LIN54) and RbAP48 persists through the cell cycle. In quiescent cells, this core module interacts with p130, DP1 and E2F4 establishing a repressor complex named DREAM. In S-phase, this interaction is lost and the MuvB core now associates with the transcription factor B-MYB, forming a transcriptional activator complex that is essential for the expression of key mitotic genes (Osterloh et al., 2007; Pilkinton et al., 2007; Sadasivam and DeCaprio, 2013). The active complex is termed MMB, when FOXM1 is recruited by MMB in G2/M, it is named MMB-FOXM1 (Sadasivam et al., 2012; Down et al., 2012).

DREAM can function as a transcriptional repressor of cell cycle dependent genes, (Litovchick, 2007). MMB, in contrast, is a transcriptional activator important for activating G2/M gene expression (Osterloh et al., 2007; Schmit et al., 2007; Pilkinton et al., 2007; Kittler et al., 2007; Knight et al., 2009; Schmit et al., 2009; Reichert et al., 2010; Sadasivam et al., 2012; Wolter et al., 2017). Stable repression of developmental genes by RNAi mediated depletion of several subunits underlines the importance of DREAM leading to cell cycle arrest and delayed entry into mitosis (Osterloh et al., 2007; Schmit et al., 2009).

Transcriptional regulation and control of cell cycle genes is mediated through promotors, which contain common recognition sites such as cell cycle-dependent element (CDE), cell cycle genes homology region (CHR) and CCAAT boxes that are often found near the transcription start (Müller et al., 2011). Tandems of CDE and CHR sites regulate the promotors by repression in G0 and G1, therefore CCAAT boxes are essential for transcriptional activation (Lange-zu Dohna et al., 2000). it has been shown that DREAM binds to CHR elements or CDE/CHR tandem sites of late cell cycle gene promotors. In quiescent cells, binding of DREAM to CHR element is mediated by LIN54 through 2 cysteine-rich domains with the DNA consensus motif TTYRAA (Schmit et al., 2009). In contrast, binding of MMB to CHR elements of late cell cycle gene promoters' functions independently of the CDE (Müller et al., 2012; Sadasivam et al., 2012; Chen et al., 2012; Müller et al., 2017). The MMB members B-MYB and FOXM1 themselves exhibit additional DNA-binding potential such as B-Myb binding sites (MBS) and forkhead binding sites (FBS), which are supposed to be important for the recruitment of the complex to target promoters (Knight et al., 2009; Schmit et al., 2009; Müller et al., 2012; Sadasivam et al., 2012).

In vivo studies in *Lin9* mutant mice revealed that Lin9 is essential for early embryonic mouse development because the lack of LIN9 leads to embryonic lethality (Reichert et al. 2010). Furthermore, adult *Lin 9* mutant mice showed atrophy of the intestinal epithelium, which resulted in rapid mortality among these animals (Reichert et al., 2010). In mice with deficient DREAM (*p107ΔD/ΔD; p130−/−* mice), defects in endochondral ossification have been observed so that these mice die shortly after birth (Cobrinik et al., 1996; Forristal et al., 2014).

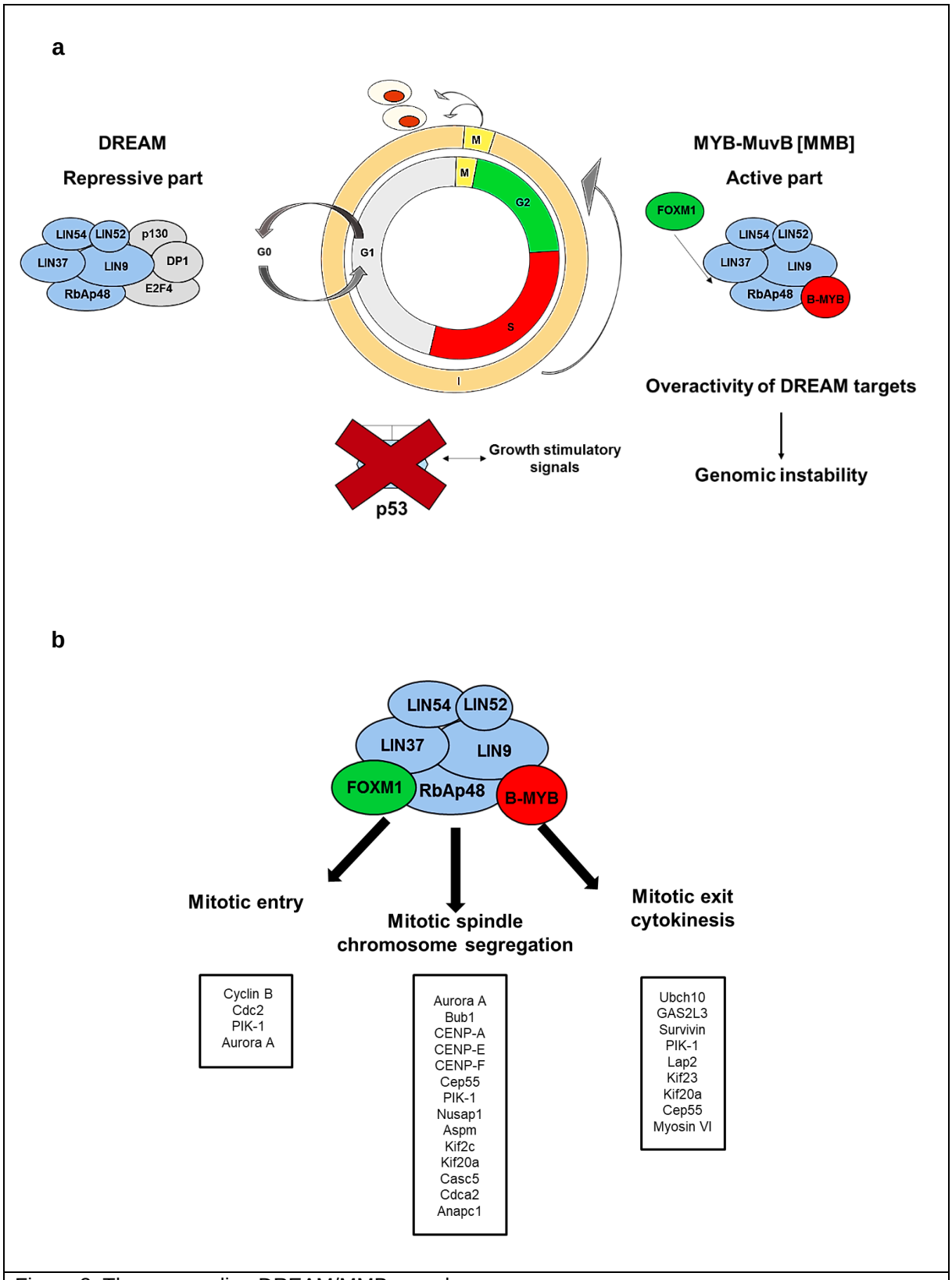

Figure 2: The mammalian DREAM/MMB complex
a) The mammalian DREAM/MMB complex regulates gene expression in a cell cycle dependent manner. In G0/early G1, DREAM consists of the MuvB-core module (blue) and p130E2F4/DP1 (grey) forming the repressive part of the complex. In S-phase, this binding is lost and B-Myb (red) associates with the complex later FoxM1 (green) forming a transcriptional activator complex called MMB. Loss of p53 results in constitutively active MMB which can lead to genomic instability.
b) The MMB complex serves as master regulator of mitotic genes.

1.3. MYBL2 (B-MYB)

The v-Myb myeloblastosis viral oncogene homolog (avian)-like 2 (MYBL2 or B-MYB) is a 110 kDa sequence-specific DNA binding protein and belongs to the MYB oncoprotein family of transcription factors. In contrast to his family members A-MYB and C-MYB, B-MYB is expressed in all proliferating cells (Charasse et al., 2000). C-MYB is the homolog of the v-MYB oncogene and is mainly expressed in immature hematopoetic cells. In contrast, A-MYB is involved in spermatogenesis and highly expressed in the developing central nervous system and in B-lymphocytes (Tanaka et al., 1999; Campanini et al., 2015). At the structural level, all three members show a homology in three domains: The N-terminal DNA-binding domain and two regions in the C-terminal region (Nomura et al, 1988; Sakura et al., 1989). In addition, an acidic transactivation domain conserved in A-MYB and C-MYB is responsible for transcriptional activation (Lipsick et al., 2001; Foos et al., 1992; Bergholtz et al., 2001). Although B-MYB harbour this domain, the C-terminal portion is associated to be the region required for transcriptional activation (Tashiro et al.; 1995; Oh et al., 1998). Regulation of B-MYB occurs in a cell cycle dependent manner, which is reliant on the antagonistic effects of cyclin D1 and A. Cyclin A/Cdk2 triggers B-MYB transactivation activity by phosphorylation but it rather reduces the B-MYB protein level. In addition, cyclin A mediates the rate of B-MYB degradation via a ubiquitination and proteasome-mediated pathway. The C-terminal domain of B-MYB is important in mediating this effect of Cyclin A (Charasse et al., 2000).

1.3.1 Physiological Role of B-MYB

One important function of B-MYB is the role in early embryonic development supported by the elevated expression levels of B-MYB in embryonic stem cells (Lang et al., 2005; Nordhoff et al., 2001). Additionally, the analysis of *B-Myb* deficient embryos revealed that B-MYB is necessary for inner cell mass (ICM) formation in an early stage of development. Moreover, *B-Myb* mutation results in embryonic growth defects, which leads to lethality (Tanaka et al., 1999). Furthermore, it has been shown *in vivo* that B-MYB is an essential regulator of hematopoietic stem cell and myeloid progenitor cell development (Baker et al.,2014). Apart from its role in activating mitotic genes as subunit of MMB, B-MYB is also essential for progression through S phase and therefore important for chromosomal stability shown in megakaryocytes and embryonic stem cells (Garcia and Frampton, 2006; Lorvellec et al., 2010; Tarasov et al., 2008). A transcription independent function for B-MYB has also been identified: B-MYB affects mitosis forming a MYB-Clafi complex, which is needed for the stabilisation of kinetochores and the localisation of clathrin at the mitotic spindle. The absence of B-MYB

reduces the amount of clathrin leading to mitotic arrest (Yamauchi et al., 2008; Werwein et al., 2013).

It has been shown that the overexpression of B-MYB in keratinocytes leads to an undifferentiated phenotype shown by the suppression of differentiation markers or the retention of proliferative activity. In contrast, the suppression of B-MYB resulted in the retention of the differentiation capacity. These results indicate that B-MYB plays an essential role in the maintenance of the undifferentiated phenotype of keratinocytes (Marujama et al., 2014). Furthermore, B-MYB together with FOXM1 are identified to serve as master regulators of proliferation in germinal centres (Lefebvre et al., 2010). Many studies reveal that B-MYB play a role in apoptosis and in the response to DNA-damage. In this context, data suggest that B-MYB promotes cell survival through the regulation of apoptotic genes (Sala, 2005). Several target genes of B-MYB have been identified including the pro survival gene Bcl2. In contrast, B-MYB inhibits the transcription of apototic genes indicating that B-MYB play a role in apoptosis (Grassilli et al., 1999; Sala, 2005). In addition, the overexpression of B-MYB in CTLL-2 cells causes resistance against apoptosis induced by doxorubicin. Furthermore, the loss of B-MYB in cells leads to a higher susceptibility to DNA-damage induced via UV-irradiation or alkylation, which results in higher genomic stability (Ahlbory, 2005; Mowla et al., 2014). Moreover, B-MYB is required for neuronal apoptosis (Liu et al., 2004). Additionally, it has been reported that B-MYB has a function in the cellular DNA-damage signalling by supporting G2/M arrest and that B-MYB suppression promotes a DNA checkpoint response (Henrich et al., 2017; Klein et al., 2015). B-MYB has also been implicated in senescence (Mowla et al., 2014; Martinez and Dimaio, 2011; Zhou et al., 2017). B-MYB is highly downregulated upon senescence (Mowla et al., 2014). Conversely, it has been reported that B-MYB can rescue senescence induced by an activated Ras oncogene in rodent cells *in vitro* (Masselink et al., 2001).

1.3.2 B-MYB in cancer

In cytogenic analysis of different cancer types, it has been shown up that chromosome 20q13, where B-Myb is located, is amplified (Bar-Shira et al., 2002; Tanner et al., 2000). Furthermore, the overexpression of B-MYB is often associated with the promotion of cell growth linked to aggressive tumor growth and poor patient outcome (Jin et al., 2017; Musa et al., 2017; Tao et al., 2014; Thorner et al., 2009). In neuroblastoma, constant expression levels of B-MYB repress the differentiation of cells into neurons, whereas high B-MYB expression correlates with a poor survival prognosis (Raschella et al., 1995; Raschella et al., 1999). In many studies, B-MYB overexpression is connected with a poor long-term prognosis for patients affected by salivary gland malignancies, acute myeloid leukaemia, glioma, cervical, gallbladder, prostate

and colorectal cancer (Fujii et al., 2017; Fuster et al., 2013; Zhang et al., 2017; Astbury et al., 2011; Liang et al., 2017; Bar-Shira et al., 2002; Ren et al., 2015). In breast cancer, the overexpression of B-MYB is implicated in the development and progression of breast cancer. B-MYB plays a critical role in stimulating genes that promote cell proliferation, migration and invasion in breast cancer and on the other hand, in supressing differentiation and apoptosis of breast cancer cells (Tao et al., 2014; Thorner et al., 2009; Budczies et al., 2015; Drabsch et al., 2010). In contrast, loss of function of B-MYB in zebrafish leads to an increased rate of tumors by causing genomic instability (Shepard et al., 2005). Also in myeloid malignancies, the downregulation of B-MYB is associated with a poor outcome (Heinrichs et al., 2013).

1.4 DREAM/MMB as potential target for cancer therapy

Gain of function mutation in protooncogenes are very frequent in human cancer (Malumbres and Barbacid, 2009; Collins et al., 1997). One prominent example is the activation of oncogenic K-RAS having an activating mutation at codon 12. K-RAS belongs to a class of small GTPases which regulate signal transduction underlying diverse cellular activities, including proliferation, survival, growth, migration and differentiation (Inoue and Nukiwa, 2005). N-RAS and H-RAS are also part of the RAS protein family and as G-proteins they function as binary signalling switches meaning they switch between the active GTP-bound form and the inactive GDP-bound form. Activation of RAS family leads to signal transduction into several downstream pathways mainly the RAF-MEK-ERK pathway as well as the PI3K-AKT-mTOR pathway (Takashima and Faller, 2013; Fang, 2016). Mutation in RAS family members or the molecular components of their downstream pathways often results in cancer formation. K-RAS is most frequently mutated among these three isoforms in malignancies, especially prominent in non-small cell lung cancer (16–40%) (Takashima and Faller, 2013). Therefore, targeting RAS downstream signalling in form of inhibitors against components of the PI3K-AKT-mTOR and RAF-MEK-ERK pathways is a promising approach in cancer therapy. However, these blocks central physiological RAS signalling pathways which are required for the viability of all cells, both normal and malignant. Therefore, the ability to utilize them in effective doses is limited (Takashima and Faller, 2013; Fang, 2016). To identify cellular drug targets whose inhibition leads to the selective killing of cancer cells while sparing normal cells, the group of Stephen Elledge undertook a genome-wide RNAi screen to identify synthetic lethal interactions with the K-RAS oncogene. They found a set of proteins whose depletion selectively impaired the viability of Ras mutant cells mainly genes with mitotic functions like the mitotic kinase Plk1 (Luo et al., 2009). Their data indicate that the mitotic machinery could be the Achilles' heel for Ras mutant cancer cells suggesting that pathways, which are involved in regulating the mitotic machinery are attractive for a potential treatment of cancers harbouring Ras mutations (Luo et

al., 2009). In this context, the MMB complex could be an attractive target for a potential treatment of RAS cancer, because it is the master regulator of key mitotic genes including Plk1.

Loss of function mutations in tumor suppressor genes such as in p53 are also very frequent in human cancer. Under normal conditions, the p53 protein level is low. Upon cellular stress (e.g. hypoxia, DNA and spindle damage), p53 is activated through phosphorylation by ATM, ATR, Chk1 and MAPKs. Thereafter, p53 protein level increases to mediate growth arrest, DNA repair or apoptosis (Vogelstein et al., 2000). An important function of p53 is to regulate cell cycle and as “guardian of the genome” to maintain genomic stability. Therefore, p53 is able to induce cell cycle arrest by activating p21 at G1/S phase or GADD45 at G2/M. Furthermore, proapoptotic members of the Bcl-2 family like Bax and Puma are targets of p53. The pivotal function to maintain genomic stability and so prevent cancer formation define the p53 gene as a tumor suppressor gene (Yue et al., 2017). Inactivation of p53 is very frequent in human cancer. Loss of p53 often leads to enhanced expression of mitotic genes leading to genomic instability, which is a hallmark of cancer (Hanahan and Weinberg, 2011). Interestingly, it has been shown that p53 triggers the switch to the repressive DREAM. Conversely, loss of p53 leads to a constitutively active MMB, which results in an enhanced expression of key mitotic genes. Therefore, one prediction is that MMB contributes to tumorigenesis by mediating overactivity of mitotic genes after loss of p53 (Mannefeld et al., 2009).

Differences in the expression of genes involved in cell cycle progression and regulation are often found when expression profiles of normal tissue and cancer tissue are compared. In many cancer types, increased levels of cell cycle genes are observed, which is often associated with a higher fraction of proliferating cells in contrast to normal tissue (Whitfield et al., 2006; Rhodes et al., 2004). Therefore, factors which promote late cell cycle gene expression and which trigger proliferation are frequently overexpressed in tumors and associated with a poor outcome (Perou et al., 2000). It has been reported that the MMB members B-MYB and FOXM1, as well as their targets, belong to this group of factors (Thorner et al., 2009). FOXM1 overexpression correlates with poor prognosis in glioblastoma, breast and ovarian cancer (Liu et al., 2006; Francis et al., 2009; Lok et al., 2011). Furthermore, FOXM1 is part of the chromosomal instability 70 (CIN70) and CIN25 gene signatures as well as MMB target genes like kinesins (Lok et al., 2011; Carter et al., 2006; Wolter et al., 2017). Moreover, in the MammaPrint (Agendia) breast cancer profile that is used to predict the risk of metastasis, LIN9 is included (Tian et al., 2010). As described above, senescence is a process which is induced after deregulation of certain oncogenes to prevent tumorigenesis. In this context, it has been shown that loss of MMB members like LIN9 and LIN54 leads to the induction of cellular senescence in fibroblasts (Hauser et al., 2012). Furthermore, a lack of

LIN9 enables cells to overcome cellular senescence, which results in oncogenic transformation and growth (Hauser et al., 2012).

1.5 Lung cancer

Lung cancer is one of the most common cancers and remains the leading cause of cancer related mortality worldwide (Jin et al., 2017). Although new therapeutic advances have been obtained over the years, the diagnosis for patients with lung cancer remains poor and the mechanisms of tumor progression is still largely uncharacterised (Hirsch et al., 2017; Winslow et al., 2011). Depending on stage and regional differences, the 5-year survival rates vary in a low range from 4-17% (Hirsch et al., 2017). Although the use of tobacco remains the main cause of lung cancer also asbestos, air pollution and genetic alterations are identified as important risk factors (Hirsch et al., 2017). For therapeutic purposes, two major classes are distinguished: non-small-cell lung carcinoma (NSCLC, about 85% of all lung cancers) and small-cell lung carcinoma (SCLC, about 15%). NSCLC is further divided into three main subtypes: adenocarcinoma, squamous-cell carcinoma and large-cell carcinoma (Jin et al., 2017; Dela Cruz et al., 2011). In NSCLC, the most frequently altered pathways are the RAS and p53 pathway. Activation of oncogenic K-Ras having an activating mutation at codon 12 compared with inactivation of p53 leads to a rapid development of adenocarcinomas. In lung cancer, upregulation of mitotic genes is a characteristic feature (Feldser et al., 2010). Interestingly, these mitotic genes are direct transcriptional targets of the MMB complex. In addition, the RAS and the p53 pathway play a pivotal role for the MMB complex.

1.6 Aim of this thesis

B-MYB and MMB target genes have been identified as overexpressed in many cancer types. This suggest that the MMB complex could be required for tumorigenesis by mediating overactivity of mitotic genes. In addition, it was shown that pathways, which are involved in the mitotic machinery could be an effective target for treatment of cancers harbouring Ras mutations. Furthermore, inactivation of p53 is very frequent in human cancer. Interestingly, the tumor suppressor p53 mediates the switch to the repressive DREAM complex and inhibits the function of B-MYB. Therefore, we predict that MMB contributes to tumorigenesis by mediating overactivity of mitotic genes leading to genomic instability, which is a hallmark of cancer. However, although MMB has been well characterized biochemically, the contribution of MMB to tumorigenesis is largely unknown.

Therefore, the aim of this thesis was to identify the role of MMB in lung cancer by the inhibition of the transcription factor B-MYB. B-MYB is only part of the MMB complex and therefore a perfect factor to investigate if MMB contribute to lung tumorigenesis. To address the role of B-MYB in lung cancer *in vivo*, a conditional allele of *B-Myb* was used in a mouse model of lung cancer driven by mutant *K-Ras* and loss of *p53*. Furthermore, cell lines derived from tumors of this mouse model were established to study the importance of B-MYB for lung cancer development in more detail. In addition, the contribution of MMB to human lung tumorigenesis was investigated. RNAi-mediated depletion of B-Myb by shRNA and siRNA in several human lung cancer cell lines was used to analyse the role of MMB in human lung tumorigenesis in detail. Moreover, another aim was to clarify, if MMB could be used as a therapeutic tool and B-MYB could serve as a potential prognostic marker for lung cancer.

2. Materials und Methods

2.1 Materials

2.1.1 Chemical stocks and reagents

Unless otherwise noted, chemicals were purchased from AppliChem, Invitrogen, Carl Roth, Fluka or Sigma Aldrich.

A	Acetic acid
	Agarose [Peqlab]
	Ammonium acetate (5M) pH 5.7
	Ammonium hydroxide
	Ammonium persulfate (APS) 10% in H_2O

B	Bovine serum albumin fraction V (BSA) 3% in H2O
	Bromophenol blue 4 mg/ml in H_2O

C	Calcium chloride dehydrate
	Chloroform 99%
	p-Coumaric acid 90mM in DMSO
	Crystal violet 0.1% in H_2O

D	Diethylpyrocarbonate (DEPC), approx. 97%
	Dimethylsulfoxide (DMSO), >99.9%
	Dithiothreitol (DTT) 1 M in H_2O
	dNTPs (dATP, dCTP, dGTP, dTTP) [Promega] 2 mM (each NTP) in H_2O
	Doxycycline 1 µg/ml

E	Eosin-G solution (0.5%) add approximately 100 µl/100 ml acetic acid
	Ethanol absolute (99.8%)
	Ethidium bromide 10 mg/ml in H_2O
	Ethylenediaminetetraacetic acid (EDTA)

F	Formaldehyde (37%)

G	Glycine

H	Haematoxylin solution sour after Mayer
	HEPES
	Hoechst 33258 10 mg/ml in H_2O
	Hydrogen peroxide (30%)
	4-Hydroxytamoxifene (4-OHT)

I	ImmoMount [Shandon]

K	K Ketavet [Pfizer] 100 mg/ml

L	Luminol 250 mM in DMSO

M	Methanol

N	Nonfat dry milk powder

P	Paraformaldehyde
	Paraplast (Paraffin – polyisobutylene mixture)
	Phenylmethylsulphonyl fluoride (PMSF), 100 mM in isopropanol [Roche]
	Polybrene (Hexadimethrine bromide) 4 mg/ml in H_2O
	Ponceau S solution
	Propidium iodid (PI) 1 mg/ml
	Protease Inhibitor Cocktail P8340 (PIC)
	ProtoGel 30 % [Biozym]

R	Random primer, 0.5 µg/µl [Roche]
	Roti® Histokitt

S	Sodium butyrate (500 mM)
	Sodium citrate
	Sodium dodecyl sulfate (SDS) 20% in H_2O

T	Tetramethylethylenediamine (Temed) 99%
	Tissue-Tek® O.C.T. Compound
	Tris
	Triton X-100
	Tween 20
	Trizol/ Trifast (Peqlab)

X	Xylazine 2 % [CP-Pharma]
	Xylene

2.1.2. Antibiotics

Antibiotic	Stock concentration	Final concentration	Application
Ampicillin	100 mg/ml	100 µg/ml in LB-medium	DH5α (E.coli)
Blasticidin	10 µg/ml	Cell line-dependent	Selection of human lung cancer cell lines
Puromycin	10 mg/ml in ethanol absolute (25.8 mM)	2.5 µg/ml in 100% ethanol	lung tumor cell lines expressing Cre^{ERT2}

2.1.3 Enzymes

Enzymes	Company
Absolute QPCR SYBER Green Mix	ThermoFisher
DNase I, RNase free	Roche
M-MLV-RT Transcriptase (200 U/µl)	ThermoFisher
His-Taq DNA Polymerase (15 U/µl)	Provided by AG Prof. Gessler
Phusion High Fidelity DNA Polymerase (2 U/µl)	Finnzymes
Restriction Endonucleases	New England Biolabs (NEB), Fermentas
RiboLock RNase-Inhibitor (40 U/µl)	Fermentas
RNAse A (10 mg/ml)	Sigma-Aldrich®
T4-DNA Ligase (400 U/µl)	New England Biolabs (NEB)

2.1.4 Buffers and solutions

2.1.4.1 General buffers

Buffer	Ingredients
DNA Loading Buffer (5x)	15% ficoll 0.05% bromophenol blue 0.05% xylene cyanol 0.05 M EDTA in 1 X TAE
Miniprep Solution S1	25 mM Tris/HCl, pH 8.0 10 mM EDTA 100 µg/ml RNAse A
Miniprep Solution S2	200 mM NaOH 1% SDS
Miniprep Solution S3	29.44 g KCH_3COO 11.5 ml CH_3COOH 28.5 ml H_2O
Phosphate buffered saline (PBS) (1x)	13.7 mM NaCl 0.3 mM KCl 0.64 mM Na_2HPO_4 0.15 mM KH_2PO_4 adjust pH to 7.4 with HCl
TAE buffer (1x)	40 mM Tris base 5 mM CH_3COOH 10 mM EDTA, pH 8.0
Tris buffered saline (TBS) (1X)	50 mM Tris/HCl, pH 7.4 150 mM NaCl
TE buffer (1x)	10 mM Tris/HCl, pH 7.5 1 mM EDTA

2.1.4.2 Buffers for whole-cell lysates

Buffer	Ingredients
Bradford solution	50 mg Coomassie Brilliant Blue G250 23.75 ml ethanol 50 ml 85% (v/v) H_3PO_4 ad 500 ml H_2O / filter twice
TNN lysis buffer	50 mM Tris/HCl, pH 7.5 120 mM HCl 5 mM EDTA 0.5% NP-40 10 mM $Na_4P_2O_7$ 2 mM Na_3VO_4 100 mM NaF add to 500 ml H_2O Protease Inhibitor cocktail (PIC) 1:1000 (add fresh) 1 M DTT (add fresh): 1:1000 10 µg/ml PMSF (add fresh): 1:100

2.1.4.3 Buffers for immunoblotting

Buffers	Ingredients
Acrylamide solution	30% (w/v) acrylamide 0.8% (w/v) N,N´-methylenbisacrylamide
Blotting buffer (1x)	0.6 g Tris base 2.258 g glycine 150 ml methanol add to 1 l H_2O
Blocking Solution	3% milk poweder in TBS-T (w/v)
Electrophoresis sample buffer (ESB) (3x)	300 mM Tris/HCl, pH 6.8 15 mM EDTA 150 mM DTT 12% (w/v) SDS 15% (w/v) glycerol 0.03% (w/v) bromophenol blue
Enhanced chemiluminescence (ECL) solution	10 ml 100 mM Tris/HCl, pH 8.5 50 µl 250 mM luminol 22 µl 90 mM p-Coumaric acid 3 µl 30% H_2O_2
Ponceau S	0.1% Ponceau S 5% CH_3COOH
SDS running buffer (10x)	144 g glycine 30 g Tris 10 g SDS add to 1 l H_2O
Separating gel buffer	1.5 M Tris/HCl, pH 8.8
Stacking gel buffer	0.8 M Tris/HCl, pH 6.8
TBS-T	0.5% Tween-20 (v/v) in TBS

2.1.4.4 Buffers for flow cytometry (FACS)

Buffer	Ingredients
Sodium citrate	38 mM in 1x PBS

2.1.4.5 Buffers for immunostaining

Buffer	Ingredients
Blocking solution	3% BSA in PBS (w/v)
PBST	0.1-0.3% Triton-X in 1x PBS (v/v)
PSP (3% paraformaldehyde, 2 % sucrose)	15 g paraformaldehyde 10 g sucrose add to 500 ml in 1x PBS, store at -20ºC
4% PFA	4% PFA in PBS (w/v), store at -20°C

2.1.4.6. Buffers for immunohistochemistry

Buffer	Ingredients
4% PFA	4% PFA in PBS (w/v) adjust pH to 7.0 with NaOH, store at -20°C
Citrate buffer	100 mM, pH 6.0
Blocking solution	3 % BSA in 1x PBS

2.1.4.7. Buffers for genomic DNA extraction (HotSHOT)

Buffer	Ingredients
1x Base buffer	25 mM NaOH 0.2 mM EDTA, pH 8.0 adjust pH to 12.0 with NaOH
1x Neutralization buffer	40 mM Tris-HCl, pH 5.0

2.1.5 Transfection reagents

Tranfection reagent	Company
Lipofectamine® RNAiMAX reagent	Life Technologies
HEPES buffer solution (HBS) (2x)	8.2 g NaCl 5.95 g HEPES, acid 0.105 g Na_2PO_4 add to 500 ml ddH_2O adjust to pH 6.95, 7.00, 7.05 (with 5 M NaOH) Storage at 4°C sterile filtered
1x PEI solution	100x PEI stock diluted 1:100 in 0.15M NaCl
2.5 M $CaCl_2$	sterile filternd

2.1.6 Antibodies

2.1.6.1 Primary antibodies

Lab ID	Name	Origin & Clonality	Application & Dilution	Vendor	Catalog
-	B-MYB	Mouse monoclonal	WB 1:5	Gift from Watson laboratory (Hybridoma)/ self-made	Tavner et al. 2007
#158	α-tubulin	Mouse monoclonal	IF 1:100	Sigma-Aldrich	T6074
#185	KI-67	Rabbit polyclonal	IHC 1.200	Thermo Scientific	RM-9106
#196	B-ACTIN	Mouse monoclonal	WB 1:5000	Santa Cruz Biotechnology	sc-47778
#232	CENPF	Rabbit polyclonal	IHC 1:2500	Abcam	ab5
#233	p-B-MYB (Phospho T487)	Rabbit monoclonal	IHC 1:600	Abcam	ab76009
#234	NUSAP1	Rabbit polyclonal	WB 1:1000 IHC 1:1500	Gift of Geert Carmeliet, against protein sequence	
#258	PRC1	Rabbit polyclonal	WB 1:2000	Santa Cruz Biotechnology	sc-8356
#289	Phospho p44/42 MAPK	Rabbit monoclonal	IHC 1:400	Cell Signaling	cs-4376

2.1.6.2 Secondary antibodies

Name	Application & Dilution	Vendor
Anti-mouse HRP conjugated	WB 1:5000	GE Healthcare
Anti-rabbit HRP conjugated	WB 1:5000	BD Biosciences
Anti-Protein A HRP	WB 1:5000	BD Bioscience
Anti-mouse Alexa Fluor 488	IF 1:500	Invitrogen

2.1.7 Plasmids

Lab ID	Plasmid	Description
#210	pBabe-puro-empty	Empty vector control for retroviral transfection
#746	pBabe-H2B-GFP	GFP control for retroviral transfections
#924	pBabe-puro-Cre^{ERT2}	Retroviral expression vector for inducible Cre-recombinase
#1348	pCMV-VSV-G	Lentiviral packaging plasmid
#1368	U6-shRNA pgkCre (lenti)	Lentiviral vector allows constitutive Cre-expression, used for infection of mice (Young and Jacks, 2010); gift from Tyler Jacks (Addgene plasmid # 24971)
#1369	pINDUCER10 (Blasticidin resistance)	Backbone for inducible miR30-shRNA expression (Meerbrey et al., 2011), blasticidin resistance was cloned into the vector by Marc Fackler.
#1386	psPAX2	Lentiviral packaging plasmid

2.1.8 Primer sequences

2.1.8.1 Murine primer for quantitative real-time PCR

Lab ID	Gene	Sequence (5' to 3')	Directionality
SG 783	Hprt (house keeper)	TCCTCCTCAGACCGCTTTT	fw
SG 784		CCTGGTTCATCATCGCTAATC	rev
SG 820	B-Myb	TTAAATGGACCCACGAGGAG	fw
SG 821		TTCCAGTCTTGCTGTCCAAA	rev
SG 1026	Aspm	GATGGAGGCCGAGAGAGG	fw
SG 1027		CAGCTTCCACTTTGGATAAGTATTTC	rev
SG 1030	Nusap1	TCTAAACTTGGGAACAATAAAAGGA	fw
SG 1031		TGGATTCCATTTTCTTAAAACGA	rev
SG 1038	Cenpf	AGCAAGTCAAGCATTTGCAC	fw
SG 1039		GCTGCTTCACTGATGTGACC	rev
SG 2193	Top2a	CAAAAGAGTCATCCCCCAAG	fw
SG 2194		GGGGTACCCTCAACGTTTTC	rev

2.1.8.2 Human primer for quantitative real-time PCR

Lab ID	**Gene**	**Sequence (5' to 3')**	**Directionality**
SG 568	Birc5	GCCCAGTGTTTCTTCTGCTT	fw
SG 569		CCGGACGAATGCTTTTTATG	rev
SG 570	Bub1	GGAGAACGCTCTGTCAGCA	fw
SG 571		TCCAAAAACTCTTCAGCATGAG	rev
SG 574	Ccnb1	CGCCTGAGCCTATTTTGGT	fw
SG 575		GCACATCCAGATGTTTCCATT	rev
SG 645	Gapdh (house keeper)	GCCCAATACGACCAAATCC	fw
SG 646		AGCCACATCGCTCAGACAC	rev
SG 630	B-Myb	TCCACACTGCCCAAGTCTCT	fw
SG 631		AGCAAGCTGTTGGTCTTCTTTGA	rev
SG 1022	FoxM1	ACTTTAAGCACATTGCCAAGC	fw
SG 1023		CGTGCAGGGAAAGGTTGT	rev
SG 1060	Nusap1	TTTTGAAGAACACAATTCCATGA	fw
SG 1061		GTCCTGACCCCTCCCTTATT	rev
SG 1083	Cenpf	GAGTCCTCCAAACCAACAGC	fw
SG 1084		TCCGCTGAGCAACTTTGAC	rev

2.1.8.3 Primer for cloning

Lab ID	**Name**	**Sequence (5' to 3')**	**Directionality**
SG 1161	3'-miR30PCREcoRIF	CTAAAGTAGCCCCTTGAATTCCGAGGCAGTAGGCA	fw
SG 1164	amplifysmir30shRNA	CAGAAGGCTCGAGAAGGTATATTGCTGTTGACAGTGAGCG	rev

2.1.8.4 Primer for sequencing

Lab ID	Name	Sequence (5' to 3')
SG 1162	SG1162-Mir5	GCTTCGGCAGCACATATACTA

2.1.8.5 Primers for genotyping

Lab ID	Allele	Sequence (5' to 3')	Product size
SG 1499	Lox stop lox cassette (LSL) *K-Ras* for tails	TCTCGACCAGCTTCTGATGGAA	LSL 645
SG 1500		CAACCTCCCCTTCTACGAGCG	
SG 1556	Floxed (fl) *p53* for tails	GGTTAAACCCAGCTTGACCA	390 bp fl
SG 1557		GGAGGCAGAGACAGTTGGAG	270 bp wt
SG 1601	Floxed (fl) *B-Myb* for tails	TAATAAAGGAGTGTCTCAGA	410 bp fl
SG 1602		TACATGGTACAAGTAGGCA	360 bp wt
SG 2023/P1	Deletion of floxed (fl) *B-Myb* sequence for tumors	TACTACTTAGAGAGACTGCC	340 bp fl
SG 2024/P2		TCCTGGTAGTGTAACTCATC	300 bp wt
SG 2025/P7		CTCTTTAGACAGGCCATTC	249 bp Δfl
SG 2031/P1	Deletion of floxed stop cassette (LSL) *K-Ras* for both tails and tumors	GTCTTTCCCCAGCACAGTGC	500 bp LSL
SG 2032/P2		CTCTTGCCTACGCCACCAGCTC	622 bp wt
SG 2033/P3		AGCTAGCCACCATGGCTTGAG TAAGTCTGCA	650 bp ΔLSL
SG 2034/P1	Deletion of floxed (fl) *p53* sequence for tumors	CACAAAAACAGGTTAAACCCAG	288 bp wt
SG 2035/P2		AGCACATAGGAGGCAGAGAC	370 bp fl
SG 2036/P3		GAAGACAGAAAGGGGAGGG	612 bp Δfl

2.1.9 siRNA sequences

Lab ID/ name	Gene	siRNA Sequence (5' to 3')	Reference
S1 siRNA mBMYB1	*B-Myb* (mouse)	GCCCAUAAAGUCCUGGGU AAC	Knight et al., Oncogene (2009)
S2 siRNA mBMYB2	*B-Myb* (mouse)	GGU GCG ACC UGA GUA AAU U	Tarasov et al., Plos One (2008)
S7 siRNA MYB5	B-Myb	GCAGAGGACAGUAUCAACATT	Mannefeld M et al, 2009
S53 siCtrl	Control	UAGCGACUAAACACAUCAA	siGENOME
S55 siFoxM1	FoxM1	GGACCACUUUCCCUACUUU	Wu Qi-Fei et al., 2010

2.1.10 Lentiviral shRNA sequences

List of the 97-Oligo sequences used in the thesis:

Gene: B-Myb, Plasmid lab ID: #1485, Oligo lab ID: SG 1792 TGCTGTTGACAGTGAGCGagaggacagacaatgctgtgaaTAGTGAAGCCACAGATGTAttcacagcattgtctgtcctccTGCCTACTGCCTCGGA
Gene: B-Myb, Plasmid lab ID: #1486, Oligo lab ID: SG 1794 TGCTGTTGACAGTGAGCGaacagacaatgctgtgaagaatTAGTGAAGCCACAGATGTAattcttcacagcattgtctgtcTGCCTACTGCCTCGGA
Gene: B-Myb, Plasmid lab ID: #1487, Oligo lab ID: SG 1796 TGCTGTTGACAGTGAGCGccaggtatcaaagaagacaacaTAGTGAAGCCACAGATGTAtgttgtcttctttgatacctgaTGCCTACTGCCTCGGA
Gene: B-Myb, Plasmid lab ID: -, Oligo lab ID: SG 1921 TGCTGTTGACAGTGAGCGagacagacaatgctgtgaagaaTAGTGAAGCCACAGATGTAttcttcacagcattgtctgtccTGCCTACTGCCTCGGA

2.1.11 Cell lines

2.1.11.1 Murine cell lines

Cell line	Tissue	Disease	Medium	Additives
KR1 (pbabe Cre^{ERT2})	Lung	Own generated primary lung tumor cell line (*K-Ras* mutated, *p53* deficient) with 4-OHT inducible Cre-recombinase expression, control	DMEM	+5 µg/ml for infection: +2.5 nM OHT
KR2 (pbabe Cre^{ERT2})	Lung	Own generated primary lung tumor cell line (*K-Ras* mutated, *p53* deficient) with 4-OHT-inducible Cre-recombinase expression, control	DMEM	+5 µg/ml for infection: +2.5 nM OHT
BC1 (pbabe Cre^{ERT2})	Lung	Own generated primary lung tumor cell line (*K-Ras* mutated, *p53* deficient, partial *B-Myb* ko) with 4-OHT inducible Cre-recombinase expression	DMEM	+5 µg/ml for infection: +2.5 nM OHT
BC2 (pbabe Cre^{ERT2})	Lung	Own generated primary lung tumor cell line (*K-Ras* mutated, *p53* deficient, partial *B-Myb* ko) with 4-OHT inducible Cre-recombinase expression	DMEM	+5 µg/ml for infection: +2.5 nM OHT

2.1.11.2 Human cell lines

Cell line	Tissue	Cell type	Disease	Medium	Antibiotic concentration for selection
MDA-MB-231	Mammary gland	epithelial	adenocarcinoma	DMEM	Blasticidin 10 µg/ml
A549	Lung	epithelial	carcinoma	RMPI 1640	Blasticidin 5.0 µg/ml
H460	Lung	epithelial	carcinoma; large cell lung cancer	RMPI 1640	Blasticidin 5.0 µg/ml
HOP62	Lung	epithelial	adenocarcinoma, carcinoma	RMPI 1640	Blasticidin 5.0 µg/ml
H23	Lung	epithelial	adenocarcinoma; non-small cell lung cancer	RMPI 1640	Blasticidin 5.0 µg/ml

Packaging cell lines	Medium	Description
Plat-E	DMEM	Packaging cell line for retroviral infection
HEK 293T	DMEM (After transfection, medium was replaced by the medium of the target cell line at the next morning)	Packaging cell line for lentiviral infection

2.1.12 Media and additives

2.1.12.1 Media for cell culture

- DMEM (4.5 g Glucose/L-Glutamine) Gibco®, Life Technologies
- RPMI 1640 (4.5 g Glucose/L-Glutamine) Gibco®, Life Technologies
- Opti-MEM® Gibco®, Life Technologies

2.1.12.2 Additives

- Fetal Calf Serum (FCS) Gibco®, Life Technologies
- Penicillin/Streptomycin (10 U/µl each) Cambrex/Lonza
- Trypsin/EDTA (0.05 %) Gibco®, Life Technologies
- Trypsin/EDTA (0.25 %) Gibco®, Life Technologies
- TrypLE™ Express Gibco®, Life Technologies
- DMSO

2.1.12.3 Media for bacterial cell culture

- Luria Bertani (LB) Agar 40 g powder in 1 l H2O, autoclaved
- Luria Bertani (LB) Medium 25 g powder in 1 l H2O, autoclaved

2.1.13 Bacterial strains

E.coli DH5α or XL1-blue competent cells for transformation of plasmid DNA

2.1.14 Mouse strains

All strains were maintained on a C57BL/6 background. The B6.129-*K*ras^{tm4Tyj} mice were a generous gift from Dr. Daniel Murphy, whereas B6.129P2-Trp53^{tm1Brn}/J mice were purchased at the Jackson Laboratory (Bar Harbor, ME, USA) (Jackson et al., 2001; Marino et al., 2000). The C57BL/6- B-Myb^{tm1PGa} mouse strain was a gift from Paloma Garcia (Garcia et al., 2005).

B6.129-*K*ras^{tm4Tyj} mice:	carrying a latent point mutation of *K- Ras* (G12D). Cre-recombinase-mediated deletion of a transcriptional termination sequence (loxP-stop-loxP, LSL) results in oncogenic protein expression.
B6.129P2-Trp53^{tm1Brn}/J mice:	carrying conditionally targeted Trp53 locus (floxed *p53*). Cre-recombinase- mediated deletion of exons 2-10 results in non-functional protein expression.
Mybl2tm1.1Jof$_{mice}$:	carrying conditionally targeted *B-Myb* allele (floxed *B-Myb*). Cre-recombinase-mediated excision of exon 2-5 results in frame shift abolishing functional protein expression.

For infection experiments, mice were inter-crossed yielding the following mutant strains:

K-Ras$^{LSL-G12D/+}$*p53*$^{fl/fl}$ mice:	carrying a removable stop cassette (LSL) for a mutant *K-Ras* allele (G12D) and floxed *p53* alleles
K-Ras$^{LSL-G12D/+}$*p53*$^{fl/fl}$ *B-Myb*$^{fl/+}$ mice:	carrying a floxed stop cassette for a mutant *K-Ras* allele (G12D), floxed *p53* alleles and one floxed *B-Myb* allele
K-Ras$^{LSL-G12D/+}$*p53*$^{fl/fl}$*B-Myb*$^{fl/fl}$ mice:	carrying a floxed stop cassette for a mutant *K-Ras* allele (G12D), floxed *p53* alleles and floxed *B-Myb* alleles

2.1.15 Markers

Marker	Company
GeneRuler 1 kb DNA ladder	Thermo Scientific (Fermentas)
GeneRuler 100 bp DNA ladder	Thermo Scientific (Fermentas)
PageRuler Prestained Protein Ladder	Thermo Scientific (Fermentas)

2.1.16 Kits

Kit	Company
GeneJET Gel Extraction Kit	Thermo Scientific
QIAquick PCR Purification Kit	QIAGEN
PureLink HiPure Plasmid Midi-/Maxiprep kit	Life Technologies

2.1.17 Devices

Device	Company
Agarose gel electrophoresis system	Peqlab
SDS-PAGE gel electrophoresis system	BIORAD
Trans-Blot wet transfer apparatus	BIORAD
FACS Cytomics FC500	Beckman Coulter
Incubators	Heraeus and Nunc
Centrifuge 5417R, 5804 and 5414D	Eppendorf
Flow cytometer Cytomics FC500	Beckman Coulter
Frigocut 2800E Microtome Cryostat	Leica
STP 120 Spin Tissue Processor	Thermo Scientific
Microm EC 350 tissue embedding center	Thermo Scientific
Hyrax M40 microtome	Zeiss
SMZ1500 Stereomicroscope	Nikon
Centrifuge Megafuge 1.0R	Heraeus
Thermocycler	Biometra
Mx3000P qPCR System	Agilent
NanoDrop 2000	Thermo Scientific
Confocal microscope NikonEclipse Ti C1	Nikon
Fluorescence microscope Leica DMI 6000B	Leica
Spectrometer Ultrospec 2100 pro	Biosciences
Multiskan Ascent	Labsystems
GS Gene Linker® UV chamber	BIORAD

2.2 Methods

2.2.1 Cell culture

2.2.1.1 Passaging of cells

Materials:

- Cell culture medium (DMEM or RPMI) with 10% FCS and 1%P/S, preheated to 37°C
- 1x PBS, pH 7.4
- Trypsin/EDTA (0.05%)
- Trypsin/EDTA (0.25%) murine tumor cell lines

Method:

Murine and human cell lines were cultivated in a tissue culture incubator at 37°C, 95% humidity and 5% carbon dioxide (CO_2). For passaging, cell culture medium was removed followed by a washing step with PBS. According to adhesion of cells to the cell culture dish surface, cells were treated with either Trypsin/EDTA (0.05%) or Trypsin/EDTA (0.25%) staying in the incubator until cells detaches from the dish via gentle shaking and observation under the microscope. The enzymatic reaction of trypsin was stopped through adding fresh culture media. Finally, cells were resuspended and seeded at the desired density onto new cell culture dishes.

2.2.1.2 Cryopreservation and Resuscitation of frozen cell lines

Materials:

- Cell culture medium (DMEM or RPMI) with 10% FCS and 1% P/S, preheated to 37°
- Freezing medium: 50% Cell culture medium + 40%FCS +10% DMSO (v/v), 4°C
- 1x PBS, pH 7.4
- Trypsin/EDTA (0.05% or 0.25%)
- Cryotubes

Method:

Cells were trypsinized as described above. Then, cells were centrifuged for 5 minutes at 300 g. Finally, supernatant was removed and the cell pellet was resuspended in 1 ml freezing media, transferred into cryotubes. After storage on ice for a few minutes, cryotubes were stored at -80 °C (short term) or in liquid nitrogen (long term).

For recovery, the cell suspension was quickly warmed up at 37°C and added to 9 ml warm fresh media and centrifuged for 5 minutes at 300 g. The supernatant was discarded; cell pellet was resuspended in fresh warm media and seeded onto new cell culture dishes.

2.2.1.3 Counting cells

Materials:

- Neubauer Chamber

Method:

10µl of a well resuspended suspension was loaded on a Neubauer chamber to determine the cell number. Cells in 4 large squares were counted and the number of cells per ml in suspension was calculated according to the formula:

Cells/ml = (Cells counted/ number of counted large squares) x 10^4

2.2.1.4 Cell treatment with different reagents

4 Hydroxytamoxifen (4-OHT):	Cells were treated with 2.5 nM 4-OHT and 5 µg/ml puromycin for indicated time.
Doxycycline:	Lentiviral shRNA expression was induced by adding the desired concentration of doxycycline for indicated time.

2.2.1.5 Establishing of tumor cell lines

Materials:

- Cell culture dish
- Razor blades
- Scissors
- Scalpel
- Tryple E
- 70% ethanol for sterilization
- 1x PBS
- Cell culture medium (DMEM) with 10% FCS and 1% P/S, preheated to 37°
- Ice

Method: modified after Basseres et al., 2010

Lung tumors from Lenti-Cre virus infected *K-Ras*$^{LSL\text{-}G12D/+}$*p53*$^{fl/fl}$*B-Myb*$^{+/+\ or\ fl/+\ or\ fl/fl}$ mice were isolated via scalpel, placed and washed in a cell culture dish on ice containing PBS. After transfer into the cell culture hood, each lung tumor was placed in a 10 cm cell culture dish containing Tryple E. Tumor tissue was finely minced with sterile razor blades in 1 ml Tryple E and incubated for 30 min at 37 ºC in a tissue culture incubator. Afterwards, the reaction of Tryple E was stopped by adding 5 ml fresh media to the dish. Remaining tissue was comminute via vigorous pipetting. Next, cell suspension was transferred to a 15 ml tube. Cell suspension were left 10 minutes standing in which fibroblasts and trypsinized debris could settle in the sediment. Next, 5 ml cell culture medium and supernatant/cell suspension were mixed and plated on a new cell culture dish. To the remaining sediment 10 ml culture medium was added a plated on a new culture dish. Cells were cultured until confluency was reached and then genotyped.

2.2.1.6. Transient transfection

2.2.1.6.1 Plasmid transfection with calcium phosphate

Materials:

- 2x HBS, pH 7.05: 500 µl; preheated 37°C
- 2.5 M $CaCl_2$: 50 µl; preheated 37°C
- ddH_2O: up to 450 µl
- plasmids [pbabeCreERT2 and pbabepuro]: 30 µg

Method:

Transfection of the retroviral packaging cell line Plat-E for the infection of murine tumor cell lines

At the first day, a confluent 10 cm culture dish with Plat-E cells was split 1:4 to reach 80% confluency on the next day. Cells were plated on a new 10 cm dish. On the second day, one hour before transfection, the culture medium was removed and fresh one was added. In an Eppendorf tube, 50 µl of 2.5 M $CaCl_2$ were mixed with 30 µg plasmid DNA resulting in a calcium phosphate co-precipitation with DNA. The mixture was then filled up with ddH_2O to 500 µl and blended again. Next, 500 µl prewarmed HBS was transferred to a 15 ml tube. Under continuous bubbling of the HBS, the $CaCl_2$/DNA mix was slowly added dropwise to the HBS. The HBS/$CaCl_2$/DNA mix was slowly added dropwise to the Plat-E cells. In the evening, medium

was removed, 8 ml fresh medium was applied and cells were incubated for 48 hours. The infection procedure of murine tumor cell lines is described in 2.2.1.7.

Materials:

- 2x HBS, pH 7.05: 250 µl; preheated 37°C
- 2.5 M $CaCl_2$: 25 µl; preheated 37°C
- ddH_2O: up to 250 µl
- plasmids: pCMV-VSV-G: 1.5 µg
  psPAX2: 2.25 µg
  construct [pInducer or shRNAs against B-Myb or Luciferase]: 3 µg

HEK 293T cells were used as lentiviral packaging cell line for the infection of human cell lines (2.2.1.7).

On the first day, a confluent 10 cm culture dish of HEK 293T cells were splitted 1:12 into 6 cm culture dishes. On the second day, one hour prior transfection, the medium was replaced by 3 ml fresh medium. Under S2 conditions, 1.5 µg of the pCMV-VSV-G plasmid, 2.25 µg of the psPAX2 plasmid and 3 µg construct plasmid were blended in an Eppendorf tube followed by mixing 25 µl 2.5 M $CaCl_2$. Next, mixture was filled up to 250 µl with ddH_2O and mingled again. Then, 250 µl of 2x HBS was transferred to a 15 ml tube. Under continuous bubbling of the HBS, the CaCl2/DNA mixture was slowly added dropwise to the HBS. The HBS/$CaCl_2$/DNA mixture was slowly added dropwise to the HEK 293T cells to covering the plate completely and incubated in the cell culture hood of S2. On the third day, in the morning, the old medium was removed and 3 ml of fresh medium was applied to the cells. Cells were incubated further. The infection procedure of human cell lines is described in 2.2.1.7.

Materials:

- 15 ml cell culture dish
- Pur DMEM medium
- Cell culture medium (DMEM) with 10% FCS and 1% P/S, preheated to 37°
- 500 mM Sodium butyrate
- ddH_2O: up to 250 µl
- plasmids: pCMV-VSV-G: 10.2 µg
  psPAX2: 15.4 µg
  construct [SG 1368: U6-shRNA pgkCre (lenti)]: 20.4 µg
- 1x PEI: 100x PEI stock diluted 1:100 in 0.15M NaCl
- 2.5 µl 1x PEI/µg DNA

Method:

On the first day, HEK 293T were seeded on 15 cm culture dishes to reach 70-80% confluency on the next day. On the second day, one hour prior transfection, the medium was replaced by 12.5 ml medium. Under S2 conditions, 10.2 µg of the pCMV-VSV-G plasmid, 15.4 µg of the psPAX2 plasmid and 20.4 µg construct plasmid were blended in an Eppendorf tube followed by filling up to 1700 µl with pur DMEM medium. 115 µl 1x PEI-solution was mingled with 1585 µl pur DMEM medium. Next, PEI-mixture was added to DNA-mixture, blended and incubated for 30 minutes at RT. Transfection-mix was added dropwise to the HEK 293T cells to covering the plate completely and incubated in the cell culture hood of S2. On the third day, in the morning, the old medium was replaced by 15 ml fresh medium and 150 µl 500 mM sodium butyrate was applied to the cells. Cells were incubated further until infection. Infection procedure of Lenti-Cre-virus is described in 2.2.1.7 (Tiscornia et al., 2006).

2.2.1.6.2 Liposomal transfection

Materials:

- Opti-MEM® (life technologies)
- Cell culture medium (10% FCS, without P/S)
- Transfection reagent: Lipofectamine® RNAiMAX reagent (Life Technologies)
- siRNAs

Method:

The transfection was performed according to the manufacturer's protocol Lipofectamine® RNAiMAX Reagent Protocol 2013 Protocol Pub. No. MAN0007825 Rev.1.0 on www.lifetechnologies.com/support.The following table shows a list of seeded cell numbers:

Cell line	6 cm culture dish
BC2	$2.5x10^5$
H23	$4.5x10^5$
HOP62	$3.0x10^5$
H460	$2.0x10^5$

On the first day, cells were seeded in an appropriate cell number in 4.5 ml antibiotic free cell culture medium to reach 60-80% confluency next day at transfection. 5 µl Lipofectamine RNAi Max Reagent was diluted in 245 µl Opti-Mem in an Eppendorf tube and incubated for 5

minutes. In another Eppendorf tube, 3.4 µl [50 nM] siRNA was diluted in 246.6 µl Opti-Mem and also incubated for 5 minutes. The diluted siRNA was added to the diluted Lipofectamine RNAi Max Reagent (1.7:2.5 ratio), mixed and incubated for 20 minutes. Finally, the siRNA-lipid complex was added to the cells incubated in the cell culture hood. Cells were harvested 72 h posttransfection and processed for RNA or protein analysis (see section 2.2.2.1 and 2.2.3.1)

The siRNA was mainly transfected in a concentration of 50 nM from a 75 µM stock. In BC2 a concentration of 100 nM was tested, too.

2.2.1.7. Cell infection

2.2.1.7.1 Retroviral infection of murine tumor cell lines

Materials:

- Polybrene (4 mg/ml): 1:1000
- Filter (0.45 µm)

Method:

One day before infection, $1x10^5$ murine tumor cells were seeded into a 6 well plate. The next morning, the virus-containing supernatant (medium of calcium phosphate transfected Plat-E cells) was filtered (0.45 µm) and transferred into a 15 ml tube. 8 ml fresh media was added to the Plat-E cells to use them for second infection. The tumor cells were incubated with the viral supernatant containing polybrene during the day. In the evening, the medium was replaced. The following day, a second infection round was started. Target cells were selected with the appropriate antibiotic and tested for positive infection.

2.2.1.7.2 Lentviral infection of pINDUCER-shRNAs

Materials:

- Polybrene (4 mg/ml): 1:1000
- Filter (0.45 µm)

Method:

One day before infection, $1\text{-}2x10^5$ human cells were seeded into a 6 well plate. The next morning, the virus-containing supernatant (medium of calcium phosphate transfected HEK 293T cells) was filtered (0.45 µm) and transferred into a 15 ml tube. The HEK 293T cells were

discarded. The cell lines were infected for 24 h in 2 ml of the viral supernatant containing polybrene. On the next morning, the medium was and the selection process was started in the evening. Infection process was repeated once.

2.2.1.8 Concentration of Lenti-Cre virus

Materials:

- Filter (0.45 µm)
- 50 ml tubes
- Ultracentrifuge: Centrifuge tubes + TST41.14 rotor
- Pur DMEM medium

Method:

On the next morning, the virus-containing supernatant (medium of calcium phosphate transfected HEK 293T cells) was harvested, spun down at 300 x g for 5 min and filtered (0.45 µm) and transferred into a 50 ml tube. Lenti-Cre virus particles were concentrated by ultracentrifugation in a TST41.14 rotor for 2 hours at 27500 rpm. The supernatant was discarded and tubes were filled with the remaining virus and centrifuged again until all virus was concentrated. The virus pellet as dissolved in 30 µl medium for 2 hours at 4°C.

2.2.1.9 Lenti-Cre virus titer determination with NIH3T3 zeG reporter cell line

Materials:

- Polybrene (4 mg/ml): 1:1000

Method:

To determine the lentiviral titer, a NIH3T3 zeG reporter cell line (NIH3T3 stably transfected with the GFP-reporter plasmid pZ/EG), which expresses GFP after Cre-mediated recombination, was utilized (Novak et al., 2000). One day before infection, 3.5 x 105 NIH3T3 zeG cells were seeded into 6 well plates. For virus-titer determination, the NIH3T3 zEG was infected with serial diluted lentivirus containing polybrene. The fraction of GFP-positive cells was determined by fluorescence activated cell sorting. $1x10^6$ lentivirus particles were aliquoted in 50 µl medium in Eppendorf tubes and stored until use by -80°C.

2.2.1.10 Cell proliferation assay with crystal violet staining (Growth curves)

Materials:

- 1x PBS, pH 7.4
- 10% formalin (3.7% paraformaldehyde)
- Tap water
- Staining solution: 20% ethanol + 0.1% crystal violet
- Drugs: 4-Hydroxytamoxifen + puromycin (2.5 nM +5 µg/ml) or doxycycline (1 mg/ml)
- 10% acetic acid for dye extraction

Cell number:

Cell line	24 Well plate
KR1	250
KR2	300
BC1	250
BC2	300
H23	8000
HOP62	1500
H460	1000
A549	400

Method:

Cells were seeded in an appropriate number at a 24 well plate as triplicates and treated with either different drugs (4-OHT + puromycin or doxycycline) or solvent for 10 days. Every second day, fresh media and drugs were applied. Furthermore, every second day the provided plate for this day (time point plate) was rinsed with 1x PBS, fixed for 10 minutes with 10% formalin (3.7 % formaldehyde) at room temperature, rinsed with tap water and air dried. At day zero reference plate was fixed 8 hours after plating the cells. At day 10, all time point plates were stained with 0.1 % crystal violet (in 20% ethanol) for 30 minutes at RT, washed with tap water until they appear clear and then air-dried. The plates were scanned and stored at 4°C.

For quantification, the dye was extracted with 0.5 ml 10 % acetic acid for 30 minutes at RT on a shaker. The crystal violet was quantified using a volume of 100 µl extract in a 96-well plate. The absorbance was measured at 595 nm at an Elisa Reader. If absorbance was above 1.0; samples were diluted. The results were normalized to the control (100 µl acetic acid).

2.2.1.11 Flow cytometry analysis using the intercalating dye Propidium Iodide

Materials:

- Cell culture medium (DMEM or RPMI) with 10% FCS and 1% P/S, preheated to 37°
- 1x PBS, pH 7.4
- Trypsin/EDTA (0.05% or 0.25%)
- 80% ethanol (-20°C): 1 ml
- Sodium citrate (38 mM): 500 µl
- Propidium iodide (1 mg/ml): 15 µl
- RNAse (10 mg/ml): 25 µl

Method:

The cell cycle phase was determined by quantitatively assessing the DNA content of a cell using the intercalating dye Propidium Iodide (PI). Cells were trypsinized, transferred in a 15 ml tube, centrifuged for 5 minutes at 300 g at 4 °C and washed with cold 1x PBS. Cells were fixed by adding 1 ml ice cold 80 % ethanol while slowly vortexing and stored at -20 °C before further processing. 1-2 hours before measurement, cells were centrifuged for 10 minutes at 210 g and washed once with cold 1x PBS. Cells were resuspended in 500 µl 38 mM sodium citrate, mixed with 25 µl RNase and incubated 1 h at 37ºC in a water bath. Finally, cell suspension was transferred to FACS tubes, stained with15 µl PI and measured in a Cytomics FC500 Flow cytometer.

2.2.2. Molecular biological methods

2.2.2.1 RNA isolation

Materials:

- Trizol or the analogue RNA isolation reagent TriFast
- Chloroform
- 75% and 100% ethanol in DEPC
- DEPC-H_2O
- Ammonium acetate (5 M), pH 5,7

Method:

Total RNA from cells was extracted with Trizol or TriFast. First, medium was removed, 1 ml Trizol was applied covering the whole plate. Then cells were scraped, transferred into a Eppendorf tube and incubated for 5 minutes at RT. Next, 200 µl chloroform was added and the mixture was vortexted thoroughly for 30 seconds. Centrifugation for 10 minutes at 12000 g in a cooling centrifuge results in formation of 3 phases. The upper aqueous phase containing RNA was transferred into a new reaction tube. RNA was precipitated with 0.1 volume 5 M ammonium hydroxide and with 2 volumes 100% ethanol for an hour or overnight at -20°. Samples were centrifuged for 10 minutes at 12000 g at 4 °C. The supernatant was removed and the pellet was washed with 1 ml 75% ethanol and vortexed. Samples were centrifuged by 7000 g at 4°C. Finally, the supernatant was removed to allow the samples to air dry. Samples were resuspended in 25 µl RNase free water and heated at 55°C for 10 min under slow shaking. Purity and concentration of the RNA was determined in a NanoDrop 2000 spectrophotometer. RNA samples were stored at -80°C.

2.2.2.2 Reverse transcription (RT-PCR)

Materials:

- DEPC-H_2O
- Random primer (0.5 mg/ml)
- dNTP’s (2mM)
- Ribolock RNAse inhibitor (Fermentas, 40U/µl)
- RevertAid Reverse Transcriptase (Thermo Scientific, 250 U/µl)
- 5x RevertAid reaction buffer (Thermo Scientific)

Method:

2 µg RNA in a final volume of 9.5 µl DEPC water were mixed on ice with 0.5 µl random primers. After denaturing at 70 °C for 5 minutes, samples were kept at 4 °C and the following mixture was added:

5 µl 5x RevertAid reaction buffer

6.25 µl dNTP

0.5 µl RiboLock RNase inhibitor

0.5 µl RevertAid Reverse Transcriptase

2.75 µl DEPC water

The solution was mixed carefully by pipetting and incubated for 1 h at 37 °C. 15 minutes heat inactivation at 70 °C stopped the synthesis process. Until use, cDNA was stored at -20 °C.

2.2.2.3 Quantitative real-time PCR (qRT-PCR)

Materials:

- AbsoluteTM QPCR SYBR Green Mix (Thermo Scientific).
- Primer mix (10 mM): Primer 1 (fw, 5 mM) and Primer 2 (rev, 5 mM)
- ABgene® PCR Plates (Thermo Scientific)
- ddH_2O (autoclaved)

Method:

The following set-up was used and measured in triplicate at the Mx3000P qPCR System by Agilent:

PCR mix:

10.0 µl Absolute™ QPCR SYBR Green Mix

0.4 µl forward primer (10 µM)

0.4 µl reverse primer (10 µM)

1 µl cDNA

8.2 µl H_2O

Thermal profile set-up:	activation	95 °C	15 min
	amplification	95 °C	0.5 min
	(40 cycles)	60 °C	1 min
		95 °C	15 min
	dissociation	95 °C	1 min
		60 °C	0.5 min
		95 °C	0.5 min

The relative expression of a specific mRNA compared to a housekeeping gene was calculated according to the formula:

$2^{-\Delta\Delta Ct}$

$\Delta\Delta Ct = \Delta Ct\ (sample) - \Delta Ct\ (reference)$

$\Delta Ct = Ct\ (gene\ of\ interest) - Ct\ (housekeeping\ gene)$

The standard deviation of ΔΔCt was calculated according to this formula:

$s = \sqrt{s_1 2 + s_2^2}$

s1 = standard deviation (gene of interest)

s2 = standard deviation (housekeeping gene)

The margin of error of $2^{-\Delta\Delta Ct}$ was determined according to this formula: $2^{-\Delta\Delta Ct} +/- s$

2.2.2.4 Isolation of plasmid DNA from bacteria

2.2.2.4.1 Mini preparation

Materials:

- LB medium (+ Ampicillin 1:1000)
- Buffer S1, 4°C
- Buffer S2
- Buffer S3
- 100% ethanol
- 70% ethanol
- TE buffer

Method:

DNA Mini preparation was performed of single colonies of transformed E.coli. colonies picked from a LB agar plate and incubated overnight in 3 ml ampicillin-containing LB media at 37 °C under vigorous shaking. On the next day, 1.5 ml of the bacterial culture were transferred into an Eppendorf tube and centrifuged for 2 minutes at maximum speed. The pellet was resuspended in 150 µl miniprep solution S1. For cell lysis, 150 µl miniprep solution S2 was added, the samples were mixed by gently inverting the Eppendorf tube 5 times and incubated 5 minutes at RT. After 5 minutes, miniprep solution S3 was added for neutralisation and mixed by gently inverting the Eppendorf tube 5 times. Samples were centrifuged for 10 minutes at maximum speed. The aqueous phase (~ 400 µl) was transferred into a fresh reaction tube, mixed with 800 µl absolute ethanol and vortexed thoroughly. Precipitated DNA was pelleted by spinning for 10 minutes at maximum speed and washed with 500 µl 70 % ethanol. After a second centrifugation step under same conditions, the supernatant was discarded, the pellet was dried and dissolved in 20 µl TE buffer. Plasmid DNA concentration and purity was determined with a NanoDrop 2000 spectrophotometer. The plasmid was stored at -20°C or used for a control digestion to test the correct ligation of vector and insert.

The endonuclease Kpn1 were used for digestion for 1 h at 37°C using the following pipetting scheme:

KPN1 digestion
1-3 µl Plasmid (vector and Insert)
0.1 µl Kpn1
2 µl KPN1 buffer (10x)
Add up to 20 µl ddH_2O

2.2.2.4.2 Midi/Maxi preparation

Materials:

- PureLink HiPure Plasmid Midi-/Maxiprep kit (Life Technologies)
- LB medium (+ Ampicillin 1:1000)
- TE buffer

Method:

After sequencing the mini preparation, the plasmids were purified using Midi and Maxi preparations. Therefore, a pre- culture (a single colony was picked from an LB agar plate) was incubated 8 hours in 2 ml ampicillin-enriched LB media. For high copy number plasmids, 1.5 ml of the pre-culture was added to 100-200 ml of LB medium (+ Ampicillin 1:1000) at 37°C overnight under vigorous shaking. Bacterial cultures were harvested by centrifugation for 10 minutes at 4200 g at 4°C. The LB medium was removed and plasmid DNA was extracted with PureLink HiPure Plasmid Midi-/Maxiprep Kit according to the manufacture's instruction. Concentration and purity was determined with a determined with a NanoDrop 2000 spectrophotometer and samples were stored at -20 °C.

2.2.2.5. Isolation of plasmid DNA fragments from agarose gels

Materials:

- Scalpel
- GeneJET Gel Extraction Kit (Thermo Scientific)

Method:

After digestion of plasmid DNA with respective restriction endonucleases, fragments were separated on 0.8-2 % agarose gels containing ethidium bromide (0.35 µg/ml) by electrophoresis for 1-2 h at 100 V. Desired bands were excised under UV light and DNA was extracted with GeneJET Gel Extraction Kit according to manufacturer's protocol.

2.2.2.6. Isolation of genomic DNA from tumor slides

Materials:

- Forceps
- Xylene

- Ethanol (100%)
- Bunsen burner

Method:

Tumor tissue was isolated under a stereomicroscope with forceps and added to an Eppendorf tube containing 1 ml pure xylene. Samples were by centrifuged for 5 minutes at full speed at RT and washed two times with 1 ml absolute ethanol. The genomic DNA pellet was further processed (see section 2.2.2.7) and genotyped (see section 2.2.2.8).

2.2.2.7. Extraction of genomic DNA (HotSHOT)

For extraction of genomic DNA (gDNA) followed by a genotyping PCR, ear biopsies were lysed in 75 µl base buffer for 30 minutes at 95 °C. After heating, samples were cooled down for 5 minutes and mixed with 75 µl of neutralizing buffer by inverting the Eppendorf tubes. For isolated tumor material only 10 µl base buffer/10 µl neutralisation buffer was applied and the heating step was reduced to 10 minutes.

2.2.2.8. Genomic DNA PCR

For genotyping of ear biopsies 1-5 µl of the final gDNA were used for each PCR reaction according to the following program:

Genomic PCR for LSL-KRasG12D:

PCR mix	PCR program		
2.5 µl 10x ReproFast buffer	95 °C	5 min	
2.5 µl dNTPs (2 mM)	95 °C	30sec	34 cycles
1 µl forward primer (10 µM)/ SG 1499	64 °C	30 sec	
1 µl reverse primer (10 µM)/ SG 1500	72 °C	1 min	
0.3 µl His Taq polymerase (15 U)	72 °C	3 min	
ad 25 µl H_2O	4 °C	hold	

Genomic PCR for p53 floxed:

PCR mix	PCR program		
2.5 µl 10x ReproFast buffer	95 °C	5 min	
2.5 µl dNTPs (2 mM)	95 °C	30sec	
1 µl forward primer (10 µM)/ SG 1556	56 °C	1 min	29 cycles
1 µl reverse primer (10 µM)/ SG 1557	72 °C	1 min	
0.2 µl His Taq polymerase (15 U)	72 °C	3 min	
ad 25 µl H_2O	4 °C	hold	

Genomic PCR for B-Myb floxed:

PCR mix	PCR program		
2.5 µl 10x ReproFast buffer	95 °C	5 min	
2.5 µl dNTPs (2 mM)	95 °C	30sec	
1 µl forward primer (10 µM)/ SG 1601	56 °C	1 min	34 cycles
1 µl reverse primer (10 µM)/ SG 1602	72 °C	1 min	
0.2 µl His Taq polymerase (15 U)	72 °C	3 min	
ad 25 µl H_2O	4 °C	hold	

For genotyping of isolated tumor material. 5 µl of the final gDNA were used for each PCR reaction according to the following program:

Genomic PCR for ∆LSL-KRasG12D:

PCR mix	PCR program		
4.0 µl 5x Phusion HF buffer	98 °C	1 min	
2.0 µl dNTPs (2 mM)	98 °C	15 sec	
1 µl primer (10 µM)/ SG 2031	67 °C	30 sec	34 cycles
1 µl primer (10 µM)/ SG 2032	72 °C	10 sec	
0.1 µl primer (10 µM)/ SG 2033	72 °C	10 min	
0.2 µl Phusion DNA polymerase (2 U)	4 °C	hold	
ad 20 µl H_2O			

Genomic PCR for ΔB-Myb floxed:

PCR mix	PCR program		
4.0 µl 5x Phusion HF buffer	98 °C	1 min	
2.0 µl dNTPs (2 mM)	98 °C	10 sec	34 cycles
1 µl primer (10 µM)/ SG 2023	59 °C	30 sec	
1 µl primer (10 µM)/ SG 2024	72 °C	10 sec	
1 µl primer (10 µM)/ SG 2025	72 °C	10 min	
0.2 µl Phusion DNA polymerase (2 U)	4 °C	hold	
ad 20 µl H_2O			

2.2.2.9. Cloning of lentiviral shRNAs (miR30 shRNAs for the pINDUCER vector system)

Potential shRNA sequences for the gene of interest were predicted via the Designer of Small Interfering RNA tool (DSIR. http://biodev.extra.cea.fr/DSIR/DSIR.html). Several criteria, which were described in Dow et al. (2012) were used to select positive candidates. These candidates were purchased as 97 bp long cloning template in a mir30-based format and restriction sites were introduced by PCR according to the following reaction:

PCR mix	PCR program (30 cycles)	
5.0 µl 10x ReproFast buffer	95 °C	3 min
5.0 µl dNTPs (2 mM)	95 °C	45 sec
2 µl Primer SG 1161 (10 µM)	54 °C	30 sec
2 µl Primer SG 1164 (10 µM)	72 °C	1 min
0.5 µl His-Taq polymerase (15 U/µl)	72 °C	10 min
ad 34.5 µl H_2O	4 °C	hold

2.2.2.10. Agarose gel electrophoresis

Materials:

- 1x TAE buffer
- DNA loading buffer (5x XB)
- 100 bp or 1 kb DNA ladder (Fermentas)
- Ethidium bromide solution (10 mg/ml)

Method:

Separation and purification of fragments of varying size was conducted by electrophoresis in agarose gels. Agarose powder was added to 1x TAE buffer, boiled in a microwave until complete dissolution of the agarose. To visualize the DNA banding pattern with a UV light source, ethidium bromide (0.35 µg/ml final concentration) was added and the complete mixture was solidified in a gel chamber. DNA samples were mixed with 5x loading buffer including bromophenol blue to monitor the progress of electrophoresis and loaded into pockets of the gel. A DNA ladder of 100 bp or 1 kb was utilized as a marker to determine the size. Electrophoresis ran for 1-2.5 hours at 100 V. DNA bands were visualized in a UV transilluminator, photographed and - if necessary - excised for further processing.

2.2.2.11 Restriction digestion

Both. PCR product and pINDUCER vector were digested with the same endonucleases for 4 h at 37°C according to the following pipetting scheme:

Vector digestion	**PCR digestion**
5 µg pINDUCER10 (#1369)	All PCR product
5µl NEB4	5 µl NEB4
0.5 µl BSA	0.5 µl BSA
3 µl Xho1	1 µl Xho1
1.5 µl EcoR1 (High fidelity)	0.5 µl EcoR1 (High fidelity)
Add to 50 µl ddH_20 add to	Add to 50 µl ddH_2O

Digested DNA fragments were purified by gel electrophoresis or column purification using GeneJET PCR Purification Kit or QIAquick PCR Purification Kit according to manufacturer's protocol. The DNA concentration of the purified PCR product and the pINDUCER vector was measured using the NanoDrop 2000c spectral.

2.2.2.12 Ligation

Materials:

- T4-DNA-Ligase
- 10x T4-DNA-Ligase buffer

Method:

For standardisation, DNA fragments were used in a molar ratio of 1:3-5 (vector to insert). The reaction was incubated for 1 h at room temperature according to the following pipetting scheme:

Ligation
4 ng Insert
100 ng Vector
0.5 µl T4-DNA-Ligase
1 µl 10x T4-DNA-Ligase buffer
Add to 10 µl ddH_2O

2.2.2.13 Transformation

Materials:

- Chemically competent DH5α E.coli bacteria, -80°C
- LB medium, pre-warmed 37°C
- LB agar plates (+ Ampicillin 1:1000)
- Heating block (37°C and 42°C)
- Ice

Method:

50 µl competent DH5α E.coli were thawed on ice, mixed with 5 µl ligation sample solution and left on ice for 10 minutes. DNA uptake was achieved via heating bacteria for 45 seconds at 42 °C in a heating block followed by a cool down on ice. Then, 400 µl pre-warmed LB media was added and the transformation mixture was incubated for 45 minutes at 37 °C in a heat block shaker with moderate agitation. The transformation mixture was centrifuged for 1 minute at maximum. 400 µl supernatant was discarded; bacteria were resuspended in the rest of the media and spread over an ampicillin-containing LB agar plate. Selection plates were incubated at 37 °C overnight and single colonies were picked for plasmid isolation.

2.2.2.14 Sequencing

Materials:

- Sequencing primer (SG 1162)
- QIAquick PCR Purification kit (QIAGEN)

Method:

Purification of the plasmid was achieved using the QIAgen PCR purification kit. For sequencing, the plasmid was sent to LGC genomics. Therefore, DNA was prepared to the company's specifications seen in the following table:

Sequencing
1 µg Plasmid
2 µl Primer SG 1162 (1:10)
Add to 14 µl ddH_2O

The results were analysed with the freeware computer software ApE (A plasmid editor).

2.2.3 Biochemical methods

2.2.3.1 Whole cell lysates

Materials:

- 1x PBS, pH 7.4 at 4°C
- Plastic cell scraper
- 3x ESB protein sample buffer
- TNN lysis buffer. 4°C:
  Add fresh before use
- 1mM DTT (1M): 1:1000
- 10 µg/ml Protease inhibitor cocktail (PIC): 1:1000
- 10 µg/ml PMSF (100 mM): 1:1000

Method:

The cell culture dish was placed on ice, the cell culture medium was removed, washed with an appropriate amount of ice cold PBS, scraped via a plastic cell scraper and transferred into a 15 ml tube. After centrifugation for 5 minutes at 950 g at 4 °C, the PBS was discarded and the cell pellet was resuspended in 1 ml ice cold PBS followed by a transfer to an Eppendorf tube. The tube was centrifuged for 5 minutes at 950 g at 4 °C. Then the supernatant was aspirated and pellet was lysed in adequate volume of TNN lysis buffer containing DTT, PIC and PMSF for 20 minutes on ice. Cell debris was removed by spinning for 10 minutes at 20000 g at 4°C whereas the clear supernatant was transferred into fresh reaction tube. The protein concentration was determined via Bradford assay (see section 2.2.3.2). Lysates were used further or flash frozen and stored at -80 °C until use.

2.2.3.2 Bradford assay

Materials:

- Bradford solution
- BSA (10 mg/ml)
- 0.15 M NaCl
- 3x ESB protein sample buffer
- Half-micro-cuvette

Method:

The protein concentration was determined after the method established by Bradford (Bradford. 1976). Therefore, 100 µl 0.15M NaCl was applied into half-micro-cuvette. Then, 1 µl of the protein lysate or a BSA dilution series was added. Next, 1 ml Bradford solution was added and mixed well for the spectrometric measurement. Finally, the extinction was measured at 595 nm compared to a standard BSA dilution series and used for the calculation of the protein concentration of the whole cell lysates. After calculation of the protein concentration of the whole cell lysates, an appropriate amount of 3x ESB protein sample buffer was added to the protein samples.

2.2.3.3 SDS polyacrylamide gel electrophoresis (SDS-PAGE)

Materials:

- ddH_2O
- 1.5 M Tris. pH 8.8
- 0.5 M Tris. pH 6.8
- Protogel (30% Acrylamide. 0.8% Bisacrylamide)
- 20% SDS
- 10% APS
- Protein marker
- SDS-running buffer

Method:

SDS-PAGE was performed using the discontinuous method described by Laemmli (Laemmli. 1970). A separating gel solution (ranging from 8-14 %) was prepared and applied into the gap of the glass plates. After polymerisation, it was overlaid with a stacking gel (5 %). In the table below, the composition of 1.5 mm gels is summarized:

Separating gel				
Gel percentage:	**8%**	**10%**	**12.5%**	**14%**
ddH_2O	3.54 ml	3.04 ml	2.5 ml	2.2 ml
1.5 M Tris. pH 8.8	1.85 ml	1.85 ml	1.85 ml	1.85 ml
Protogel	2 ml	2.5 ml	3.1 ml	3.5 ml
20% SDS	55 µl	55 µl	55 µl	55 µl
10% APS	50 µl	50 µl	50 µl	50 µl
TEMED	5 µl	5 µl	5 µl	5 µl

Stacking gel	
Gel percentage:	**5% gel**
ddH_2O	990 µl
0.5 M Tris. pH 6.8	1.0 ml
Protogel	0.5 ml
20% SDS	60 µl
10% APS	40 µl
TEMED	4 µl

The electrophoresis was performed in SDS-running buffer with constant amperage of 35 mA/gel for approximately 1.5 hours.

2.2.3.4 Immunoblotting

Materials:

- PVDF membrane
- 4 Whatman filter paper
- 2 blotting pads from Biorad system
- 100% methanol
- Blotting buffer. 4°C
- Ponceau S
- TBS-T (0.05-0.1%)
- Blocking solution (TBS-T 3% milk powder)
- 1 M Tris, pH 8.5
- Enhanced chemiluminescence (ECL) solution

Method:

The PVDF membrane was equilibrated 1 minute in 100 % methanol and the blotting pads and Whatman filter papers were wet in blotting buffer. The blot was assembled in the following order: on the white site of the blotting frame a blotting pad, two Whatman filter papers, PVDF membrane, gel, two Whatman filter papers and a blotting pad is placed and closed. The “sandwich” was transferred into a wet blot Biorad chamber; a cooling unit from -20°C freezer was placed next to the sandwich and the chamber was filled up with ice cold blotting buffer. Depending on the protein size, transfer was conducted for 1-2 h at constant voltage (100 V).

Successful and equal protein transfer was visualized by staining of the membrane in Ponceau S solution.

Membranes were blocked for 30 minutes in 3 % nonfat dry milk powder in TBST to reduce unspecific binding followed by the incubation with primary antibodies overnight at 4 °C. Unbound antibody was removed by three washing steps with TBST for 10 minutes under gentle shaking. Incubation with respective secondary antibodies for 1 hour at RT followed by another three washing steps with TBST for 10 minutes. Next, the ECL components were mixed together in 1 M Tris (pH 8.5). activated by H_2O_2. The PVDF membrane was developed for 1 min in the staining solution. After removing excess liquid, membrane was wrapped in plastic foil and exposed to X-ray films in a dark room.

2.2.3.5 Immunofluorescence

Materials:

- 1x PBS, pH 7.4
- Fixative: PSP (PBS + 3% paraformaldehyde + 2% sucrose)
- 1x PBS, pH 7.4 + 0.2% Triton-X
- PBST: 1x PBS, pH 7.4 + 0.1% Triton-X
- Blocking solution: 3% BSA diluted in 1x PBS
- Antibodies
- Humid chamber
- Hoechst 33258
- Shandon Immu-Mount (Thermo Scientific)
- Colourless nail polish

Method:

For immunostaining, cells were seeded with an appropriate cell number in a 6 well plate on coverslips. Coverslips were washed carefully with 1x PBS, fixed for 10 min with PSP and afterwards rinsed two times then washed once with PBS. Then, the cells were permeabilized with PBS + 0.2% Triton-X for 5 min, rinsed and washed 5 minutes with 1x PBST followed by a blocking step with 3% BSA for 30 minutes. After blocking, the coverslips were transferred to humid chambers and incubated for 1 h with the first antibody on parafilm followed by three washing steps with PBST for 3 minutes. After transfer to humid chambers, coverslips were incubated for 30 min with the secondary antibody in PBS (1:500). After three washing steps with PBST for 3 minutes in 6 well plate, Hoechst 33258 (1:1000) was applied for nuclear

staining. The cells were rinsed and washed 5 minutes with PBS and the coverslips were mounted onto a prepared slide. After drying in the dark, the slides were sealed by colourless nail polish and stored at 4°C in the dark.

2.2.4 Immunohistochemical methods

2.2.4.1 Preparation of paraffin sections

Materials:

- Dissecting set: very small surgical scissors and forceps
- 1 ml Syringe
- 1x PBS. pH 7.4
- Fixative: 4% PFA
- 50%, 70%, 80%, 90%, 95% and 100% Ethanol
- Paraffin

For preparation of lung paraffin sections, the mouse was sacrificed by cervical dislocation. For revealing the lung, laparotomy by a longitudinal incision was performed. Furthermore, separation of the diaphragm from the lung and detachment of the lung from the ribs was achieved by cutting with very small surgical scissors. Next, lungs were perfused with 5 ml 1x PBS to remove the remaining blood. After revealing the trachea, instillation of 4% PFA fixative by a syringe was mediated through a minimal surgical cut in the trachea until lung was inflated. Then the lung was isolated and washed in 1x PBS. Excess tissue was removed and the lung was fixed in 4% PFA overnight at 4°C in a horizontal shaking platform. To document the appearance of the lungs, images providing an overview of the lungs were created on the Keyence microscope. Lungs were washed twice in 1x PBS and once in 0.9 % NaCl for 10 minutes. Next, lungs were treated with 50 % and 70 % ethanol for 1 h each on a rotating wheel at RT. Serial dehydration of the lungs was performed automatically overnight in a TissueSpin Processor:

70 % ethanol 1 h

80 % ethanol 1 h

90 % ethanol 1 h

95 % ethanol 1.5 h

100 % ethanol (2 times) 1 h

Xylene (2 times) 1.5 h

Paraffin (2 times) 2 h

After the last dehydration step, tissue samples were embedded in paraffin using a Microm EC 350 modular tissue embedding center. The blocks were allowed to solidify and stored at 4 °C. Paraffin blocks were sectioned into 5 µm (for immunohistochemical applications) or 10 µm thick slices (for tumor gDNA isolation) with a Hyrax M40 microtome.

2.2.4.2 H&E staining

Materials:

- Haematoxylin solution sour after Mayer
- Eosin-G solution (0.5%) add approximately 100µl/100ml acetic acid
- Xylene
- 50%, 70%, 80%, 90%, 95% and 100% Ethanol
- Roti® Histokitt

Method:

For staining, dry slides were deparaffinized two times in xylene for 10 minutes and rehydrated in a decreasing ethanol dilution series (100 %, 95 %, 80 %, 70 %, 50 %) for 3 minutes each. After rinsing in H_2O for 3 minutes, nuclei were stained in haematoxylin solution for 10 minutes followed by washing with running tap water for 15 minutes to accelerate blueing of sections. Slides were incubated in Eosin-G solution for 5 minutes, then rinsed with water to remove excess stain. Next, slides were dehydrated in increased serial ethanol dilutions (70 %, 95 %, 100 %) for 3 minutes each, two times xylene for 10 minutes. Finally, slides were mounted with Roti® Histokitt and observed under an Upright Microscope DMI6000B. Images of the lungs were taken with Upright Microscope DMI6000B and evaluated to determine their tumor area with ImageJ software and their tumor grade.

2.2.4.3 Antibody staining of tissue sections

Materials:

- 50%, 70%, 80%, 90%, 95% and 100% Ethanol
- Xylene
- 3 % H_2O_2 diluted in 1x PBS

- Blocking solution: 3% BSA diluted in 1x PBS
- Antibodies in 3% BSA
- DAB staining solution: 250µl 1% DAB solution containing 200 µl 10 N HCl + 250 µl 0.3% H_2O_2 + 4.5 ml 1 M Tris, pH7.5
- Marking pencil

Lung sections were deparaffinized in xylene two times for 5 minutes and rehydrated in a decreased ethanol dilution series (100 %. 95 %. 80 %. 70 %. 50 %) for 3 minutes each followed by H_2O treatment for 3 minutes. Endogenous peroxidase activity was blocked by incubating in 3 % H_2O_2. Next, sections were washed 3 times in 1x PBS for 5 minutes each. Lung sections were placed in a coplin jar containing 10 mM sodiumcitrate buffer (pH 6.0) and boiled 8 minutes for an acidic heat induced antigen retrieval. Sections were cooled down to RT and rinsed 3 times with 1x PBS for 5 minutes. Lung tissue on the sections was surrounded with a marking pencil to avoid the merge of different antibodies. Next, 200µl-300µl BSA was applied to these lung tissue to block and minimize unspecific staining. Overnight, lung tissue was incubated with 200-300 µl primary antibody at 4 °C in a humidified chamber. Next morning, sections were washed with 1x PBS three times for 2 minutes to remove excess antibody. Then, secondary antibody was applied for 1 h at RT in a humidified chamber followed by three washing steps with 1x PBS for 2 minutes to remove excess antibody. Visualization of binding reaction was shown via 3.3'-Diaminobenzidine (DAB) staining. Therefore, 200-300 µl DAB staining solution was applied on lung tissue for 10 minutes yielding a brown precipitate. Next, sections were washed three times in H_2O for 2 minutes and stained with haematoxylin for 3 minutes followed by washing with running tap water for 15 minutes. Finally, sections were dehydrated in serial ethanol dilutions (70 %, 95 %, 100 %) for 3 minutes each. two times in xylene for 10 minutes and mounted with Roti® Histokitt. Images were taken ant an Upright Microscope DMI6000B and evaluated.

2.2.5. Mouse husbandry

All animal experiments were conducted according to regulatory guidelines and protocols that were approved by an institutional committee (Tierschutzkommission der Regierung von Unterfranken).

2.2.5.1 Mouse facility

An open cage system using type II polycarbonate cages were utilized to keep mice and to ensure species-appropriate husbandry. Furthermore, standard rodent diet and water were provided every day. Moreover, cages were cleaned regularly and health monitoring of sentinel mice was performed every 3-6 months. Preservation of strains was assured by continuous breeding of respective pairs in a ratio of 1:2 (male to female). After three weeks, pups were weaned, genotyped and separated from their parents before achieving maturity. All mice were registered with identity number (ear clip), gender, genotype, date of birth and parental breeding pair name. Mice were sacrificed with CO_2 or cervical dislocation (virus-infected mice).

2.2.5.2 Anaesthesia of mice

Materials:

- Xylazine
- Ketamine
- 0.9% NaCl
- 25 gauge needle
- 1 ml Syringe
- Weighing scale

Method:

Injection anaesthesia was performed using a combination of Ketamine and Xylazine. To determine the correct dose for anaesthesia, mice were weighed four hours before infection. Prior to infection, 150 µl Xylazine and 450 µl Ketamine were mixed with 1800 µl 0.9 % NaCl. Then, 175 µl suspension per 25 g body weight were administered with a 25 gauge needle intraperitoneally to the mice. To ensure that the mice are fully anesthetized, it was controlled if they lack the toe reflex.

2.2.5.3 Infection of mice with Lenti-Cre

Materials:

- Intubation platform
- Fiber-Lite Illuminator

- Exel Safelet IV catheter
- Flat forceps
- 1 ml Syringe
- 100 µl pipette with pipette tips
- Paper
- Lenti-Cre virus placed in ice box

Method:

Under a biosafety level 2 environment, infection of mice was performed with high precaution. Delivery of Lenti-Cre was carried out using the intratracheal infection method. Therefore. 6-8 weeks old mice were anesthetized and intratracheal intubation was performed according to DuPage et al. (DuPage et al., 2009). For infection, the mice were placed on a platform hanging from its top front teeth on the bar and adjusted to the right position for inserting the catheter. A Fiber-Lite Illuminator was used to shine on the mouse's chest to control breathing and later inhalation of the virus. Then, the catheter was prepared, the mouth was opened and the tongue was gently pulled out with flat forceps. The catheter was slid into the trachea until the top of the catheter reaches the mouse's front teeth and the needle was immediately removed from the mouth to ensure that the mice can breathe through the catheter. Then, the platform containing mouse and catheter was moved into the biosafety hood. $1x10^6$ Lenti-Cre virus particles diluted in 50 µl medium was pipetted directly into the opening of the catheter and the mice started inhaling the virus immediately. The catheter was removed from the trachea when the virus was no longer visible in the opening of the catheter and the entire volume was travelled down the catheter. The mice were then placed on paper, breathing was controlled and loss of liquid was noticed and documented. Finally, the mice were wrapped round with paper to ensure that the mice become not hypothermic and the head of the mice were propped up in the cage. Mice were regularly monitored until their recovery from anaesthesia.

2.2.6 Statistical analysis

Statistical significance was determined using Student's t-test or Chi Square test with post-hoc Fisher's Exact test and defined as significant according to following P values: *: $p<0.05$; **: $p<0.01$; ***: $p<0.001$. ****: $p<0.0001$. All statistical analyses were performed with GraphPad Prism 6 (GraphPad Software. Inc. La Jolla. CA. USA).

3. Results

3.1 Role of MMB in lung tumorigenesis *in vivo*

The MMB complex serves as a transcriptional activator, which is essential for the expression of key mitotic genes. It has been shown, that B-MYB, FOXM1 and target genes of the MMB are a part the CIN signature and play a crucial role in many cancer types. Still there is not much known about the role of the MMB in (lung) tumorigenesis *in vivo*. Therefore, the aim of this part was to clarify if the MMB is required for lung tumorigenesis. For the investigation, I used a well characterised *in vivo* non-small cell lung cancer (NSCLC) mouse model driven by oncogenic *K-Ras* and loss of *p53,* which are the most altered pathways in NSCLC. This model is based on a Cre-LoxP system harbouring a mutant *K-Ras* allele (*K-Ras*$^{LSL\text{-}G12D/+}$) and conditional loss-of- function *p53 alleles* (*p53*$^{fl/fl}$).

3.1.1 NSCLC mouse model with conditional alleles of *B-Myb*

Our group has shown, that p53 is able to inhibit the function of B-MYB. In return, B-MYB is highly upregulated in p53 -/- cells, which is linked to its ability to promote checkpoint recovery in these cells leading to enhanced expression of mitotic genes (Mannefeld et al., 2009). Therefore, we predicted that B-MYB and MMB contribute to (lung) tumorigenesis by mediating overactivity of mitotic genes after loss of p53. Accordingly, I tested if depletion of B-MYB influences lung tumor formation. Double-mutant *K-Ras*$^{LSL\text{-}G12D/+}$*p53*$^{fl/fl}$ mice were crossed with mice with conditional loss of function alleles of *B-Myb* (Fig. 3a). In *B-Myb*$^{fl/fl}$ mice, exon 2-5 of *B-Myb* are flanked by LoxP sites. When Cre-mediated recombination takes place, the part between the LoxP sites is excised and a truncated non-functional protein is expressed resulting in a frameshift (Fig. 3c). To determine the genotype of mice, PCR was used (Fig. 3b). A first question, which was addressed, was if lung tumor formation is induced in the aforementioned mouse model. Therefore 6-8 weeks old *K-Ras*$^{LSL/G12D/+}$*p53*$^{fl/fl}$*B-Myb*$^{+/+ \text{ and } fl/+ \text{ and } fl/fl}$ mice were infected with a Cre-lentivirus. Cre was delivered by a recombinant lentivirus and used with a titer of $1x10^6$ virus particles per mouse. The virus was applied by an intratracheal infection technique described in 2.2.5.3. 13 weeks after infection, known as optimal timepoint to generate a modest number of lesions in the lung in *K-Ras*$^{LSL\text{-}G12D/+}$*p53*$^{fl/fl}$ mice, *K-Ras*$^{LSL/G12D/+}$ *p53*$^{fl/fl}$ *B-Myb*$^{+/+ \text{ and } fl/+ \text{ and } fl/fl}$ mice were sacrificed, dissected and their lungs were removed. Lungs were embedded in paraffin and sectioned (Fig. 3d). As expected a spectrum of tumors arose, which differ in size and cell appearance. This result showed that the mouse model, the lentivirus concentration and time point fits.

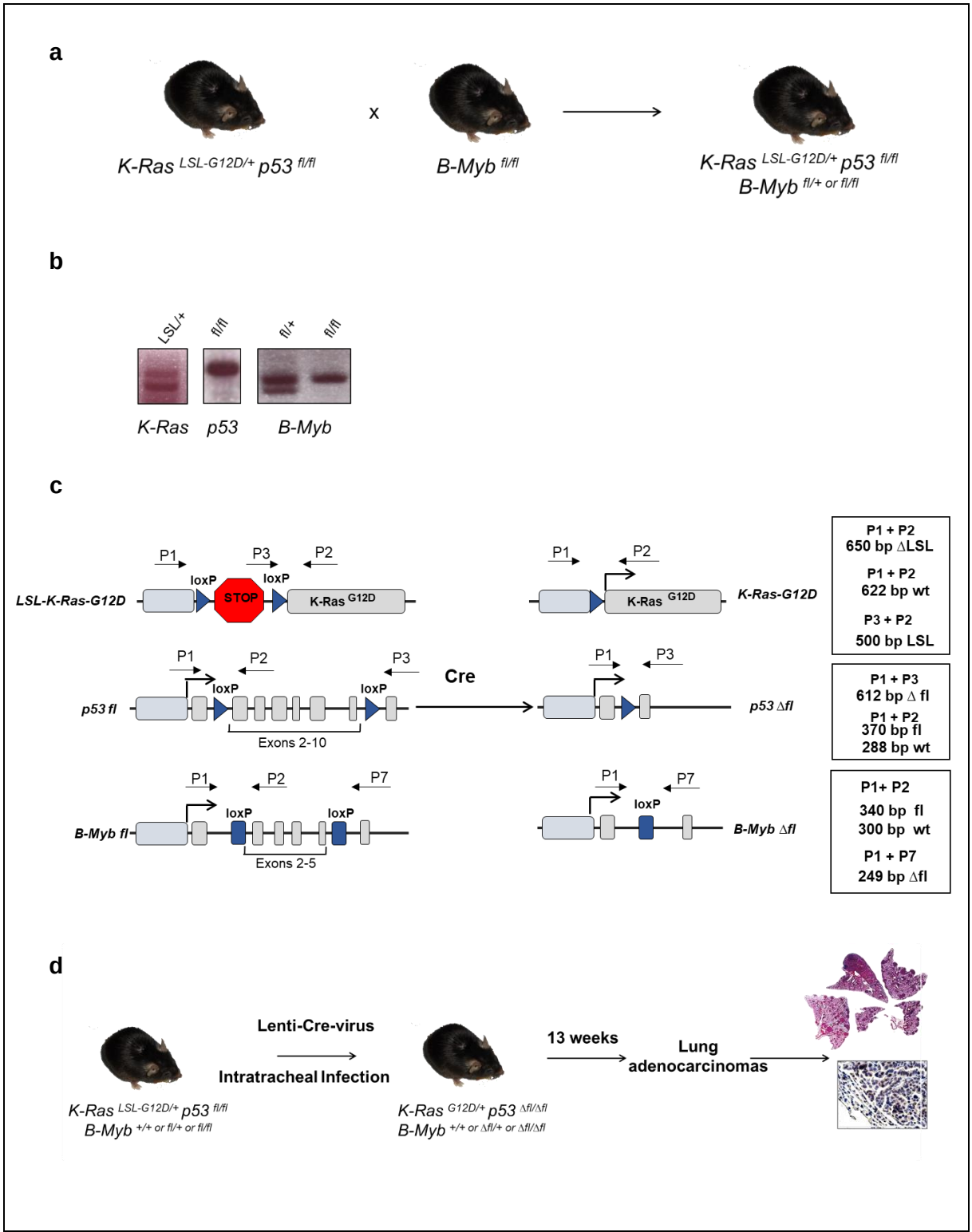

Figure 3: NSCLC mouse model to determine the requirement of B-MYB to lung tumorigenesis
(a) Double-mutant *K-RasLSL$^{G12D/+}$; p53$^{fl/fl}$* mice were crossed with conditional *B-Myb$^{fl/fl}$* mice to receive *K-Ras$^{LSL-G12D/+}$ p53$^{fl/fl}$ B-Myb$^{fl/+ or fl/fl}$* mice.
(b) For Genotyping primers for the LoxP-STOP-LoxP cassette (LSL) on K-Ras allele or LoxP sites on alleles of p53 and B-Myb were used.
(c) NSCLC mouse model is based on a Cre-LoxP system. Addition of Cre-lentivirus leads to an activation of oncogenic *K-Ras^{G12D}*, loss of *p53 (p53 Δ/Δ)* and depletion of *B-Myb (B-MybΔΔ).*
(d) 13 weeks post infection was chosen as optimal timepoint for developing lung adenocarcinomas.
C57Bl/6 mouse copyright: Wualex

3.1.2 Tumor burden is reduced when B-Myb is depleted

Next, I asked whether B-Myb deletion has an impact on the tumor burden. As reported in part 3.1.1 *K-Ras*$^{LSL\text{-}G12D/+}$*p53*$^{fl/fl}$*B-Myb*$^{+/+ \text{ and } fl/+ \text{ and } fl/fl}$ mice were infected with Cre-lentivirus. 13 weeks post infection, mice were sacrificed and the surface of the lungs was inspected and showed a lower number of tumors (white bulky spots on lung surface) in *K-Ras*$^{LSL\text{-}G12D/+}$*p53*$^{fl/fl}$*B-Myb*$^{fl/fl}$ mice than in control mice (*K-Ras*$^{LSL\text{-}G12D/+}$*p53*$^{fl/fl}$*B-Myb*$^{+/+ \text{ or } fl/+}$) (Fig. 4a). Histological lung sections were stained with H&E and examined under the microscope (Fig. 4b and S1). Determination of the tumor area revealed that *K-Ras*$^{LSL\text{-}G12D/+}$*p53*$^{fl/fl}$*B-Myb*$^{fl/fl}$ mice had a significantly lower tumor area in comparison to the control (Fig. 4c). According to the inspection of the lung surface, the reduction of the tumor area was dependent on the B-Myb status. In addition, the tumor grade was classified by a four-stage grading system (described in DuPage et al., 2009; Nikitin et al., 2004; Jackson et al., 2001) (Fig. 4e). Grade I lesions are atypical adenomatous hyperplasia short AAH. These are lesions, which have uniform nuclei, show no nuclear atypia. The lung architecture is largely preserved. Adenomas are classified as grade II tumors. They contain cells with uniform but slightly enlarged nuclei. In comparison to grade I tumors they are more solid somehow more compressed. Compared with adenomas adenocarcinomas, grade III tumors, show enlarged, pleomorphic nuclei and increased frequency of mitosis. Invasive adenocarcinomas (grade IV) harbour all the characteristic of grade III tumors but in addition they show invasive stroma. Tumors in *K-Ras*$^{LSL\text{-}G12D/+}$*p53*$^{fl/fl}$*B-Myb*$^{fl/fl}$ mice were more represented in grade 1 and 2 tumors than in grade 3 and 4 meaning they showed a shift to a lower, less aggressive tumor grade in comparison to *K-Ras*$^{LSL\text{-}G12D/+}$*p53*$^{fl/fl}$*B-Myb*$^{+/+}$ mice (Fig. 4d). Together these observations illustrate that depletion of B-Myb results in a lower tumor area and in a shift to lower, less aggressive tumor grade, which indicate a lower tumor burden. In conclusion, depletion of B-Myb significantly impairs the development of lung tumors and tumors, which arose are in most cases less aggressive. This data demonstrates, that B-Myb is required for tumorigenesis in NSCLC *in vivo*.

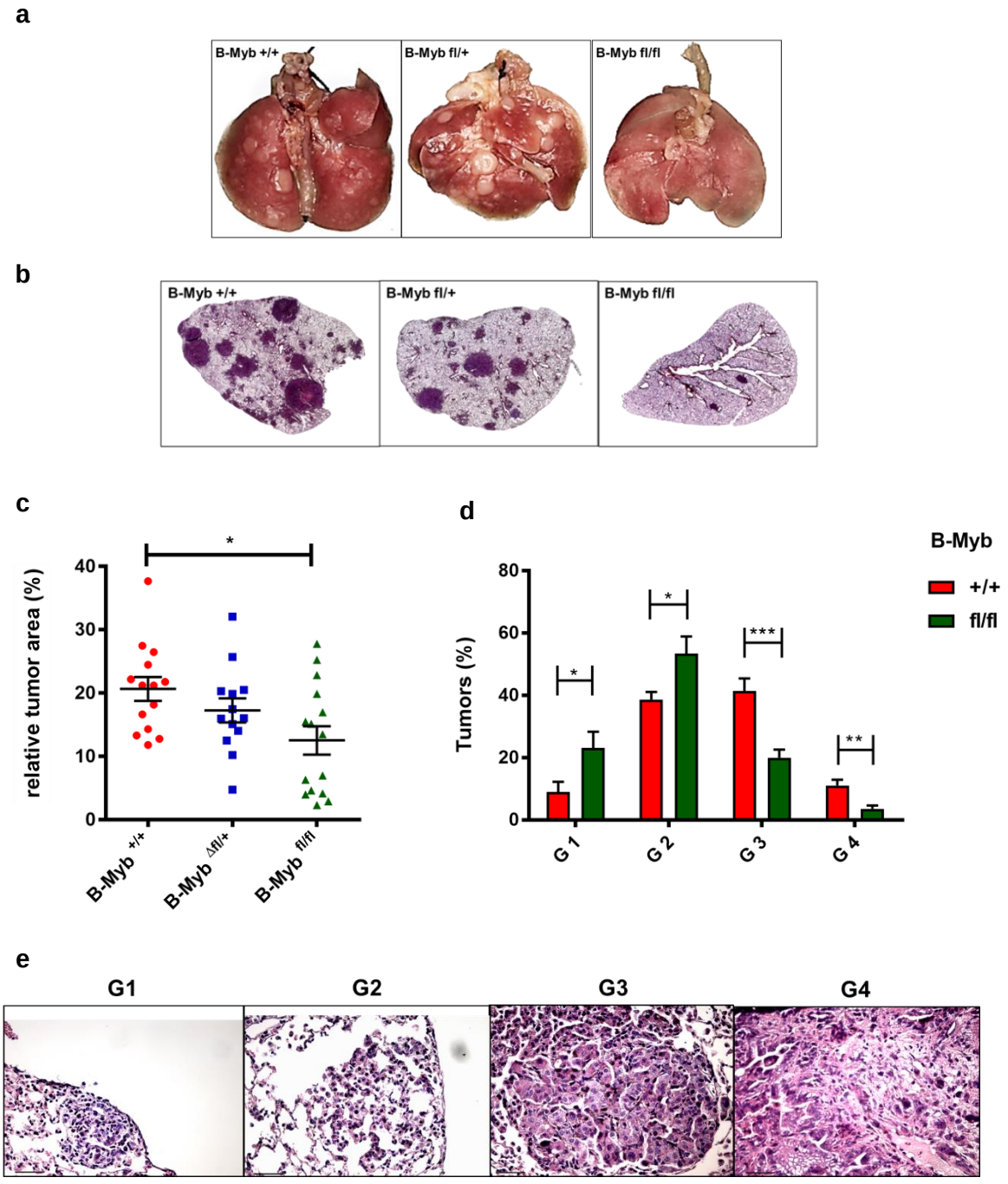

Figure 4: Requirement of B-MYB for tumorigenesis in an *in vivo* NSCLC mouse model
(a) Representative images of lungs. After 13 weeks post infection mice were sacrificed, lungs were isolated and the surface inspected.
(b) Representative H&E sections of lungs from *K-Ras*$^{LSL\text{-}G12D/+}$ *p53*$^{fl/fl}$ *B-Myb*$^{+/+ \text{ and } fl/+ \text{ and } fl/fl}$ mice.
(c) Quantification of tumor area to total area of the lung. Symbols represent individual analysis of tumor area in each mouse. Mean ± S.E.M. is given.
(d) Quantification of tumor grades (n=766 tumors *K-Ras*$^{LSL\text{-}G12D/+}$ *p53*$^{fl/fl}$ *B-Myb*$^{+/+}$ and n=652 tumors *K-Ras*$^{LSL\text{-}G12D/+}$*p53*$^{fl/fl}$ *B-Myb*$^{fl/fl}$). Error bars represent S.E.M. Statistical significance for all panels was determined as *: P < 0.05, ***: P < 0.001 (e) Representative tumor grade images of histological sections *from K-Ras*$^{LSLG12D/+}$ *p53*$^{fl/fl}$ *B-Myb*$^{+/+ \text{ or } fl/+ \text{ or } fl/fl}$ tumors. Scale bar 50µm.

3.1.3. Mitotic genes are targets of MMB in lung cancer *in vivo*

Previous microarray data have shown that genes such as Nusap1 or mitotic kinesins are direct transcriptional targets of the MMB (Esterlecher et al., 2013; Reichert et al., 2010). To analyse the regulation of MMB targets genes in lung cancer *in vivo*, immunohistochemistry staining was performed. Lung sections were rehydrated followed by an acidic heat induced antigen retrieval. After incubation with antibodies against phosphorylated B-MYB (p-B-MYB) or mitotic MMB-target genes (NUSAP1, CENPF), visualization of binding reaction was shown via DAB staining, which produces a dark brown reaction product. Afterwards, the staining was analysed. Elevated levels of active B-MYB expression was observed in high grade tumors demonstrated by staining with an antibody that detects B-MYB phosphorylated on threonine 487 by cyclin A/CDK2 during S phase (Fig. 5a). Reduced B-MYB expression was observed in majority of tumors from *K-Ras*$^{LSL\text{-}G12D/+}$ *p53*$^{fl/fl}$*B-Myb*$^{fl/fl}$ mice compared to the control (Fig. 5b). In addition, a correlation between B-MYB expression and tumor grade was found: High B-Myb expression was associated with high grade, low expression of B-MYB with low grading (Fig 5c). Related to the correlation between B-MYB expression and tumor grade, I studied if there is a correlation between the MMB target NUSAP1 and tumor grade. NUSAP1 is a MMB target gene, required for spindle microtubule organization during mitosis. Indeed, NUSAP1 was expressed in murine adenocarcinoma and its expression correlates with the tumor grade with high NUSAP1 expression in high grade tumors and low expression in low grade tumors (Fig. 6a, b). Another MMB target gene is CENPF, which is associated with the kinetochore and maintains this association through early anaphase. CENPF expression also correlates with tumor grade (Fig. 6c, d). We next wanted to know, if we can show the direct connection between B-Myb and Nusap1 in our lung cancer mouse model. Indeed, B-MYB and NUSAP1 were highly co-expressed in murine lung adenocarcinoma (Fig. 7). Together these data support the notation, that mitotic genes are targets of MMB in lung cancer *in vivo.*

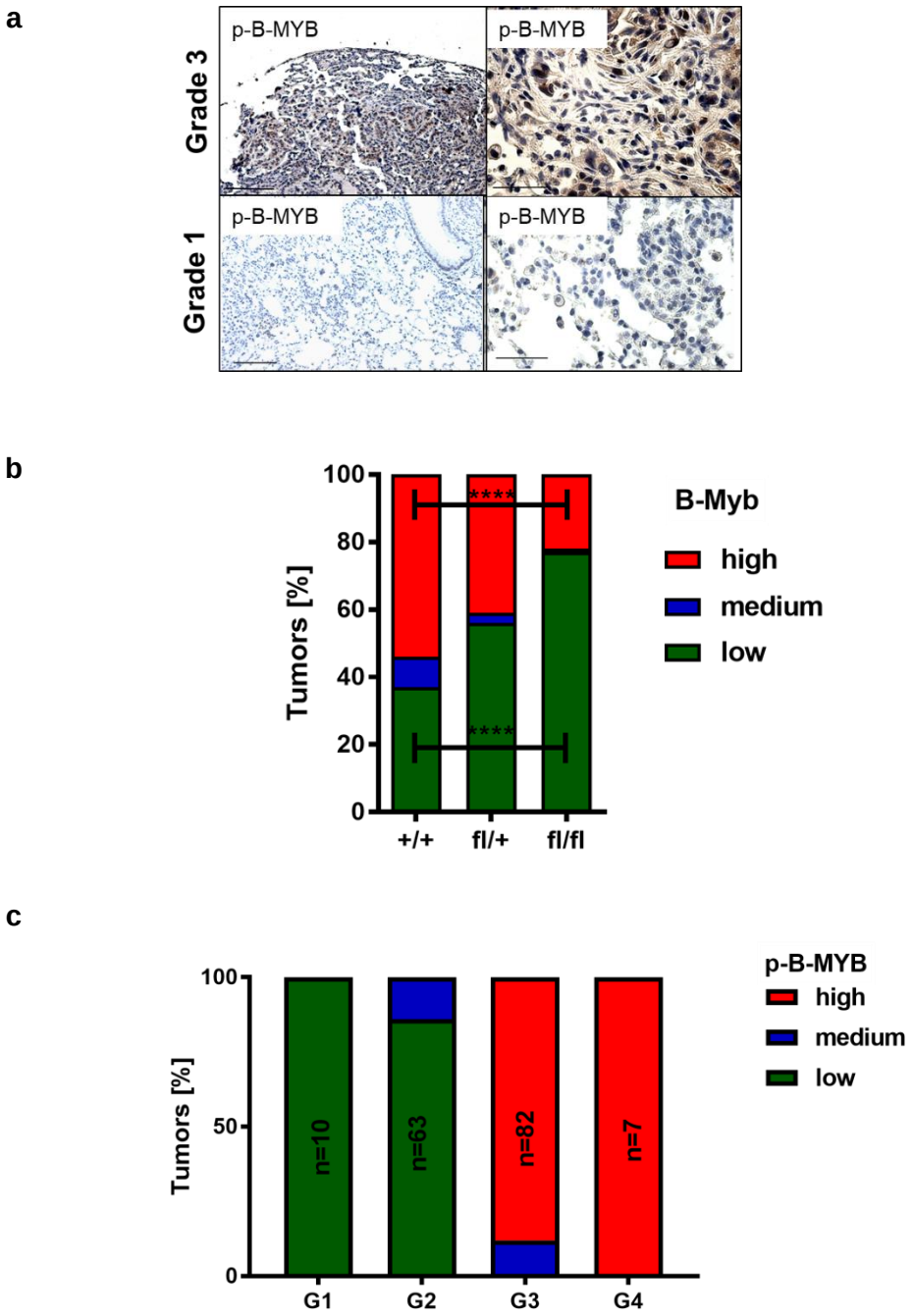

Figure 5: Expression of B-MYB in lung adenocarcinoma
(a) Immunohistochemistry staining of histological sections from *K-Ras*$^{LSL-G12D/+}$ *p53*$^{fl/fl}$ *B-Myb*$^{+/+ \text{ and } fl/+ \text{ and } fl/fl}$ mice with an antibody against p-B-MYB (phospho T487). Expression of p-B-MYB in grade 1 and 3 tumors. Left: original magnification 5x, scale bar: 150 µm; right: original magnification 20x; scale bar: 50 µm.
(b) Percentage of lung tumors expressing p-B-MYB at low (<10% of p-B-MYB positive cells), medium (10-30% of p-B-MYB positive cells) or high (>30% of p-B-MYB positive cells) levels of indicated genotypes. For each genotype, a high number of tumors (*B-Myb*$^{+/+}$=233; *B-Myb*$^{fl/+}$=284; *B-Myb*$^{fl/fl}$=108) from four different mice were analysed. Statistical significance was determined (Chi Square test) as ****P < 0.0001.
(c) P-B-MYB expression in murine lung tumors from grade 1 to grade 4 is quantified in *K-Ras*$^{LSL-G12D/+}$ *p53*$^{fl/fl}$ *B-Myb*$^{+/+}$. Correlation between p-B-Myb expression and tumor grade.

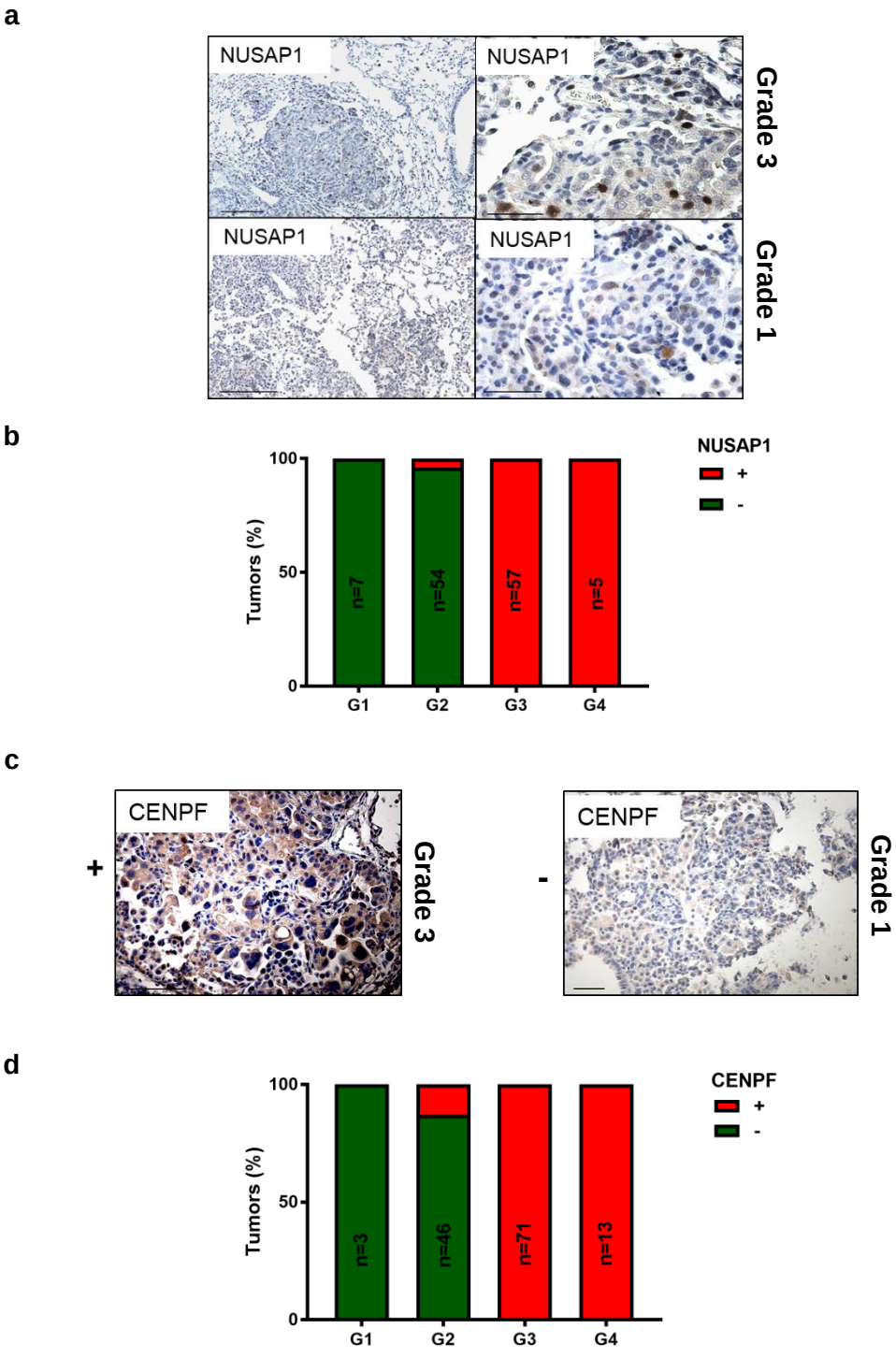

Figure 6: Expression of MMB target genes NUSAP1 and CENPF in lung tumors
(a) NUSAP1 expression in lung adenocarcinomas. Expression of NUSAP1 in grade 1 and grade 3 tumors was determined by immunohistochemistry in *K-Ras*$^{LSL-G12D/+}$ *p53*$^{fl/fl}$ *B-Myb*$^{+/+}$ mice.
Left: Magnification 5x. Scale bar:150 µm; right: magnification 20x. Scale bar: 50 µm.
(b) Quantification of NUSAP1 expression related to tumor grade.
(c) CENPF expression in lung adenocarcinomas. Expression of CENPF in grade 1 and grade 3 tumors was determined by immunohistochemistry in *K-Ras*$^{LSL-G12D/+}$ *p53*$^{fl/fl}$ *B-Myb*$^{+/+}$ mice.
Left: Magnification 20x. Scale bar: 150 µm; right: magnification 5x. Scale bar: 50 µm.
(d) Quantification of CENPF expression related to tumor grade.

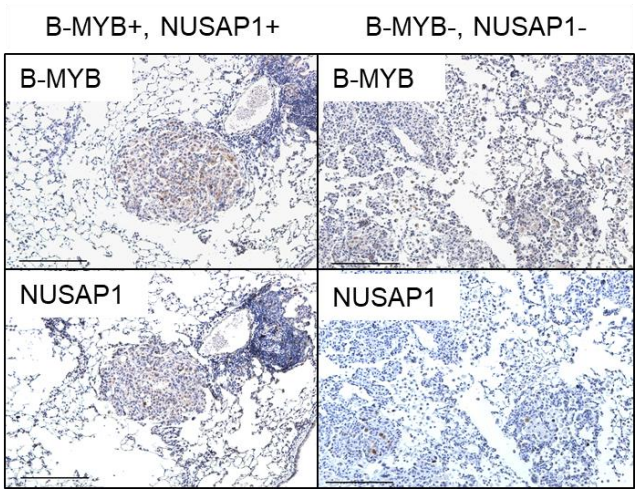

NUSAP1 \ B-MYB	-	+
-	14	0
+	3	18

Figure 7: Correlation between expression of B-MYB and its target gene NUSAP1
Coexpression of B-MYB and NUSAP1 in murine lung adenocarcinoma. The table on the right shows the number of tumors with and without B-MYB and NUSAP1 expression. Scale bar: 200 µm. Statistical significance was determined (Student's t- test, two-sided) as ****P < 0.0001.

3.1.4. Reduced expression of p-ERK and KI-67 in tumors after loss of B-Myb

Finally, the effect of B-Myb deletion on the expression of p-ERK and KI-67 was addressed. P-ERK is a kinase of the MAPK signalling pathway and serves as a marker for activated Ras signalling. Upregulation of MAPK pathway has been reported to be a characteristic feature of advanced lung tumors (Juntilla et al., 2015). Therefore, lung sections of *K-Ras*$^{LSL\text{-}G12D/+}$*p53*$^{fl/fl}$*B-Myb*$^{fl/fl}$ mice and respective controls were stained with an antibody against p-ERK and KI-67 (Fig. 8a, 9a). Expression levels were divided into low, medium and high staining. Indeed, I could demonstrate, that p-ERK expression correlates with tumorgrade (Fig. 8c) and with a high significance with genotype (Fig. 8b). The same is true for KI-67, a proliferation marker, which has been shown to be upregulated in high grade tumors (Fig 9b, c). The fraction of KI-67-positive tumor cells is often associated with the clinical course of the disease (Scholzen and Gerdes, 2000). In conclusion, these data demonstrate, that RAS signalling pathway is upregulated in advanced tumors and that loss of B-MYB impairs proliferation of lung tumors *in vivo.*

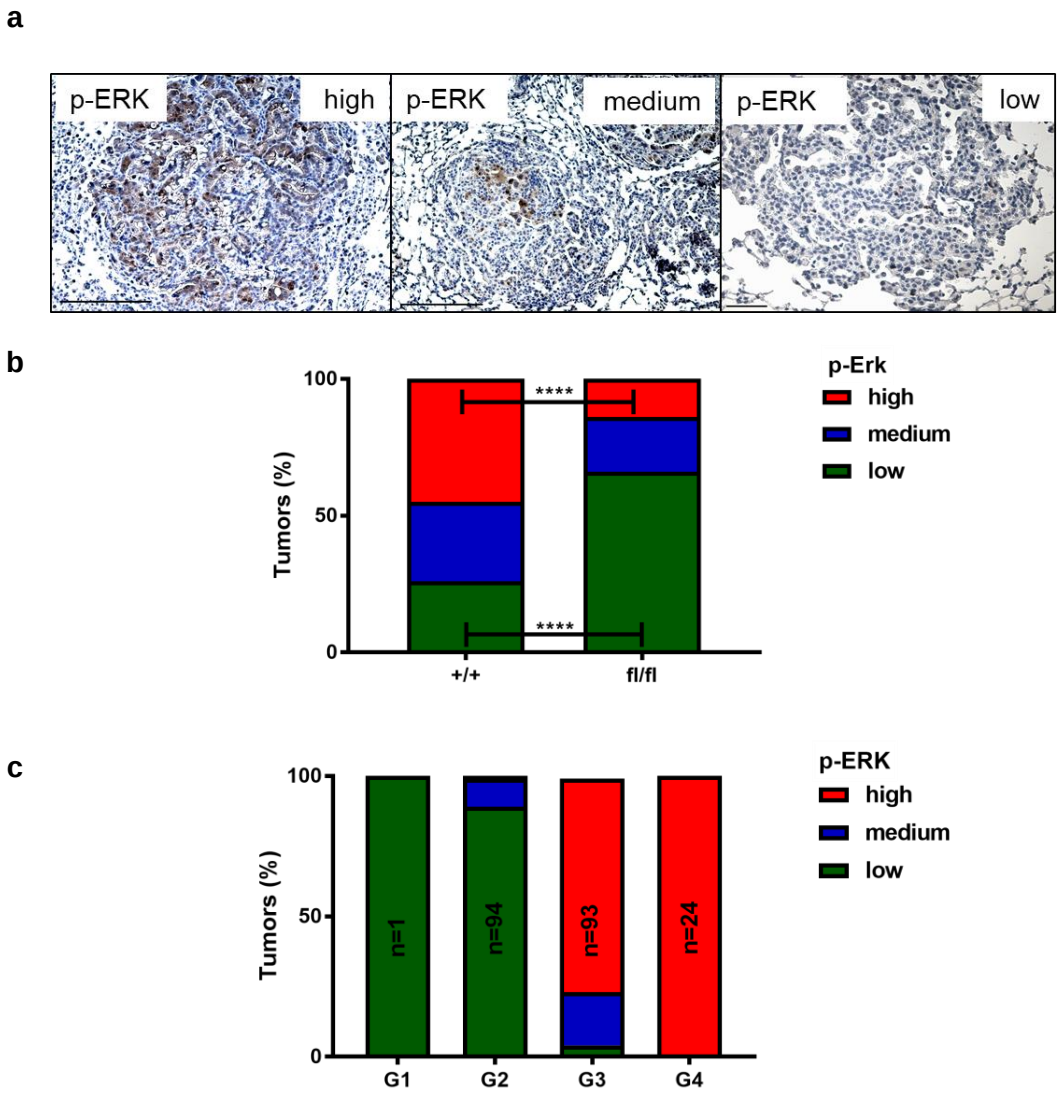

Figure 8: p-ERK expression in murine lung adenocarcinomas
(a) Immunohistochemistry staining of histological sections from *K-Ras*$^{LSL-G12D/+}$ *p53*$^{fl/fl}$ *B-Myb*$^{+/+ \text{ and } fl/+ \text{ and } fl/fl}$ mice with an antibody against p-ERK. Scale bar: 200 µm; right: 50 µm.
(b) Percentage of lung tumors expressing p-ERK on low (<10% of p-ERK positive cells), medium (10-30% of p-ERK positive cells) and high (>30% of p-ERK positive cells) levels of shown genotypes. For each genotype, a high number of tumors (*B-Myb*$^{+/+}$=221; *B-Myb*$^{fl/fl}$=95) from three different mice were analysed. Statistical significance was determined (Chi Square test) as ****P < 0.0001.
(c) P-ERK expression in murine lung tumors from grade 1 to grade 4 was quantified in *K-Ras*$^{LSL-G12D/+}$ *p53*$^{fl/fl}$ *B-Myb*$^{+/+}$ mice. Correlation between p-Erk expression and tumor grade.

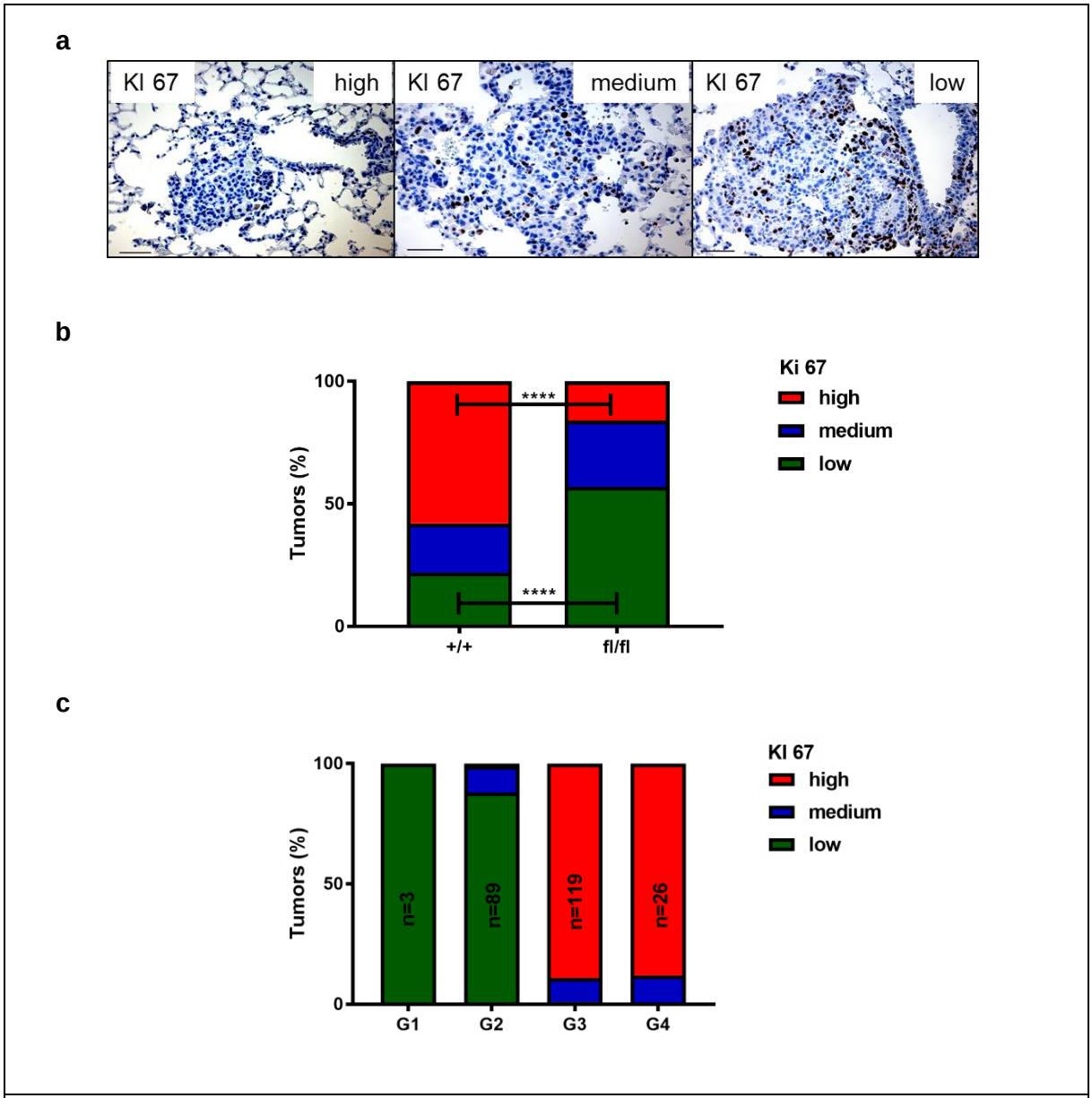

Figure 9: KI-67 expression in murine lung adenocarcinomas
(a) Immunohistochemistry staining of histological sections from *K-Ras*$^{LSL-G12D/+}$ *p53*$^{fl/fl}$ *B-Myb*$^{+/+ \text{ and } fl/+ \text{ and } fl/fl}$ mice with an antibody against KI-67. Scale bar: 50 µm.
(b) Percentage of lung tumors expressing KI-67 on low (<5% of KI-67 positive cells), medium (5-15% of KI-67 positive cells) and high (>15% of KI-67 positive cells) levels of shown genotypes. For each genotype, a high number of tumors (*B-Myb*$^{+/+}$=221; *B-Myb*$^{fl/fl}$=95) from three different mice were analysed. Statistical significance was determined (Chi Square test) as ****P < 0.0001.
(c) KI-67 expression in murine lung tumors from grade 1 to grade 4 was quantified in *K-Ras*$^{LSL-G12D/+}$ *p53*$^{fl/fl}$ *B-Myb*$^{+/+}$ mice. Correlation between KI-67 expression and tumor grade.

3.1.5 Incomplete recombination of B-Myb after lentiviral Cre-infection *in vivo*

Next, I wanted to address whether Cre-mediated recombination was efficient. In part 3.1.3 it was mentioned, that B-Myb protein expression is reduced in *K-Ras*$^{LSL-G12D/+}$*p53*$^{fl/fl}$*B-Myb*$^{fl/fl}$ mice but that it is still detectable. This could indicate, that Cre-mediated recombination was not completely efficient. To answer that question, the status of conditional alleles was determined.

Therefore, tumor material from embedded lung sections were scraped via forceps, deparaffinized, purified and analysed by genomic PCR. In all tumor samples from *K-Ras*$^{LSL\text{-}G12D/+}$ *p53*$^{fl/fl}$*B-Myb*$^{fl/fl}$ mice, a band corresponding to the unrecombined floxed *B-Myb* allele was still present indicating that the recombination was incomplete. In addition, the efficient recombination of "STOP cassette" (ΔLSL) of the *K-Ras* allele was checked and verified. A weak band, of unrecombined, floxed *K-Ras* (LSL) was detected in some tumors, which is likely a contamination from surrounding normal lung material (Fig. 10). In conclusion, these data suggest that there is a selective pressure against the complete loss of B-Myb during lung tumor formation.

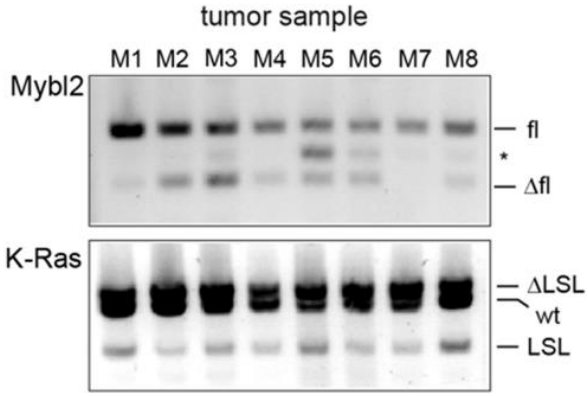

Figure 10: Incomplete recombination of *B-Myb* in primary lung tumors
Genomic PCR of *B-Myb* and *K-Ras* alleles in tumors dissected from *K-Ras*$^{LSL\text{-}G12D/+}$ *p53*$^{fl/fl}$ *B-Myb* $^{fl/fl}$ mice showing incomplete recombination (floxed allele is still present). Fl, unrecombined *B-Myb* allele; Δfl, recombined *B-Myb* allele; LSL, non-recombined *K-Ras*$^{G12D/+}$ allele; ΔLSL recombined *K-Ras*$^{G12D/+}$. *A background band.

3.1.6 Incomplete recombination of B-Myb alleles in tumor cell lines

To be able to study further B-MYB dependent proliferation *in vitro*, primary cell lines from lung tumors of *K-Ras*$^{LSL\text{-}G12D/+}$*p53*$^{fl/fl}$*B-Myb*$^{fl/fl}$ mice (BC1 and BC2) were established. Primary cell lines from *K-Ras*$^{LSL\text{-}G12D/+}$*p53*$^{fl/fl}$*B-Myb*$^{+/+}$ mice (KR1 and KR2) served as respective controls. As expected, *B-Myb* was incompletely recombined in *K-Ras*$^{LSL\text{-}G12D/+}$*p53*$^{fl/fl}$*B-Myb*$^{fl/fl}$ cell lines, seen by the presence of the floxed, unrecombined allele (fl) in genomic PCR (Fig. 11a). In contrast to BC1, in BC2 no recombination has taken part seen by the missing delta floxed allele (Δfl). To achieve full recombination, the cell lines were infected with a retroviral vector expressing a hormone-inducible Cre^{ERT2} recombinase. Unexpectedly the administration of 4-hydroxytamoxifen (4-OHT) to BC1 and BC2 cells resulted not in the complete deletion of remaining floxed *B-Myb* allele. After a second infection with retroviral Cre^{ERT2} and after administration of 4-OHT, the remaining allele was still present in BC1 cells. In contrast, the recombination pattern changed from fl/fl to Δfl/fl in BC2 cells (Fig. 11b, c). The effect on the relative mRNA expression of B-Myb for BC1 and BC2 was analysed by RT-qPCR. In BC1 there

was no effect on B-Myb mRNA expression. In contrast, 4-OHT had an effect on B-Myb in BC2 cells (Fig. 11d). The BC2 cell line was therefore used for further experiments, whereas BC1 was not further considered because of the marginal effects of 4-OHT treatment on B-Myb expression. As respective control, the KR1 cell line was utilized. Western blot analysis revealed that protein expression of B-MYB was eliminated in BC2 cells after 4-OHT treatment (Fig. 11e). Due to technical problems, the BETA ACTIN bands of BC2 cells for – and + 4-OHT differ (Fig. 11e).

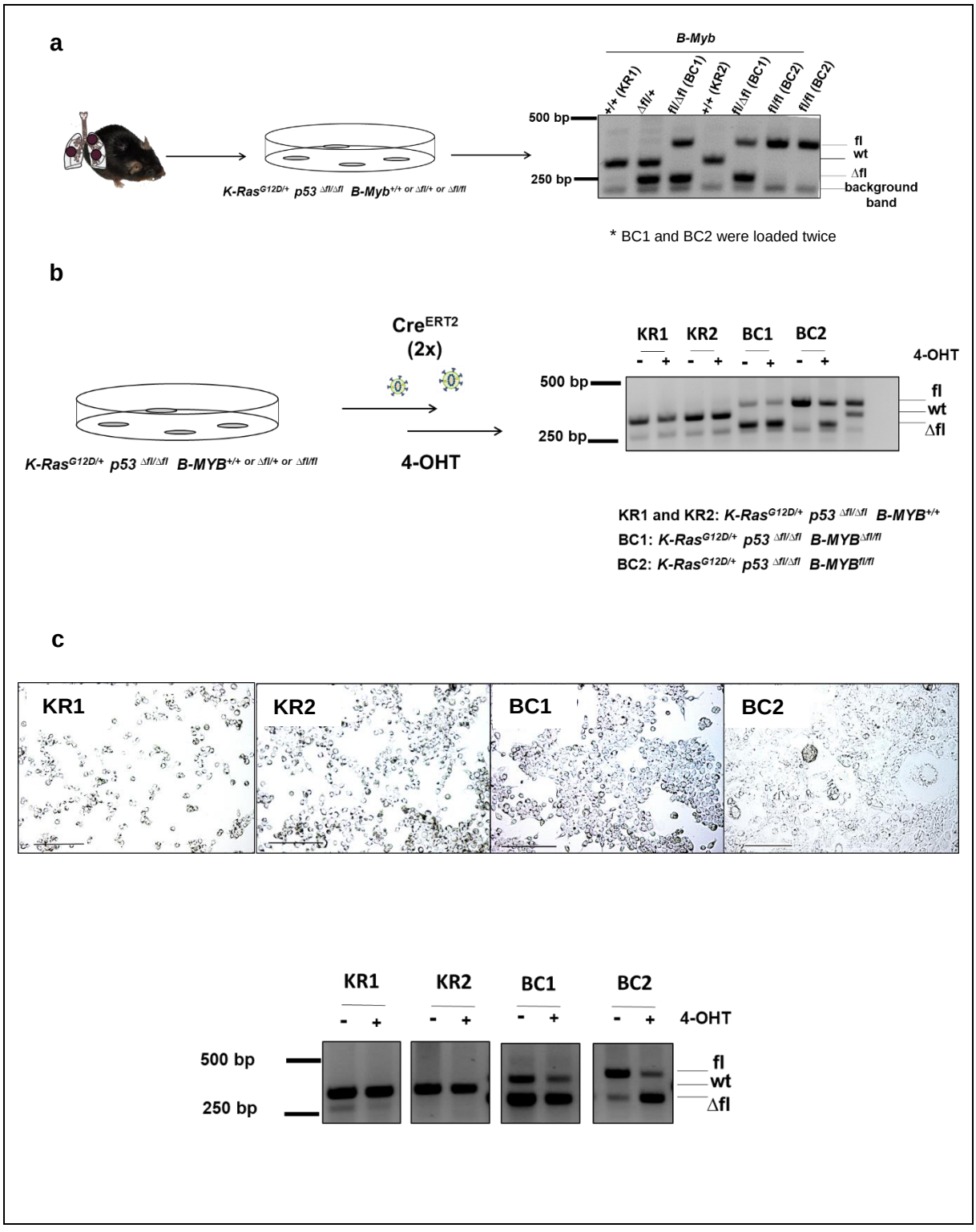

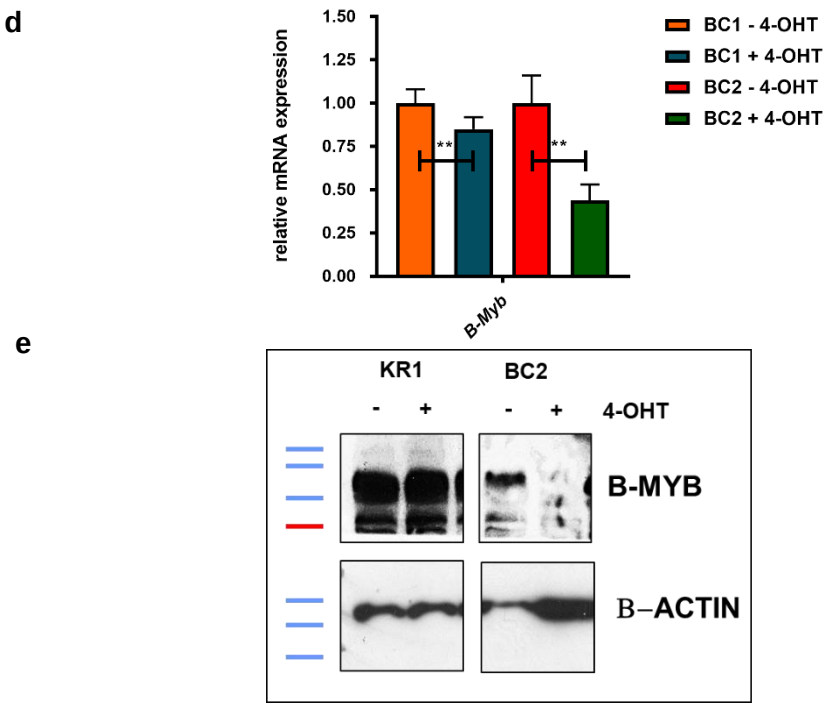

Figure 11: Incomplete recombination of *B-Myb* in lung cancer cell lines before and after multiple infection with a retrovirus encoding for Cre^{ERT2}
(a) *B-Myb* is incompletely recombined in *K-Ras*$^{LSL\text{-}G12D/+}$ *p53*$^{fl/fl}$ *B-Myb*$^{fl/fl}$ cell lines. Wt, wildtype *B-Myb* allele; fl, unrecombined *B-Myb* allele; ∆fl, recombined *B-Myb* allele.
(b) *B-Myb* lung cancer cell lines (KR1 and KR2 derived from *K-Ras*$^{LSL\text{-}G12D/+}$ *p53*$^{fl/fl}$ *B-Myb*$^{+/+}$ and BC1 and BC2 derived from *K-Ras*$^{LSL\text{-}G12D/+}$ *p53*$^{fl/fl}$ *B-Myb*$^{fl/fl}$) were stably infected twice with hormone a retrovirus encoding for inducible Cre^{ERT2} recombinase. BC1 and BC2 showed incomplete recombination after treatment with 4-OHT (2.5 nM; 5 µg/ml puromycin) for 10 days, floxed *B-Myb* allele is still present.
(c) Representative images and PCR *of K-Ras*$^{LSL\text{-}G12D/+}$ *p53*$^{fl/fl}$ *B-Myb*$^{+/+ \text{ or } fl/fl}$. Scale bar: 200 µm
(d) Expression of *B-Myb* and MMB target genes were reduced after treatment with 4-OHT (2.5 nM; 5 µg/ml puromycin) for 7 days in BC2 cell line but not in BC1. Expression of indicated genes were analysed via reverse transcriptase-quantitative PCR (RT-qPCR). One experiment has been evaluated in triplicate by qPCR. The error bars of the experiment were calculated of triplicates according to section 2.2.2.3.
(e) B-MYB protein levels were reduced in BC2 after treatment with 4-OHT (2.5 nM; 5 µg/ml puromycin) for 8 days. B-MYB protein levels were determined by immunoblotting. BETA ACTIN served as loading control.

3.1.7 Characterisation of B-Myb cell lines

Previous studies have reported that MMB serves as activator of mitotic gene expression (Schmit et al., 2007; Mannefeld et al., 2009) in mammalian cells. In part 3.1.3 it was shown, that mitotic genes are targets of MMB in lung cancer *in vivo*. I therefore next investigated, whether B-Myb has an impact on the regulation of mitotic genes in primary lung cancer cells. Therefore, relative mRNA expression of B-Myb lung tumor cell lines was analysed by RT-qPCR. As expected, the control cell line KR1 showed no change in mRNA expression after 4-

OHT treatment. In BC2 cell line, a significant effect on B-Myb and on the MMB targets after 4-OHT treatment for 7 days was observed (Fig. 12a). Here I saw, that *B-Myb* was significantly downregulated as well as some known MMB targets like *Nusap1*. These findings were comparable to the *in vivo* part where *Nusap1 e*xpression was also reduced. To independently confirm this result, I depleted, B-Myb for 72 h by two different small interfering RNAs (siRNAs), siMYB1 and siMYB2. The expression of MMB genes was analysed by RT-qPCR. Indeed, I detected also a significant effect on *B-Myb* and on the MMB target gene mRNA expression with siMYB2 compared to sictrl in BC2 cell line. Despite increasing the concentration of the siMYB2, no higher downregulation of MMB targets was observed (Fig. 12b). In contrast, siRNA siMYB1 had a weak effect on *B-Myb* mRNA expression and no effect on the expression of MMB targets (Fig. 12b).

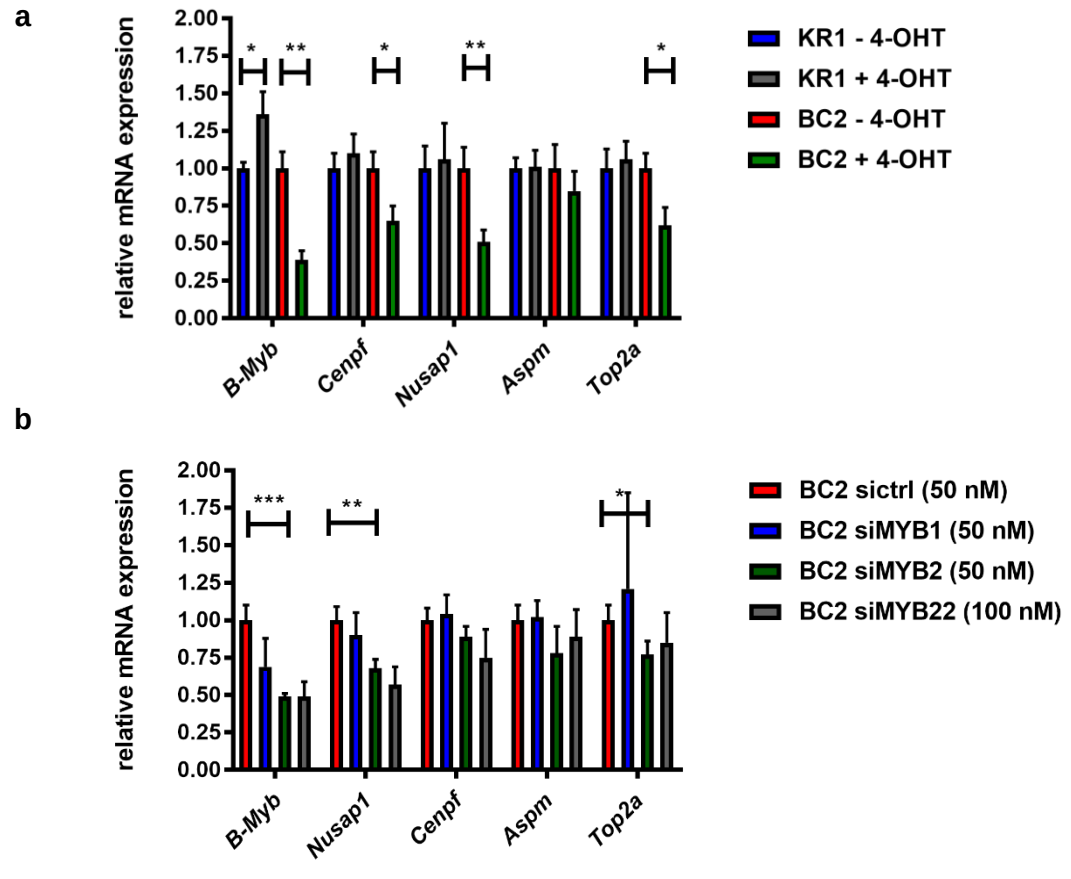

Figure 12: mRNA expression of *B-Myb* and MMB target genes in lung adenocarcinoma cell lines
(a) Expression of *B-Myb* and MMB target genes were reduced after treatment with 4-OHT (2.5 nM; 5 µg/ml puromycin) for 7 days in BC2 cells. KR1 served as control. Expression of indicated genes were analysed via reverse transcriptase-quantitative PCR (RT-qPCR). Three independent experiments have been evaluated in triplicate by qPCR. The error bars of the representative experiment were calculated of triplicates according to section 2.2.2.3. One representative experiment is shown.
(b) Depletion of *B-Myb* was achieved by RNA interference (RNAi) in BC2 cells. Two different siRNAs directed at murine B-Myb (c:50nM) were used, labelled as siMYB1 and 2. Additionally, siMYB2 was utilized with a concentration of 100 nM (siMYB22) to achieve a higher knockdown. Expression of indicated genes were analysed via reverse transcriptase-quantitative PCR (RT-qPCR). One experiment has been evaluated in triplicate by qPCR. The error bars of the experiment were calculated of triplicates according to section 2.2.2.3.

3.1.8 Proliferation is impaired in BC2 cell line after deletion of B-Myb

To investigate the requirement for MMB during proliferation of lung cancer cells *in vitro*, I determined the proliferation by using growth curves. To do so, cell lines were seeded at low density in 96 well plates and treated with 2.5 nM 4-OHT to delete B-Myb or with solvent for 10 days. Although there was no complete recombination, proliferation of BC2 cells was significantly impaired by 4-OHT-treatment in comparison to untreated cells (Fig. 13). Importantly, 4-OHT had no effect on the proliferation of control, cells. This data indicates, that B-MYB is required for proliferation of primary lung cancer cell lines.

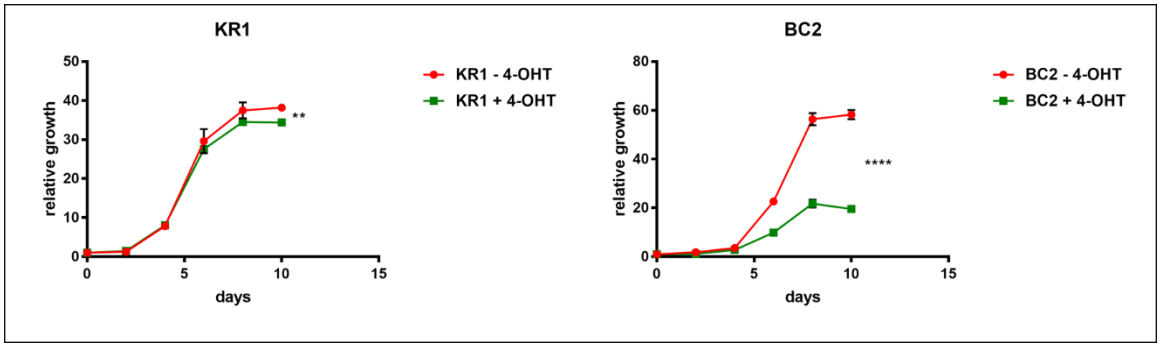

Figure 13: B-MYB is required for proliferation of lung cancer cells
Proliferation was impaired in BC2 cell line after 4-OHT treatment compared to the control cell line KR1. Cells were seeded at a low density and treated with 2.5 nM 4-OHT and 5 µg/ml puromycin or solvent for 10 days (growth curve). Three independent experiments have been evaluated. One representative experiment is shown.

3.1.9 Loss of B-Myb results in a higher frequency of cellular abnormalities and an abnormal cell cycle profile

In order to address whether loss of B-Myb has an effect on cytokinesis, examination under a fluorescence microscope for determination of mitotic defects and PI- FACS for cell cycle profile analysis were used. KR1 control cells and BC2 cells were treated with 2.5 nM 4-OHT for 10 days, fixed and stained with Hoechst and then evaluated under the fluorescence microscope. 200 cells were counted and mitotic defects were quantified. A high frequency of mitotic defects including bi/multi nucleated cells, giant cells, multilobed cells and micronuclei was observed (Fig. 14).

In addition, the cell cycle profile was studied after 4-OHT treatment (2.5 nM OHT) for 10 days. The analysis revealed that the cell cycle profile for BC2 was abnormal in comparison to the control cell line after 4-OHT treatment (Fig. 15a). Specifically, the percentage of cells in G1 was strongly reduced after deletion of B-Myb. In addition, an increase in subG1 fraction, indicative of apoptotic cells, and a high percentage of polyploid cells was observed.

Taken together, the partial loss of B-Myb in primary lung cancer cells leads to a high frequency of mitotic defects and an abnormal cell cycle profile (Fig. 14 and 15).

Together these experiments can explain the requirement for B-MYB for lung tumorigenesis *in vivo*.

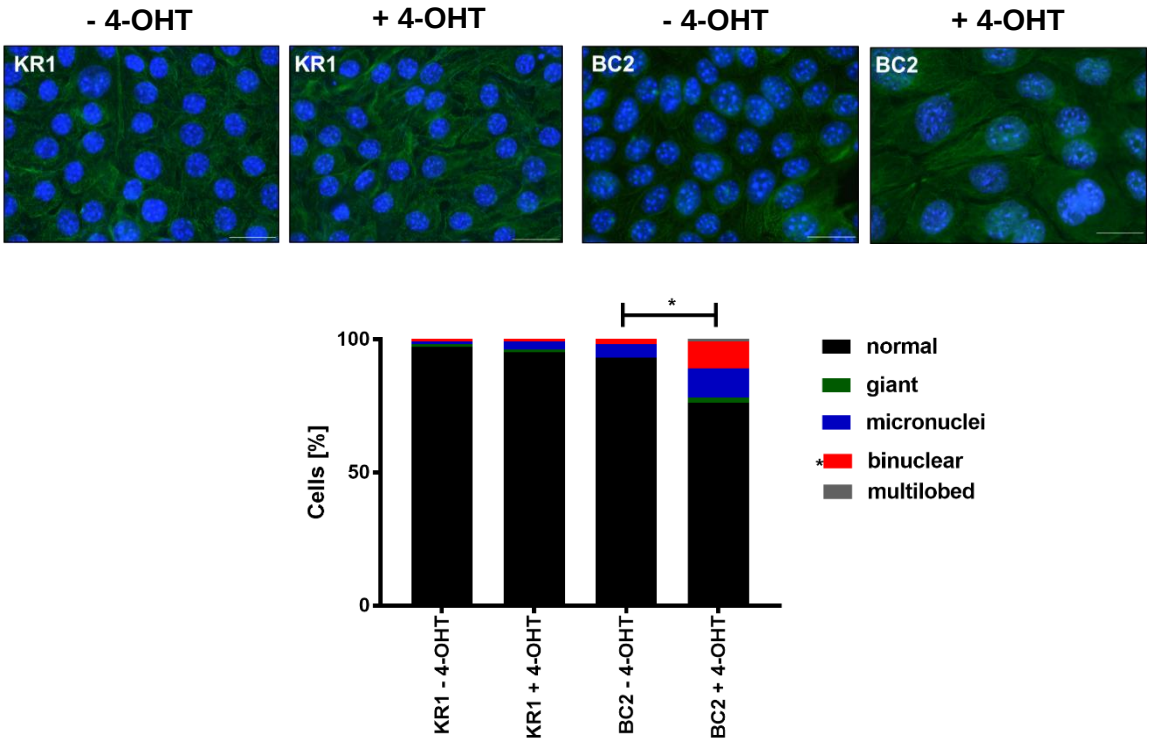

Figure 14: Cytokinesis defects in BC2 cell line after 4-OHT treatment compared to KR1 cell line
BC2 cells show significant mitotic defects after treatment with 4-OHT (2.5 nM; 5 µg/ml puromycin) for 10 days. Per condition, 200 cells were counted and mitotic defects quantified. Three independent experiments have been evaluated. One representative experiment is shown.

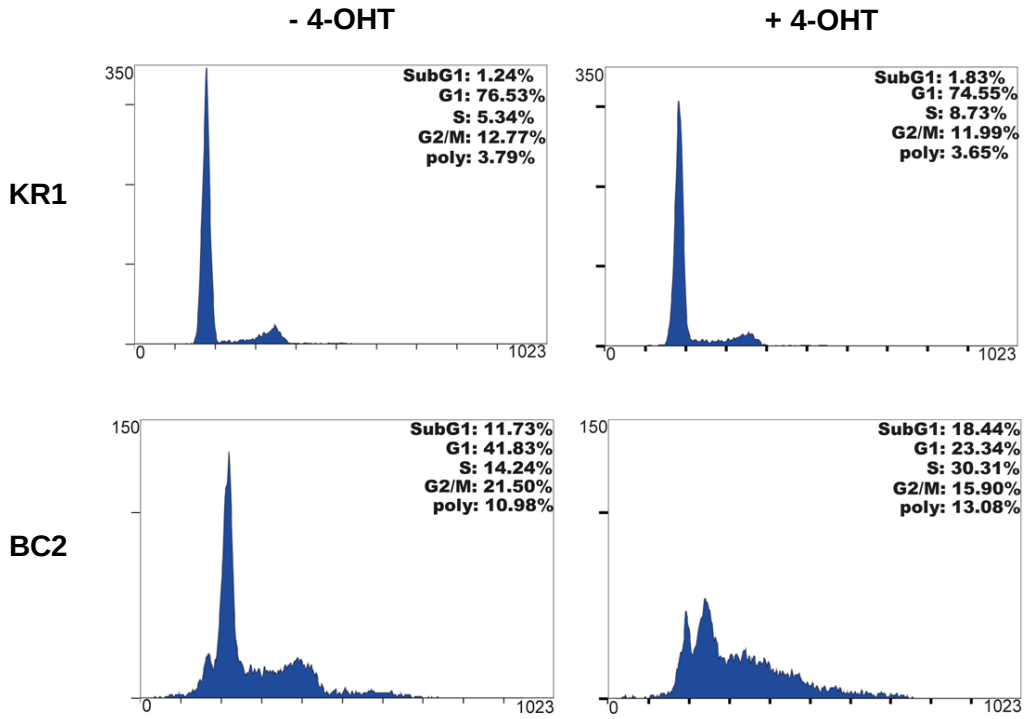

Figure 15: Abnormal cell cycle profile in BC2 cell line after loss of B-Myb
Cell cycle profile of BC2 cell line showed an abnormal cell cycle distribution (reduced G1, more polyploid and higher number of cells in SubG1) after treatment with 4-OHT (2.5 nM; 5 µg/ml puromycin) for 10 days. PI-FACS was used to receive cell cycle profile. Three independent experiments have been evaluated. One representative experiment is shown.

3.2 ShRNA mediated depletion of B-Myb in human lung cancer cell lines

Examination of recently published microarray data sets showed that high expression levels of B-MYB are associated with a poor prognosis for lung adenocarcinoma patients (Iltzsche et al., 2016). Recently, we showed that B-MYB is highly expressed in human lung adenocarcinoma (Iltzsche et al., 2016). Furthermore, our group demonstrated, that human lung cancer cell lines possess high levels of B-MYB (Iltzsche et al., 2016). These observations suggest, that B-MYB could be involved in human lung tumorigenesis and might serve as a marker or a therapeutic target. One central question is therefore whether B-MYB is required for proliferation of human lung tumor cell lines. To address this possibility, lung cancer cell lines stably expressing shRNAs directed at B-Myb were established.

To create several stable lung cancer cell lines that express doxycycline-inducible small hairpin RNAs (shRNAs) directed at B-Myb (Fig. 16a), I used the multifunctional lentiviral vector pInducer (Meerbrey et al., 2011). The advantage of the pInducer system is that it is a single vector system, so that specialized cell lines or multiple vectors are not required. Furthermore,

it has a minimal basal expression of shRNAs and high inducibility in polyclonal populations, which controls gene silencing. Moreover, it has a cistron encoding for both rtTA and a sortable marker in the same transcription unit, which enables cells with higher rtTA expression and shRNA inducibility to be identified and isolated in polyclonal populations (Meerbrey et al., 2011).

The design of the shRNAs was conducted with an online siRNA prediction tool (per Dow et al., 2012). Subsequently, I cloned promising candidates into the lentiviral pINDUCER vector. Lentiviral supernatants were used to transduce MDA-MB-231 cells (breast cancer cell line) by pINDUCER-shRNAs and the cells were subsequently selected for lentiviral integration by blasticidin. At the beginning, I tested if the shRNA was induced by measuring the expression of RFP 48 h after treatment with 1 µg/ml doxycycline (Fig. 16a and S. 4) and the knockdown efficiency of the shRNAs 60 h after treatment with 1 µg/ml doxycycline by immunoblotting (Fig. 16c). As shown in figure 16c, I could identify a set of shRNAs against B-MYB with an adequate knockdown efficiency. In some early experiments, it became apparent that shRNA 1792 was most efficient (from now on abbreviated as 92). Therefore, shRNA 92 was used for further experiments. A shRNA against Luciferase (LU) were created in lab and served as a control. In the next step, the shRNA was tested in several lung cancer cell lines. To receive an adequate knockdown efficiency, lung cancer cell lines were infected twice with shRNA 92. Knockdown of B-MYB was validated 60 h after induction by different concentrations of doxycycline via immunoblotting in H23 cell line (Fig. 17). Next, in order to analyse B-Myb and MMB target expression on the transcriptional level, I treated the different lung cancer cell lines with 1 µg/ml doxycycline for 7 days. Expression of indicated genes was analysed via RT-qPCR. Surprisingly, only B-Myb expression was significantly reduced while the expression of selected MMB target genes was unchanged (Fig.18).

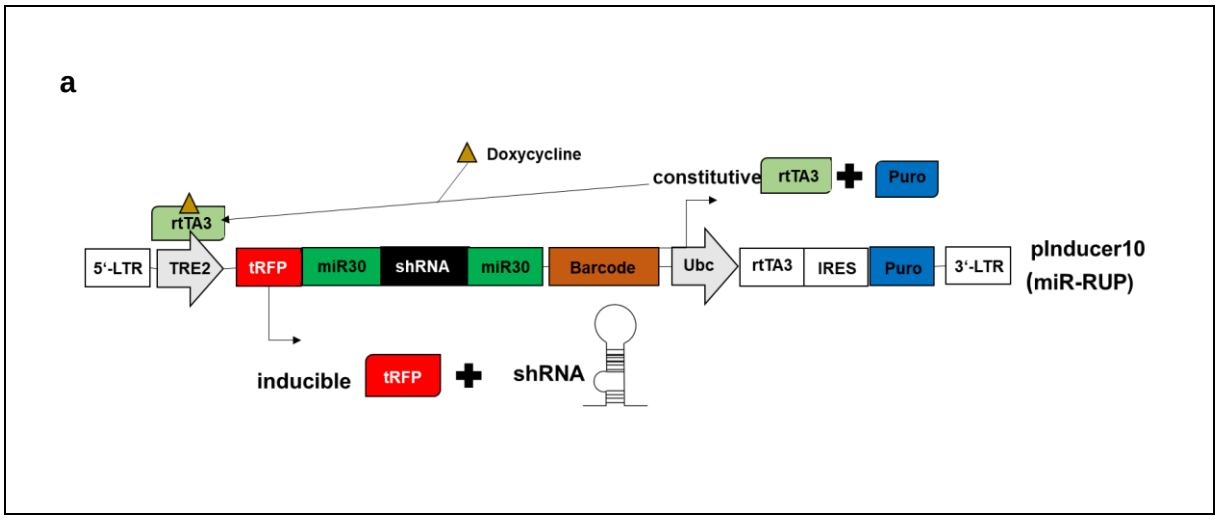

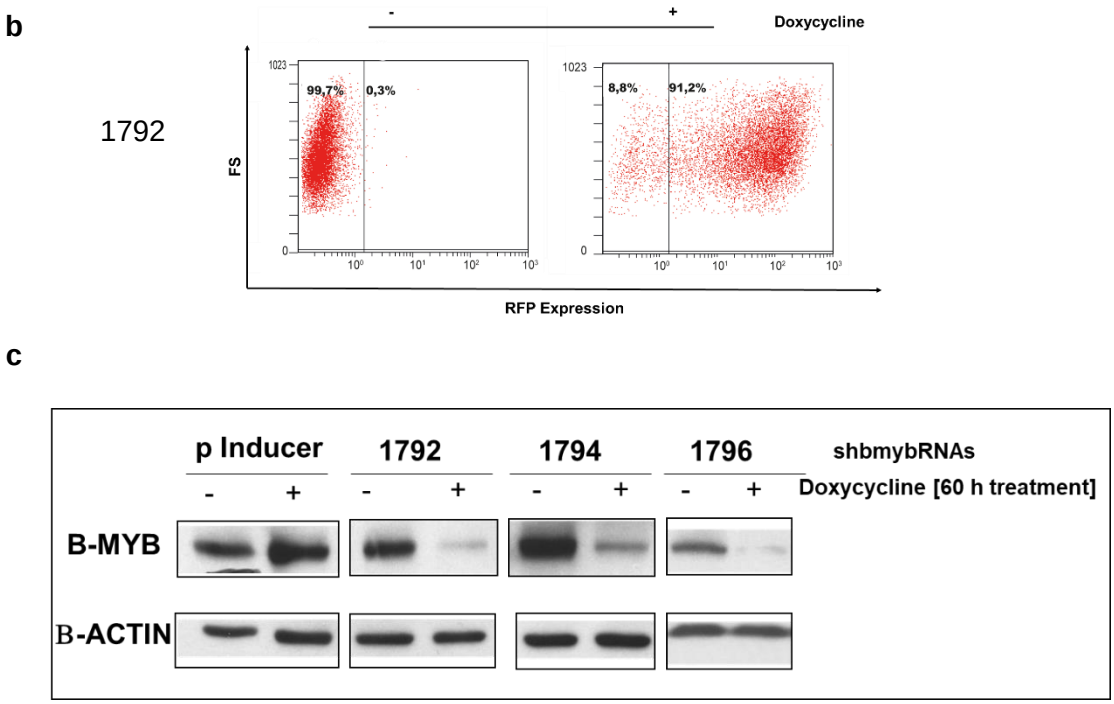

Figure 16: The knockdown efficiency of shRNAs against B-MYB was tested in the breast cancer cell line MDA-MB-231
(a) Scheme of the pInducer vector for doxycycline- inducible expression is shown.
(b) Example for a FACS profile of shRNA against B-MYB (1792) without (-) and with (+) doxycycline (1 µg/ml) treatment [RFP expression correlates with shRNA expression.
(c) Protein levels of B-MYB were efficiently downregulated after induction of the shRNAs with 1 µg/ml doxycycline after 60 hours' treatment. Beta actin served as loading control, pInducer vector as control.

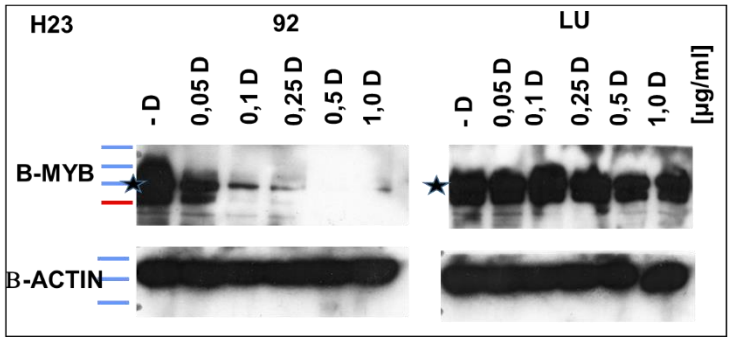

Figure 17: Knockdown of B-MYB in the human lung cancer cell line H23
Stable human lung cancer cell line H23 expressing the best shRNA (1792) against B-MYB here labelled as 92 were generated. An shRNA against Luciferase (LU) served as control. Knockdown efficiency of B-MYB after induction of the shRNA with indicated concentrations of doxycycline was tested by RFP-FACS and immunoblotting. Beta Actin served as loading control.

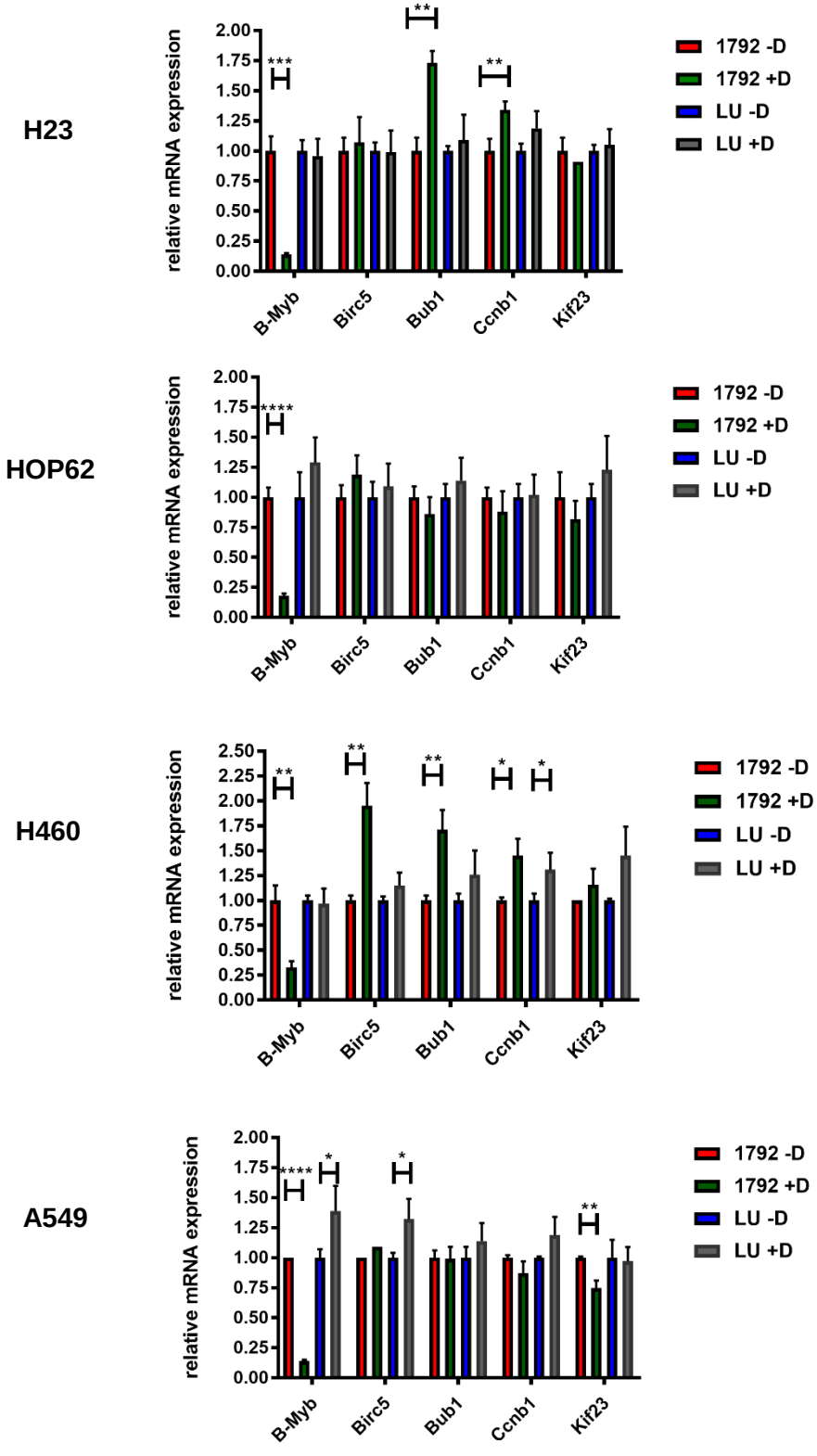

Figure 18: B-Myb but not MMB targets were efficiently downregulated on transcriptional level
Expression of B-Myb but not of MMB target genes were reduced after treatment with 1 µg/ml doxycycline for 10 days in human lung cancer cell line. Human lung cancer cell lines expressing inducible shRNA against luciferase served as control. Expression of indicated genes were analysed via reverse transcriptase-quantitative PCR (RT-qPCR). Two independent experiments have been evaluated in triplicate by qPCR. The error bars of the representative experiment were calculated of triplicates according to section 2.2.2.3 One representative experiment is shown.

3.2.1 Lentiviral system is not efficient enough for downregulation of MMB targets

Next, I determined whether B-MYB depletion has an impact on proliferation of human lung cancer cell lines. Lung cancer cell lines stably expressing the B-MYB specific shRNA were seeded at low density in a 96 well plate and treated with different concentration of doxycycline or with solvent for 10 days. Treatment with doxycycline resulted in a decrease in proliferation. However, proliferation in control cell lines was also slightly impaired by doxycycline-treatment (Fig. 19).

In addition, I asked whether depletion of B-MYB has an impact on the cytokinesis and the cell cycle profile of lung cancer cell line. Lung cancer cell lines treated with 1 µg/ml doxycycline for 10 days were fixed, stained with Hoechst and then evaluated under the microscope. 200 cells were counted and mitotic defects were quantified. A significant increase in micronuclei and in binucleation was observed in human lung cancer cell lines after treatment with doxycycline (Fig. 20a, b).

In addition, the cell cycle profile was studied after doxycycline treatment (1 µg/ml) for 10 days. However, no change in the distribution of cell cycle phases was observed after treatment with doxycycline. In addition, no increase in the subG1 fraction and no increase of polyploid cells was present (Fig. 21a).

Taken together, although B-Myb was downregulated on transcriptional level the MMB target genes were not significantly affected. Small effects on proliferation and on the upregulation in cytokinesis defects in human lung tumorigenesis could be observed. Thus, either B-MYB is not important for proliferation of human lung cancer cell lines or that the lentiviral system is not efficient enough in eliminating the expression of B-MYB.

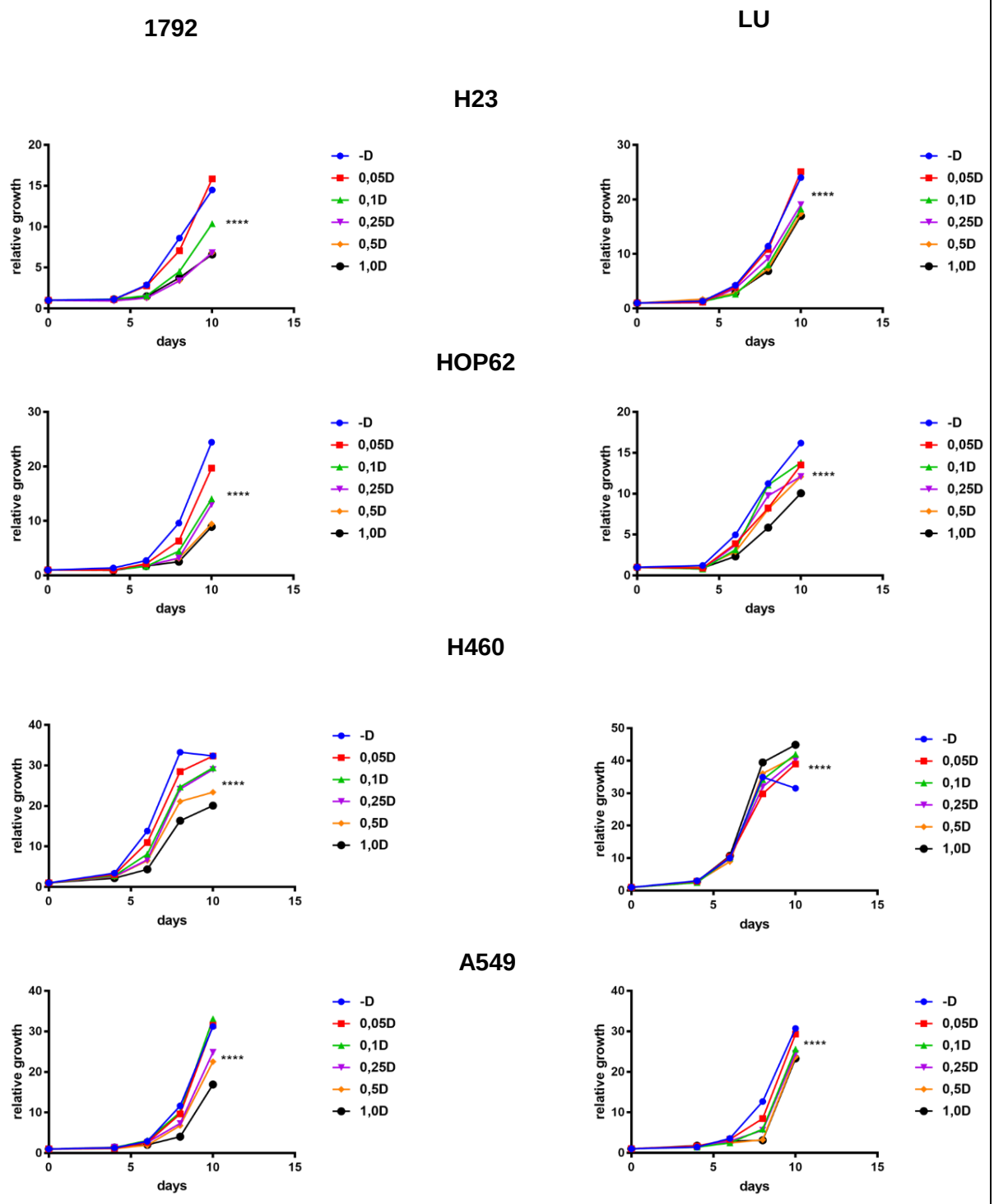

Figure 19: Impaired proliferation after loss of B-Myb in human lung cancer cell lines
Proliferation was impaired in human lung cancer cell lines after treatment with indicated doxycycline concentrations. Cells were seeded at a low density and treated with indicated doxycycline concentrations or solvent for 10 days (Growth curve). Human lung cancer cell lines expressing inducible shRNA against luciferase served as control but also show a decrease in proliferation. Three independent experiments have been evaluated. Statistical significance was determined only on day 10 (Student's t- test, two-sided) as ****P < 0.0001. One representative experiment is shown.

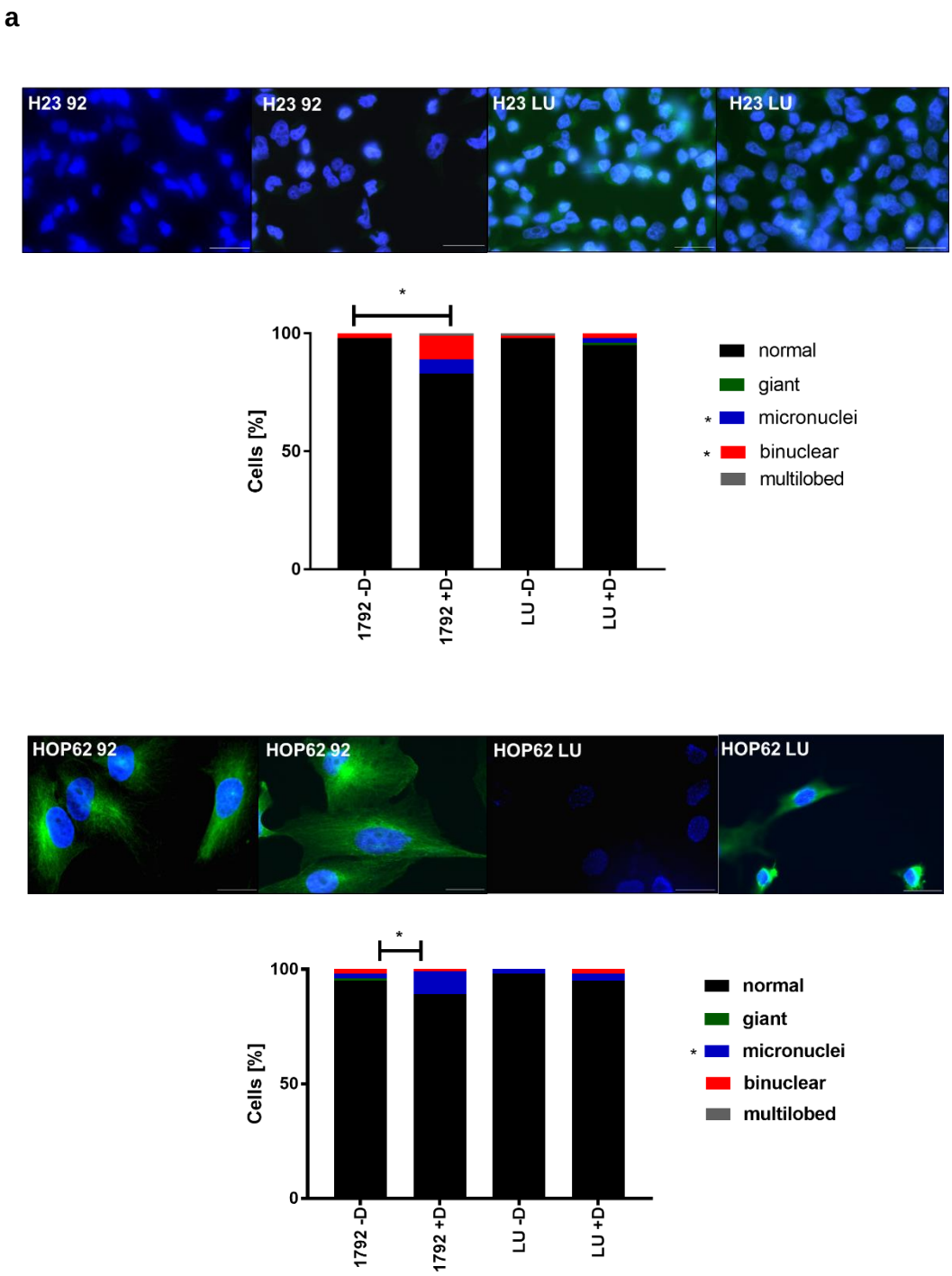

Figure 20: Cytokinesis defects in different lung cancer cell lines after loss of B-Myb
(a) H23 92 and HOP62 92 showed significant mitotic defects after treatment with 1 µg/ml doxycycline for 10 days in comparison to the Luciferase control cell lines. Per condition, 200 cells were counted and mitotic defects quantified. Two independent experiments have been evaluated. Statistical significance was determined (Fisher's exact test, two-sided) as * P < 0.05, **** P < 0.001.

b

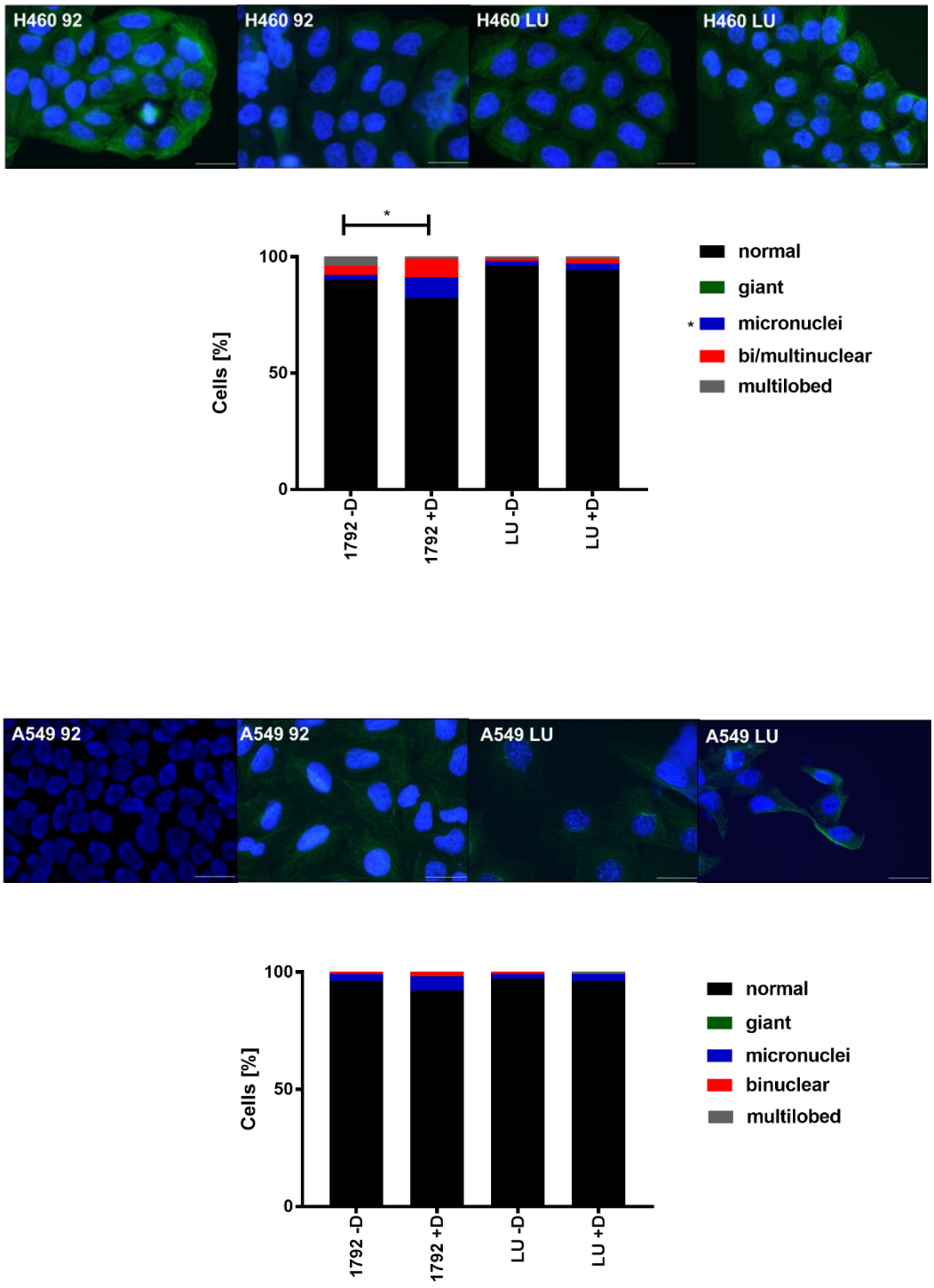

(b) H460 expressing shRNA 92 but not A549 with shRNA 92 showed significant mitotic defects after treatment with 1 µg/ml doxycycline for 10 days in comparison to the luciferase control cell lines. Per condition, 200 cells were counted and mitotic defects quantified. Two independent experiments have been evaluated. Statistical significance was determined (Fisher's exact test, two-sided) as * P < 0.05, **** P < 0.001. One representative experiment is shown.

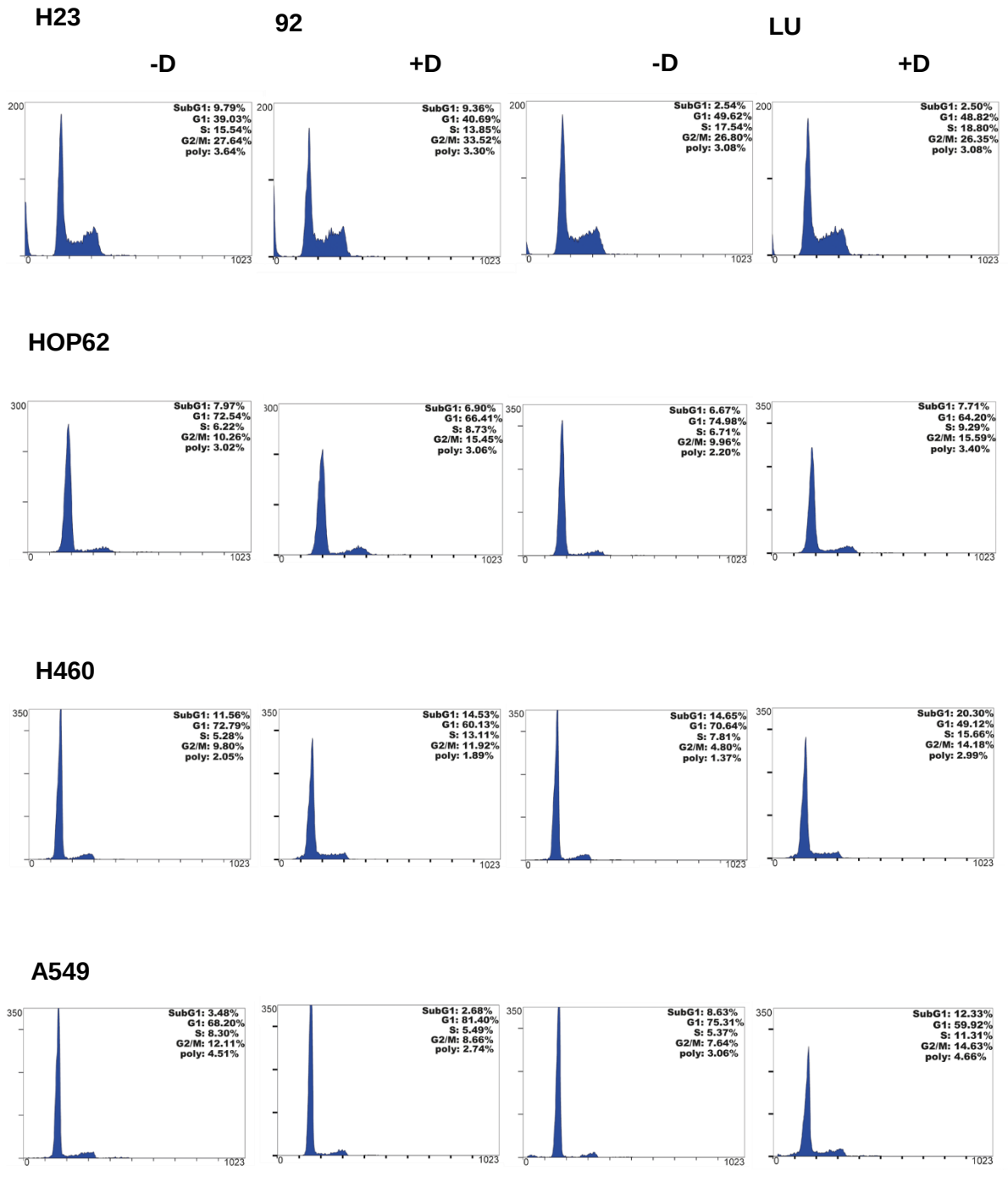

Figure 21: Cell cycle profile was largely unchanged after treatment with 1 µg/ml doxycycline
Cell cycle profile of human lung cancer cell line showed a normal cell cycle profile (after treatment with 1 µg/ml doxycycline for 10 days. PI-FACS was used to receive cell cycle profile. Two independent experiments have been evaluated. One representative experiment is shown.

3.2.2 siRNA mediated depletion of B-Myb in human lung tumor cells

Because the lentiviral shRNA system may not to work to deplete B-Myb sufficiently, I next used a siRNA approach in which B-Myb was depleted by RNAi for 72 h. Also, FoxM1 was depleted because it has been reported that inactivation of FoxM1 cause similar effects as B-Myb or MuvB inhibition. Furthermore, a synergistic activity between B-MYB and FOXM1 has been shown through network analysis to identify master regulators of B lymphocytes proliferation (Lefebvre et al., 2010). It has been assumed that FOXM1 acts downstream of B-MYB with MuvB serving as a bridge linking these two factors. Therefore, B-Myb, FoxM1 and both together were depleted by siRNA to study gene expression. Changes in the gene expression of MMB target genes in comparison to the non-specific siRNA treated control were analysed by RT-qPCR. Most of MMB target genes were strongly downregulated after depletion of B-Myb or FoxM1 or both together in comparison to the non-specific siRNA treated control (Fig. 22a, b, c). However, depletion of both, B-Myb and FoxM1, had no additive effect on the downregulation of MMB target genes (Fig. 22a, b, c). For further characterisation, the human lung cancer cell line H23, which harbour a mutation in K-Ras and in p53, was used. The H23 cell line was suitable for further testing because it is comparable to the mutation status of Ras and p53 in murine lung tumors and cell lines.

Next, I tested, if NUSAP1 was downregulated on protein level in H23 cells. Indeed, NUSAP1 was downregulated in H23 cells by siRNA mediated depletion of B-MYB (Fig. 23a).

Next, I asked whether depletion of B-MYB is associated with mitotic defects. Conditions remained the same as described before. 200 cells were counted and indicated mitotic defects were quantified. In fact, I could demonstrate, that a higher frequency of mitotic defects especially higher amount on micronuclei was detected (Fig. 23b). This result was comparable to the effect in the lentiviral shRNA system.

Finally, I analysed the cell cycle profile. Upon B-MYB depletion the fraction of cells in G1 was decreased in whereas the fraction of polyploid cells was increased (Fig. 23c).

Together, these data illustrate, that B-MYB is required for expression of mitotic genes in human lung cancer cells. In addition, these experiments showed that depletion of B-MYB by RNAi using siRNA is more effective than by lentiviral shRNA.

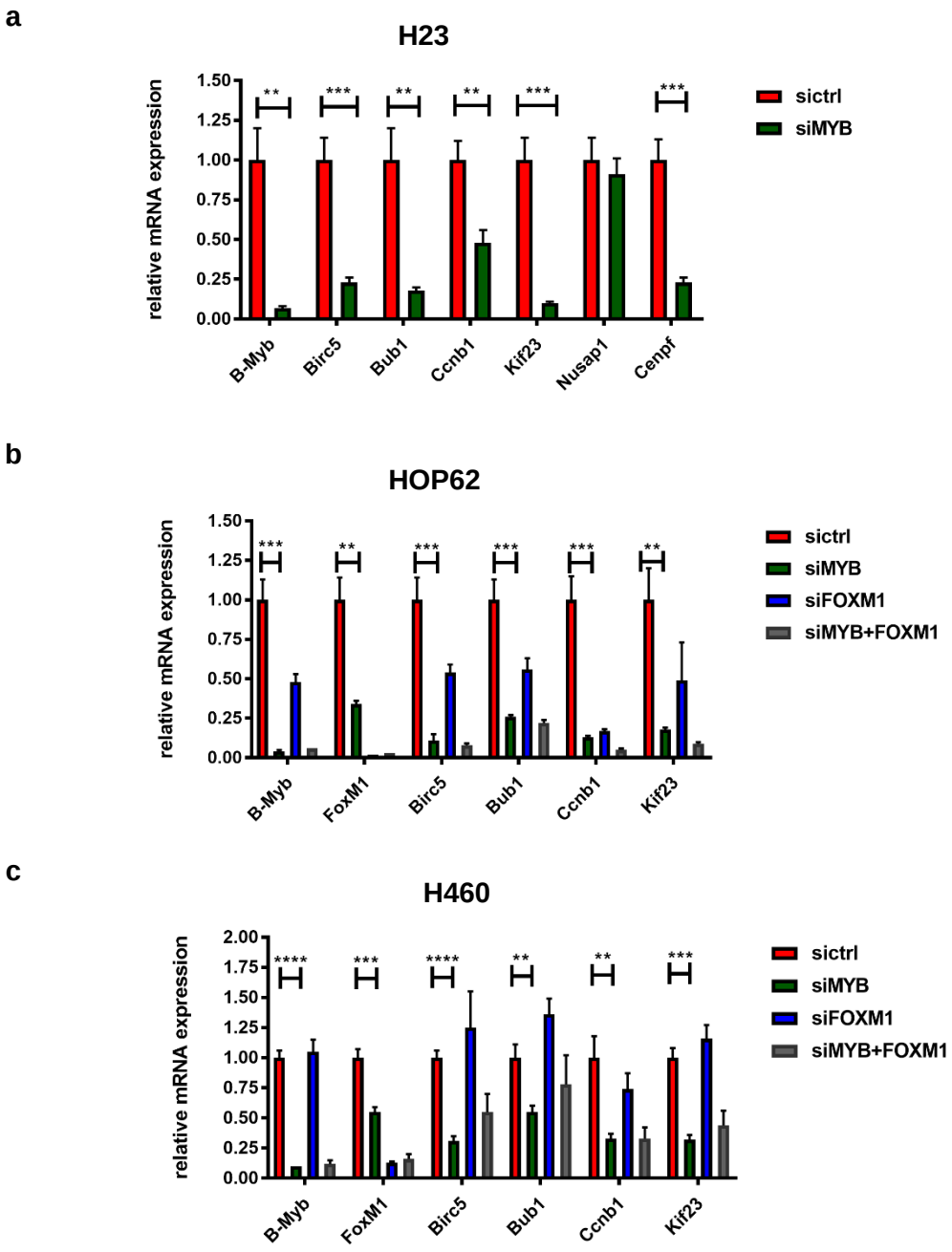

Figure 22: Gene regulation in human lung cancer cell lines after RNAi mediated depletion of B-Myb or FoxM1

(a) B-Myb was depleted by RNAi in H23 cell line for 72 hours. A non-specific siRNA was used as a control. Expression of indicated genes was analysed via reverse transcriptase-quantitative PCR (RT-qPCR). Two independent experiments have been evaluated in triplicate by qPCR. The error bars of the representative experiment were calculated of triplicates according to section 2.2.2.3. One representative experiment is shown.

(b) B-Myb and FoxM1 were depleted by RNAi in comparison to control RNAi in HOP62 cell line for 72 hours. Expression of indicated genes were analysed via reverse transcriptase-quantitative PCR (RT-qPCR). The error bars of the experiment were calculated of triplicates according to section 2.2.2.3. One experiment has been evaluated in triplicate by qPCR.

(c) B-Myb and FoxM1 were depleted by RNAi in comparison to control RNAi in H460 cell line for 72 hours. Expression of indicated genes were analysed via reverse transcriptase-quantitative PCR (RT-qPCR). One experiment has been evaluated in triplicate by qPCR. The error bars of the experiment were calculated of triplicates according to section 2.2.2.3.

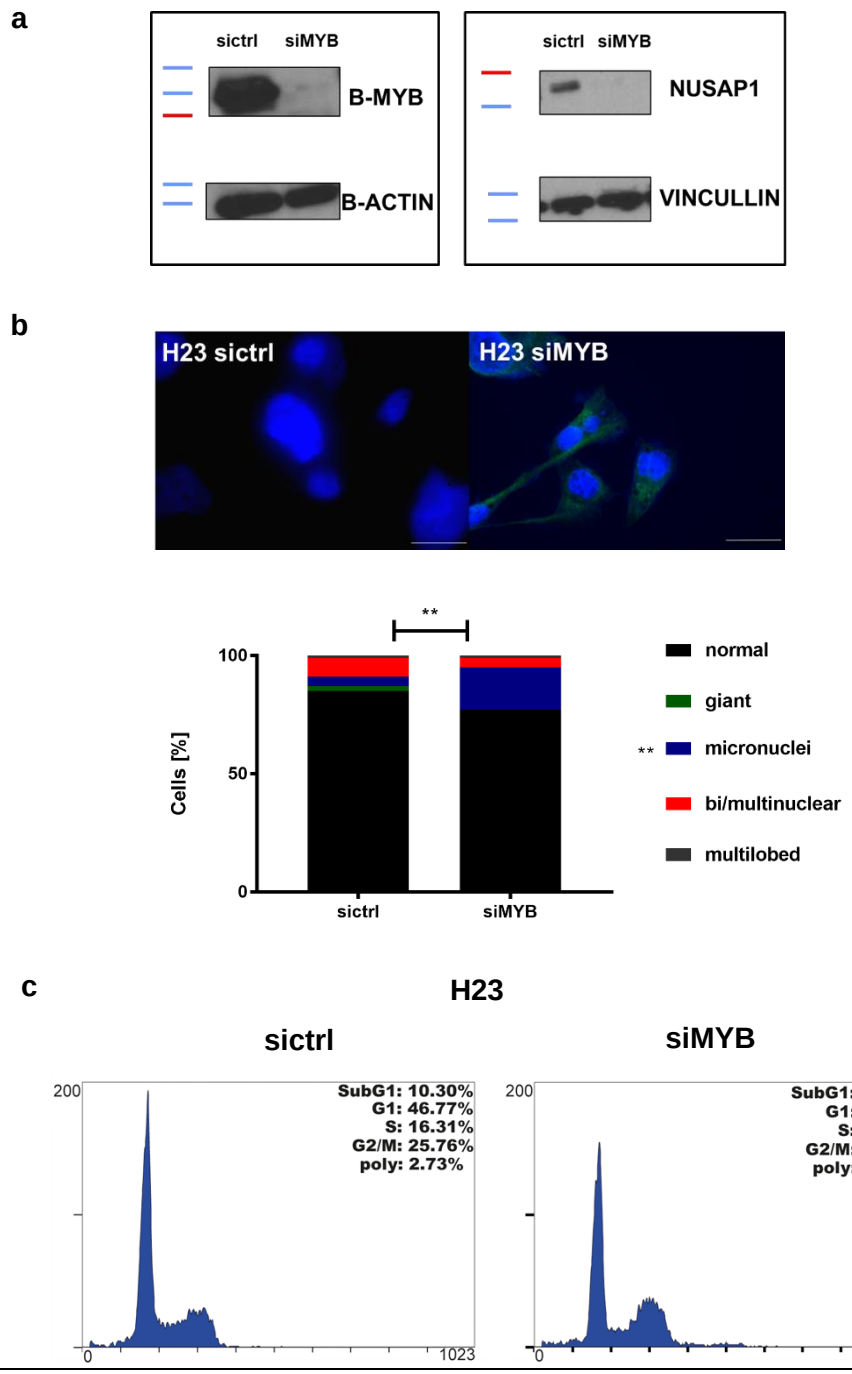

Figure 23: B-MYB is required for normal mitosis of human lung cancer cells
(a) Protein levels B-MYB and MMB target gene NUSAP1 were efficiently depleted by RNAi in comparison to control RNAi after 72 hours in H23. Beta Actin and Vincullin served as loading control. Protein levels were determined by immunoblotting. Two independent experiments have been evaluated. One representative experiment is shown.
(b) Significant mitotic defects after treatment with RNAi for 72 hours in comparison control RNAi was observed in H23. Per condition, 200 cells were counted and mitotic defects quantified. Two independent experiments have been evaluated. Statistical significance was determined (Fisher's exact test, two-sided) as * $P < 0.05$, **** $P < 0.001$. One representative experiment is shown.
(c) Cell cycle profile of H23 cell line looked abnormal after treatment with RNAi compared to control RNAi after 72 hours. PI-FACS was used to determine the cell cycle profiles. Two independent experiments have been performed. One representative experiment is shown.

4. Discussion

B-MYB has distinct physiological functions for instance in transcriptional regulation, proliferation, cell survival, apoptosis and senescence. Therefore, it is not surprising that B-MYB plays also a crucial role in cancer development and progression (Sala, 2005; Mowla et al., 2014; Martinez and DiMaio, 2011). However, whether B-MYB as part of the MMB complex is required for lung tumorigenesis *in vivo* has not been investigated. In this study, I demonstrate that deletion of B-Myb leads to a reduced tumor size (Fig. 4c) and a shift to lower less aggressive tumor grade in a K-Ras dependent mouse model for lung tumorigenesis (Fig. 4d) resulting in a lower tumor burden. Elevated levels of B-MYB and its target genes NUSAP1 as well as CENPF were observed in advanced tumors (Fig. 5a, b, c and 6a, b, c, d). Furthermore, a direct correlation between B-MYB and NUSAP1 was seen in murine lung adenocarcinoma (Fig. 7). Moreover, advanced lung tumors show up elevated p-ERK levels, a characteristic feature of these tumors (Fig. 8a, b, c). On transcriptional level, inactivation of *B-Myb* expression lead to a reduced expression on MMB target genes in a primary cell line derived from a lung adenocarcinoma (Fig. 12a). Reduced proliferation was also observed after loss of B-MYB as seen by a lower fraction of KI-67 positive cells in tumor sections (Fig. 9b) and *in vitro* by a significantly impairment of proliferation in primary cells (Fig. 13). This was accompanied by a high frequency of mitotic defects (Fig. 14). Unexpectantly, a complete suppression of tumor development was not achieved by the knockout of *B-Myb*. The analysis of the allelic status in primary tumors revealed that Cre-mediated recombination was not able to completely delete *B-Myb* (Fig. 10). Incomplete recombination of *B-Myb* was also observed in primary tumor cell lines (Fig. 11a, b).

The shRNA-mediated depletion of B-Myb in human lung cancer cell lines resulted in slight effects on proliferation and in cytokinesis defects (Fig. 19 and 20a, b). After siRNA mediated depletion of B-Myb or FoxM1, MMB target genes were strongly downregulated (Fig. 22a, b, c). Furthermore, a high frequency of mitotic defects was detected (Fig. 23b). Moreover, the fraction of cells in the G1 phase of the cells was decreased while the fraction of polyploid cells was increased (Fig. 23c). Together, these data illustrate, that B-MYB is required for gene expression and normal cell cycle progression of human lung cancer cell lines.

In this study, deletion of B-Myb leads to a reduced tumor area and a shift to lower less aggressive tumor grade in *K-Ras*$^{LSL\text{-}G12D/+}$*p53*$^{fl/fl}$*B-Myb*$^{fl/fl}$ mice compared to control resulting in a lower tumor burden. Together these data demonstrate that deletion of B-Myb significantly impairs the development of lung tumors and tumors, which arose are in most cases less aggressive. Furthermore, it illustrates that MMB is required for tumorigenesis in NSCLC *in vivo* in a p53-negative background (Fig. 4c, d). Surprinsingly, complete suppression of tumor development was not achieved by *B-Myb* knockout. Immunohistochemistry staining revealed

that B-MYB expression is reduced in *K-Ras*$^{LSL\text{-}G12D/+}$*p53*$^{fl/fl}$*B-Myb*$^{fl/fl}$ mice but that it is still there indicating that complete recombination of *B-Myb* allele failed (Fig. 4a).

Although a lentiviral Cre recombinase was utilized to ensure permanent expression by integration into the genome as well as *in vivo* delivery by intratracheal intubation, which provides the most direct and consistent method for the virus to reach the lungs, Cre-mediated recombination of *B-Myb* seemed to be inefficient (DuPage et al., 2009). (Fig. 10a). Interestingly, Cre-mediated recombination was also not efficient enough to inactivate *Lin9* in *K-Ras*$^{LSL\text{-}G12D/+}$*p53*$^{fl/fl}$*Lin9*$^{fl/fl}$ mice (Iltzsche et al., 2017). Similarly, in a lung tumor mouse model driven by K-Ras and loss of Rac1, only tumors develop and progress who are able to escape inactivation of both alleles of *Rac1* (Kissil et al., 2007). Findings in *K-Ras*$^{LSL\text{-}G12D/+}$*Luc FADD*$^{-/-}$ mice revealed that lung tumors may arise due to persistent Fadd abundance because of inefficient Cre recombination of the *Fadd* transgene (Bowman et al., 2015). Moreover, it has been reported that all c-Jun NH_2-Terminal Kinase lung tumors harbour a retained *Jnk1*^{LoxP} allele and so are incompletely recombined (Cellurale et al., 2011).

In this study, incomplete recombination was also observed in primary tumor cell lines (Fig. 11a). After expression of a hormone-inducible Cre^{ERT2} recombinase and administration of 4-hydroxytamoxifen (4-OHT) only incomplete recombination of the remaining floxed *B-Myb* allele was achieved. This was surprising, because treatment of CreER-expressing tumor cell lines derived from *K-Ras*$^{LSL\text{-}G12D/+}$*p53*$^{fl/fl}$*Lin9*$^{fl/fl}$ mice with 4-OHT resulted in the deletion of the remaining allele (Iltzsche et al., 2016).

Cre-mediated recombination is an effective tool that allows the DNA modification to be targeted to a specific cell type and generation of conditional somatic mouse mutants (Marth, 1996; Feil et al., 2009). The Cre recombinase from bacteriophage P1 catalyses site specific recombination at loxP sites to excise the intervening gene in prokaryotic as well as in eukaryotic cells (Baubonis and Sauer, 1993). However, incomplete recombination may occur due to variations in Cre activity and accessibility to chromatin (Hennet et al., 1995; Shao et al., 2002). In this context, it has been proposed that the efficiency of Cre-mediated genomic targeting is sensitive to chromosomal position effects (Baubonis and Sauer, 1993). In Hennet et al. it has been reported that enhanced Cre function could be mediated by incorporating Flp structures including eukaryotic translational and nuclear localization signals (Hennet et al., 1995). Immunohistochemistry staining revealed that tumor size and grade correlates with B-MYB expression and that only grade I lesions showed low B-MYB expression (Fig. 5a, c). Although, isolation of grade I or II tumors was performed, it was not possible to genotype this material or to establish cell lines due to absence of sufficient tumor material. A possible solution for future studies is the isolation of tumor material by laser capture microdissection. Also, other knockout tools to avoid incomplete recombination can be considered. One approach could be

the orthotopic and heterotopic implantation of cancer cell lines or freshly isolated tumors into immunodeficient mice (Kim et al., 2009). Another promising knockout tool that has emerged is the genome editing technology known as CRISPR/Cas9. Originally used by bacteria as defence mechanism, it has been modified to facilitate genetic manipulations in a variety of cell types and organisms (Horvath and Barrangou, 2010; Hsu et al., 2014). However, it is questionable whether a complete deletion of such a tumor essential gene is possible. Another alternative approach to investigate the impact of B-MYB on tumorigenesis is to overexpress B-MYB. Indeed, Jin et al. it has been shown that overexpression of B-MYB significantly increases lung cancer cell growth, migration and invasion (Jin et al., 2017).

Together, these data suggest that there is a high selective pressure on tumors against the complete loss of *B-Myb*, because only tumors that escape the complete deletion of *B-Myb* allele are able to progress. Overall these experiments demonstrate that B-MYB is essential for murine lung tumorigenesis

Similar to B-MYB, it has been shown that depletion of LIN9 significantly impairs the development of lung tumors indicating a requirement of LIN9 for tumorigenesis in NSCLC *in vivo*. LIN9 is a member of the MuvB core module and so present in both, the repressive DREAM as well as in the active MMB complex, whereas B-MYB is only part of the MMB complex. Impaired tumor development upon loss of LIN9 could therefore reflect a requirement for the repressive function of the DREAM complex. However, the similar pgenotype of B-MYB and LIN9 deletion on lung tumorigenesis and gene expression suggests a requirement for the activating MMB complex in cancerogenesis as opposed to an active role of the DREAM repressor module.

To investigate the role of B-Myb in human lung cancer cell lines, RNA interference (RNAi) was used. RNAi is a natural process through which the expression of a targeted gene can be knocked down with high specificity and selectivity. Therefore, RNA interference presents an effective tool for personalized cancer therapy. RNAi can be mediated through two types of molecules: the chemically synthesized double-stranded small interfering RNA (siRNA) or vector based short hairpin RNA (shRNA). Although shRNA and siRNA have similar functional outcomes, they have a distinct structure, differ in molecular mechanism and in RNA pathways (Rao et al., 2009). shRNA is a sequence of small RNA molecule which forms a solid hairpin turn that allows silencing of target gene expression. Expression of shRNA is achieved by delivery of plasmids or through viral or bacterial vectors (Paddison et al., 2002). The advantage to use shRNAs for experiments in contrary to siRNAs is, if inserted via an appropriate viral vector, it produces permanent gene silencing effects. Therefore, it can be utilized for long term knockdown for instance in growth curve experiments. In contrast, siRNA can be used only for

short term knockdown of genes due to the transient effect. Considering these facts, I used a multifunctional lentiviral vector (pInducer) to create several stable lung cancer cell lines that express doxycycline-inducible small hairpin RNAs (shRNAs) directed at B-Myb to be able to perform long term experiments (Fig.16a). However, although a seemingly adequate knockdown rate for B-MYB was achieved in lung cancer cell lines (Fig. 18), MMB target gene expression (Fig. 18) was only slightly affected maybe due to the late timepoint and effect on proliferation (Fig. 19) and on cytokinesis were minor (Fig. 20a, b) and not comparable to those in murine lung tumorigenesis. In contrast, siRNA treatment of human lung cancer cell lines leads to a strong downregulation of MMB targets (Fig. 21a, b, c) and to strong effects on cytokinesis defects. The knockdown of B-Myb through siRNA was more effective (up to 90%) than per shRNA (up to 80%). This difference in the knockdown efficiency seems to be the critical factor and determining for the strong effects.

It has been reported that inactivation of FOXM1 causes similar effects as B-MYB or MuvB inhibition. Forkhead box protein M1 (FOXM1) belongs to a family of evolutionary conserved transcriptional regulators. The DNA-binding domain called the forkhead box or winged helix domain is characteristic feature of FOXM1 (Wierstra and Alves, 2007). FOXM1 regulates expression of a large array of G2/M-specific genes like Plk1 or Cenpf and is therefore implicated in cell cycle progression (Grant et al., 2013). FoxM1-deficient MEFs displayed defects in G2/M transition, chromosome segregation and cytokinesis (Laoukili et al., 2005). *In vivo* studies showed that deletion of FOXM1 lead to growth defects and mitotic failures (Wang et al., 2005). FOXM1 has also been linked to cancer. Upregulation of FOXM1 was found in most of solid human cancers including lung cancer (Kim et al., 2006). Synergistic activity between B-MYB and FOXM1 has been shown through network analysis to identify master regulators of B lymphocytes proliferation (Lefebvre et al., 2010). Furthermore, recent data suggest that B-MYB is required for FOXM1 binding to promotors. Inactivation of B-MYB or MuvB proteins reduce the binding of FOXM1 to late cell cycle promotors (Saddavasim and DeCaprio, 2012; Down et al., 2012). This suggests that FOXM1 acts downstream of B-MYB with MuvB serving as a bridge linking these two factors.

To compare the effects of B-Myb depletion to FoxM1, FoxM1 depletion through siRNA was performed. In addition, it was tested if RNAi knockdown of both B-Myb and FoxM1 has additive effects on cell cycle gene expression. Knockdown of both factors has no additive effect, which is consistent with other findings (Saddavasim and DeCaprio, 2012). Interestingly, knockdown of FoxM1 through siRNA in H460 and HOP62 cell line (Fig. 22 b,c) revealed that B-Myb expression is also reduced. Zhang et al. found that downregulation of FOXM1 is associated with a significant reduction of B-MYB expression on protein level, whereas B-MYB inactivation result only in a slight reduction of FOXM1 (Zhang et al., 2017). Wiseman identified LIN9 and not B-MYB as the direct binding partner for FOXM1 in oesophageal adenocarcinoma

(Wiseman et al., 2015). However, Lefebvre investigated whether B-MYB and FOXM1 may regulate each other due to studies in which synergistic transcription factors often participate in feed-forward loops (Lefebvre et al., 2010; Palomero et al., 2006; Carro et al., 2010). B-MYB mRNA and protein levels were not affected by FOXM1 inactivation, whereas FOXM1 levels were reduced in a time-dependent manner after B-Myb silencing. This underlines that B-MYB is a transcriptional activator of FOXM1. In addition, quantitative chromatin immune precipitation assays showed that B-MYB binds *in vivo* the FOXM1 promotor suggesting that B-MYB and FOXM1 form a feed-forward loop (Lefebvre et al., 2010).

As mentioned in the introduction, data of the Stephen Elldege group indicate that the mitotic machinery could be the Achilles' heel for Ras mutant cancer cells. These data suggest that pathways, which are involved in regulating the mitotic machinery are attractive for a potential treatment of cancers harbouring Ras mutations (Luo et al., 2009). In this context, the MMB complex could be a target for a potential treatment of Ras-dependent cancer. Although it seems to be promising to use MMB as therapeutic target for the treatment of lung cancer, inhibiting its function with small molecules will be difficult due to the fact that no enzymatic activities have been identified. As transcription factor, B-MYB is not a conventional drug target. Recently a new promising tool emerged to inhibit multidomain scaffold proteins, notably transcription factors, through ligand-induced protein degradation using bifunctional ligands. One part of the bifunctional ligand is specific for the target protein whereas the other part mediates the recruitment of a cellular E3 ligase to the target protein leading to proteasomal degradation (Winter et al., 2015).

Other new therapeutic modalities for B-MYB targeting emerged. Peptides or small molecules that could be identified by high-throughput screening or rational design, could be useful (Gonda, Leo and Ramsey, 2008; Winter et al., 2015). Another approach to target B-MYB is to induce degradation of its mRNAs by siRNA. However, effective delivery *in vivo* and off- target effects remain problematic (reviewed in De Fougerolles et al., 2007). Targeting B-Myb transcription could be a promising tool, too (Gonda, Leo and Ramsey, 2008; Winter et al., 2015). Although there is no direct B-MYB inhibitor available, CDK2 inhibition could be utilized to reduce B-MYB activity in cancers, which show high B-MYB expression. Although a potent CDK2 inhibitor is lacking, other CDK inhibitors, which are in clinical trials could be also beneficial (Musa et al., 2017). Recently a promising therapeutic tool emerged underlying the molecular mechanisms of action of bromodomain and extraterminal protein inhibitors (BETi). Recent data suggest that BET inhibitors directly suppress the MuvB components Lin9, B-Myb and FoxM1 in triple-negative breast cancer (Sahni et al., 2017). BET inhibitors have also been shown to be effective in mouse models in diverse cancers and therefore currently investigated in early phase clinical trials (Shi et al., 2014).

The downstream transcriptional network of MMB could also serve as effective targets. MMB targets, which have specialized functions in mitosis might allow a more precise prognostic outcome for therapy avoiding side effects. The MMB target Survivin (Birc5), which is strongly overexpressed e.g. in human neuroblastoma tumors correlating with poor patient outcome, is already under investigation in phase I and II clinical trials (Islam et al., 2000; Giaccone et al., 2009; Lamers et al., 2011; Garg et al., 2016). Silencing of Survivin within these tumors resulted in mitotic catastrophe leading to apoptosis. Moreover, RNAi-mediated depletion of the kinesin Kif23 (MLKP1) was shown to suppress lung tumor formation *in vivo* and to induce apoptosis in lung cancer cells (Iltzsche et al., 2017). In addition, mitotic kinesins and microtubule-associated non-motor proteins, which are direct transcriptional targets of the MMB, are identified to suppress proliferation in breast cancer indicating their potential to act as prognostic markers (Wolter et al., 2017). Several inhibitors against MMB targets have already been in clinical trial for instance Aurora kinases (Gautschi et al., 2008).

Other MMB regulated genes and possible targets for therapy include NUSAP1 and CENPF. NUSAP1 (Nucleolar and Spindle-Associated Protein 1) has been identified as an essential microtubule stabilizing and bundling protein that is enriched at the central part of the spindle (Ribbeck et al., 2007; Raemaekers et al., 2003). Requisition of Nusap1 to the nucleus during interface prevents interaction with microtubules as long as mitosis begins (Raemaekers et al., 2003). Nusap1 expression is restricted to late S/G2 and M phases consistent to the fact that Nusap1 is a direct transcriptional target of the MMB. Comparable to B-Myb, Nusap1 deficiency in mice leads to early embryonic lethality caused by failures in the chromosome alignment (Vanden Bosch et al., 2010). However, increased Nusap1 levels are associated with inhibition of proliferation (Raemaekers et al., 2003; Okamoto et al., 2015). Nevertheless, elevated levels of Nusap1 are connected to cancer formation and are associated with a poor prognosis, which is consistent to the results in figure 6 a and b (Gulzar et al., 2013; Chen et al., 2015). Centromere binding protein F (Cenpf) is a 367 kDa cell cycle dependent kinetochore associated protein (Fowler et al., 1998; Rattner et al., 1993; Yang et al., 2003). It belongs to a class of proteins that are found at the centrosome in a cell cycle specific manner in contrast to those that associate throughout the cell cycle like Cenpa (Rattner et al., 1993). It localizes onto the kinetochore in late G2/M to metaphase, relocates at the spindle midzone and the intracellular bridge in late anaphase and is degraded following completion of mitosis (Fowler et al., 1998). Comparable to NUSAP1, elevated levels of CENPF are associated with cancer formation underscoring the results shown in Fig. 6 c and d (Cohen et al., 2014).

In addition to the development of efficient lung cancer therapies, the identification of prognostic markers remains indispensable. B-MYB has prognostic value for predicting outcomes in cancer patients including breast cancer, colorectal cancer, cervical cancer, acute myeloid leukemia, neuroblastoma, gallbladder cancer and prostate cancer (Shi et al., 2012; Ren et al.,

2015; Astbury et al., 2011; Fuster et al., 2013; Raschella et al., 1999; Liang et al., 2017; Bar-Shira et al., 2002). Data presented here and in Iltzsche et al. (2017) indicate that B-MYB could serve as potential target in lung cancer. Comparable results were provided by Jin et al. (2017), who showed that B-MYB is significantly upregulated in NSCLC correlating with clinicopathological parameters.

Conclusion

In this thesis, it was demonstrated that the MMB complex is required for lung tumorigenesis *in vivo* in a p53-negative background by the inhibition of the transcription factor B-Myb using a conditional B-Myb knockout NSCLC mouse model. The requirement of the MMB in murine lung tumorigenesis was shown by a reduced tumor area and a shift to lower less aggressive tumor grade in *K-Ras*$^{LSL\text{-}G12D/+}$*p53*$^{fl/fl}$*B-Myb*$^{fl/fl}$ mice compared to control. Furthermore, a direct connection between B-MYB and its target gene NUSAP1 *in vivo* was corroborated by the coexpression of both through immunohistochemistry staining. Elevated levels of either B-MYB, NUSAP1 or CENPF in advanced tumors and in contrast low levels in grade 1 or 2 tumors underlined additionally the contribution of MMB in lung tumorigenesis and the oncogenic potential of B-MYB. To further characterise physiological functions in murine lung tumorigenesis, cell lines derived from tumors of this mouse model have been established. The tumor growth promoting function of B-MYB was illustrated after loss of B-Myb by a lower fraction of KI-67 positive cells *in vivo* and a significantly high impairment in proliferation in BC2 *in vitro*. Defects in cytokinesis shown by a high frequency of cytokinesis defects and an abnormal cell cycle profile after loss of B-Myb underscore the impact of B-MYB and so MMB in lung tumorigenesis. It could be further demonstrated that B-Myb is a tumor essential gene, because only tumors that escape the complete loss of *B-Myb* allele were able to progress as seen by the incomplete recombination of *B-Myb* in murine lung tumors and in the derived cell lines.

In addition, the contribution of MMB to proliferation of human lung tumor cell lines was demonstrated. Therefore, RNAi-mediated depletion of B-Myb by shRNA and siRNA in several human lung cancer cell lines was used. On transcriptional level, B-Myb and MMB target genes were highly downregulated in comparison to the non-specific siRNA treated control. An analogues result was observed also on protein level. Furthermore, loss of B-MYB resulted in a reduced proliferation. Moreover, a higher frequency of cytokinesis defects especially higher amount of micronuclei was detected, which is equivalent to the effect in the lentiviral system. Cell cycle profile analysis showed up the switch to an abnormal profile. Interestingly, RNAi-mediated depletion of B-Myb through siRNA was more efficient than inactivation through lentiviral shRNA.

Finally, the ability of MMB to act as therapeutic target and B-MYB to serve as a potential prognostic marker in lung tumorigenesis has been elucidated. Detection of elevated B-MYB levels in human adenocarcinoma underlines the potential of B-MYB to serve as a clinical marker (Iltzsche et al., 2017; Jin et al., 2017).

5. Summary

The evolutionary conserved Myb-MuvB (MMB) multiprotein complex is a transcriptional master regulator of mitotic gene expression. The MMB subunits B-MYB, FOXM1 as well as target genes of MMB are often overexpressed in different cancer types. Elevated expression of these genes correlates with an advanced tumor state and a poor prognosis for patients. Furthermore, it has been reported that pathways, which are involved in regulating the mitotic machinery are attractive for a potential treatment of cancers harbouring Ras mutations (Luo et al., 2009).

This suggest that the MMB complex could be required for tumorigenesis by mediating overactivity of mitotic genes and that the MMB could be a useful target for lung cancer treatment. However, although MMB has been characterized biochemically, the contribution of MMB to tumorigenesis is largely unknown in particular *in vivo.*

In this thesis, it was demonstrated that the MMB complex is required for lung tumorigenesis *in vivo* in a mouse model of non small cell lung cancer. Elevated levels of B-MYB, NUSAP1 or CENPF in advanced tumors as opposed to low levels of these proteins levels in grade 1 or 2 tumors support the possible contribution of MMB to lung tumorigenesis and the oncogenic potential of B-MYB.The tumor growth promoting function of B-MYB was illustrated by a lower fraction of KI-67 positive cells *in vivo* and a significantly high impairment in proliferation after loss of B-Myb *in vitro*. Defects in cytokinesis and an abnormal cell cycle profile after loss of B-Myb underscore the impact of B-MYB on proliferation of lung cancer cell lines. The incomplete recombination of *B-Myb* in murine lung tumors and in the tumor derived primary cell lines illustrates the selection pressure against the complete loss of *B-Myb* and further demonstrats that B-Myb is a tumor-essential gene. In the last part of this thesis, the contribution of MMB to the proliferation of human lung cancer cells was demonstrated by the RNAi-mediated depletion of B-Myb. Detection of elevated B-MYB levels in human adenocarcinoma and a reduced proliferation, cytokinesis defects and abnormal cell cycle profile after loss of B-MYB in human lung cancer cell lines underlines the potential of B-MYB to serve as a clinical marker.

6. Zusammenfassung

Der evolutionär konservierte Myb-MuvB (MMB) Multiproteinkomplex ist ein transkriptionaler Meisterregulator der mitotischen Genexpression. Die MMB Untereinheiten B-MYB, FOXM1 und ihre Zielgene sind oft überexprimiert in verschiedenen Krebsarten. Die erhöhte Expression dieser Gene korreliert mit einem fortgeschrittenen Tumorstadium und einer schlechten Prognose für Patienten. Außerdem wurde berichtet, dass Signalwege, die die Mitosemaschinerie betreffen, reizvoll sind als mögliches Target für die Behandlung von Ras mutierten Krebsarten (Lao et al., 2009).

Dies weißt auf darauf hin, dass der MMB Komplex an der Tumorentstehung beteiligt sein könnte, indem er die Überexpression mitotischer Gene fördert und damit ein geeignetes Target zur Behandlung von Krebs darstellen könnte. Obwohl der MMB biochemisch eingehend untersucht wurde, ist die Beteiligung des MMB an der Tumorgenese weitestgehend unbekannt speziell *in vivo*.

In dieser Doktorarbeit wurde anhand eines NSCLC Mausmodells gezeigt, dass der MMB für die Lungentumorgenese *in vivo* erforderlich ist. Erhöhte Level von B-MYB, NUSAP1 oder CENPF in fortgeschrittenen Tumoren und im Gegenzug niedrigen Leveln in Grad 1 und 2 Tumoren unterstreichen die mögliche Beteiligung des MMB an der Lungentumorgenese und das onkogene Potential von B-MYB. Die Tumorwachstum-fördernde Funktion von B-MYB wurde veranschaulicht durch eine geringere Anzahl an KI-67 positiven Zellen *in vivo* und einem signifikant hohen Beeinträchtigung der Proliferation nach dem Verlust von B-MYB *in vitro*. Defekte in der Zytokinese und ein abnormales Zellzyklusprofil nach dem Verlust von B-MYB heben den Einfluss von B-Myb auf die Proliferation von Lungenkrebszelllinien hervor. Die unvollständige Rekombination von B-Myb in murinen Lungentumoren und den daraus hergestellten primären Tumorzelllinien veranschaulichen den Selektionsdruck auf den kompletten Verlust von B-MYB und zeigen zusätzlich, dass B-MYB ein für den Tumor essentielles Gen ist. Im letzten Teil der Doktorarbeit konnte die Beteiligung des MMB auf die Proliferation auf Lungenkrebszellen gezeigt werden durch den Verlust von B-MYB durch RNAi-Interferenz (RNAi). Detektion erhöhter B-Myb Level in humanen Adenokarzinomen und eine verminderte Proliferation, Zytokinese-Defekte und ein abnormales Zellzyklusprofil nach B-MYB Verlust in humanen Lungenkrebszelllinien unterstreichen das Potential von B-MYB als klinischer Marker zu fungieren.

7. References

Ahlbory, D., Appl, H., Lang, D., and Klempnauer, K.H. (2005). Disruption of B-myb in DT40 cells reveals novel function for B-Myb in the response to DNA-damage. Oncogene 24, 7127-7134.

Aslanian, A., Iaquinta, P.J., Verona, R., and Lees, J.A. (2004). Repression of the Arf tumor suppressor by E2F3 is required for normal cell cycle kinetics. Genes & development 18, 1413-1422.

Alberts B, Johnson A, Lewis J, Raff M, Roberts K, Walter P (2008). "Chapter 17". Molecular Biology of the Cell (5th ed.). New York: Garland Science. ISBN 978-0-8153-4111-6.

Astbury, K., McEvoy, L., Brian, H., Spillane, C., Sheils, O., Martin, C., and O'Leary, J.J. (2011). MYBL2 (B-MYB) in cervical cancer: putative biomarker. International journal of gynecological cancer: official journal of the International Gynecological Cancer Society 21, 206-212.

Baker, S.J., Ma'ayan, A., Lieu, Y.K., John, P., Reddy, M.V., Chen, E.Y., Duan, Q., Snoeck, H.W., and Reddy, E.P. (2014). B-myb is an essential regulator of hematopoietic stem cell and myeloid progenitor cell development. Proceedings of the National Academy of Sciences of the United States of America 111, 3122-3127.

Barnum, K.J., and O'Connell, M.J. (2014). Cell cycle regulation by checkpoints. Methods in molecular biology (Clifton, NJ) 1170, 29-40.

Bar-Shira, A., Pinthus, J.H., Rozovsky, U., Goldstein, M., Sellers, W.R., Yaron, Y., Eshhar, Z., and Orr-Urtreger, A. (2002). Multiple genes in human 20q13 chromosomal region are involved in an advanced prostate cancer xenograft. Cancer research 62, 6803-6807.

Basseres, D.S., Ebbs, A., Levantini, E., and Baldwin, A.S. (2010). Requirement of the NF-kappaB subunit p65/RelA for K-Ras-induced lung tumorigenesis. Cancer research 70, 3537-3546.

Baubonis, W., and Sauer, B. (1993). Genomic targeting with purified Cre recombinase. Nucleic acids research 21, 2025-2029.

Beall, E.L., Lewis, P.W., Bell, M., Rocha, M., Jones, D.L., and Botchan, M.R. (2007). Discovery of tMAC: a Drosophila testis-specific meiotic arrest complex paralogous to Myb-Muv B. Genes & development 21, 904-919.

Beijersbergen, R.L., Kerkhoven, R.M., Zhu, L., Carlee, L., Voorhoeve, P.M., and Bernards, R. (1994). E2F-4, a new member of the E2F gene family, has oncogenic activity and associates with p107 in vivo. Genes & development 8, 2680-2690.

Bergholtz, S., Andersen, T.O., Andersson, K.B., Borrebaek, J., Luscher, B., and Gabrielsen, O.S. (2001). The highly conserved DNA-binding domains of A-, B- and c-Myb differ with respect to DNA-binding, phosphorylation and redox properties. Nucleic acids research 29, 3546-3556.

Blake, M.C., and Azizkhan, J.C. (1989). Transcription factor E2F is required for efficient expression of the hamster dihydrofolate reductase gene in vitro and in vivo. Molecular and cellular biology 9, 4994-5002.

Bowman, B.M., Sebolt, K.A., Hoff, B.A., Boes, J.L., Daniels, D.L., Heist, K.A., Galban, C.J., Patel, R.M., Zhang, J., Beer, D.G., et al. (2015). Phosphorylation of FADD by the kinase CK1alpha promotes KRASG12D-induced lung cancer. Science signaling 8, ra9.

Budczies, J., Bockmayr, M., Denkert, C., Klauschen, F., Lennerz, J.K., Gyorffy, B., Dietel, M., Loibl, S., Weichert, W., and Stenzinger, A. (2015). Classical pathology and mutational load of breast cancer - integration of two worlds. The journal of pathology Clinical research 1, 225-238.

Campanini, E.B., Vandewege, M.W., Pillai, N.E., Tay, B.H., Jones, J.L., Venkatesh, B., and Hoffmann, F.G. (2015). Early Evolution of Vertebrate Mybs: An Integrative Perspective Combining Synteny, Phylogenetic, and Gene Expression Analyses. Genome biology and evolution 7, 3009-3021.

Carro, M.S., Lim, W.K., Alvarez, M.J., Bollo, R.J., Zhao, X., Snyder, E.Y., Sulman, E.P., Anne, S.L., Doetsch, F., Colman, H., et al. (2010). The transcriptional network for mesenchymal transformation of brain tumours. Nature 463, 318-325.

Cartwright, P., Muller, H., Wagener, C., Holm, K., and Helin, K. (1998). E2F-6: a novel member of the E2F family is an inhibitor of E2F-dependent transcription. Oncogene 17, 611-623.

Cellurale, C., Sabio, G., Kennedy, N.J., Das, M., Barlow, M., Sandy, P., Jacks, T., and Davis, R.J. (2011). Requirement of c-Jun NH(2)-terminal kinase for Ras-initiated tumor formation. Molecular and cellular biology 31, 1565-1576.

Charrasse, S., Carena, I., Brondani, V., Klempnauer, K.H., and Ferrari, S. (2000). Degradation of B-Myb by ubiquitin-mediated proteolysis: involvement of the Cdc34-SCF(p45Skp2) pathway. Oncogene 19, 2986-2995.

Chellappan, S.P., Hiebert, S., Mudryj, M., Horowitz, J.M., and Nevins, J.R. (1991). The E2F transcription factor is a cellular target for the RB protein. Cell 65, 1053-1061.

Chen, L., Zhuo, D., Chen, J., and Yuan, H. (2015). Screening feature genes of lung carcinoma with DNA microarray analysis. International journal of clinical and experimental medicine 8, 12161-12171.

Chen, X., Müller, G.A., Quaas, M., Fischer, M., Han, N., Stutchbury, B., Sharrocks, A.D., and Engeland, K. (2013). The forkhead transcription factor FOXM1 controls cell cycle-dependent gene expression through an atypical chromatin binding mechanism. Molecular and cellular biology 33, 227-236.

Cobrinik, D., Lee, M.H., Hannon, G., Mulligan, G., Bronson, R.T., Dyson, N., Harlow, E., Beach, D., Weinberg, R.A., and Jacks, T. (1996). Shared role of the pRB-related p130 and p107 proteins in limb development. Genes & development 10, 1633-1644.

Cohen, Y., Gutwein, O., Garach-Jehoshua, O., Bar-Haim, A., and Kornberg, A. (2014). The proliferation arrest of primary tumor cells out-of-niche is associated with widespread downregulation of mitotic and transcriptional genes. Hematology (Amsterdam, Netherlands) 19, 286-292.

Collins, K., Jacks, T., and Pavletich, N.P. (1997). The cell cycle and cancer. Proceedings of the National Academy of Sciences of the United States of America 94, 2776-2778.

Cooper GM. The Cell: A Molecular Approach. 2nd edition. Sunderland (MA): Sinauer Associates; 2000. The Eukaryotic Cell Cycle. Available from: https://www.ncbi.nlm.nih.gov/books/NBK9876/

De Fougerolles, A., Vornlocher, H.P., Maraganore, J., and Lieberman, J. (2007). Interfering with disease: a progress report on siRNA-based therapeutics. Nature reviews Drug discovery 6, 443-453.

DeCaprio, J.A., Ludlow, J.W., Figge, J., Shew, J.Y., Huang, C.M., Lee, W.H., Marsilio, E., Paucha, E., and Livingston, D.M. (1988). SV40 large tumor antigen forms a specific complex with the product of the retinoblastoma susceptibility gene. Cell 54, 275-283.

Dela Cruz, C.S., Tanoue, L.T., and Matthay, R.A. (2011). Lung cancer: epidemiology, etiology, and prevention. Clinics in chest medicine 32, 605-644.

Di Stefano, L., Jensen, M.R., and Helin, K. (2003). E2F7, a novel E2F featuring DP-independent repression of a subset of E2F-regulated genes. The EMBO journal 22, 6289-6298.

Dimova, D.K., and Dyson, N.J. (2005). The E2F transcriptional network: old acquaintances with new faces. Oncogene 24, 2810-2826.

Dow, L.E., Premsrirut, P.K., Zuber, J., Fellmann, C., McJunkin, K., Miething, C., Park, Y., Dickins, R.A., Hannon, G.J., and Lowe, S.W. (2012). A pipeline for the generation of shRNA transgenic mice. Nature protocols 7, 374-393.

Down, C.F., Millour, J., Lam, E.W., and Watson, R.J. (2012). Binding of FoxM1 to G2/M gene promoters is dependent upon B-Myb. Biochimica et biophysica acta 1819, 855-862.

Drabsch, Y., Robert, R.G., and Gonda, T.J. (2010). MYB suppresses differentiation and apoptosis of human breast cancer cells. Breast cancer research: BCR 12, R55.

DuPage, M., Dooley, A.L., and Jacks, T. (2009). Conditional mouse lung cancer models using adenoviral or lentiviral delivery of Cre recombinase. Nature protocols 4, 1064-1072.

Dyson, N. (1998). The regulation of E2F by pRB-family proteins. Genes & development 12, 2245-2262.

El-Deiry, W.S., Tokino, T., Velculescu, V.E., Levy, D.B., Parsons, R., Trent, J.M., Lin, D., Mercer, W.E., Kinzler, K.W., and Vogelstein, B. (1993). WAF1, a potential mediator of p53 tumor suppression. Cell 75, 817-825.

Elledge, S.J. (1996). Cell cycle checkpoints: preventing an identity crisis. Science (New York, NY) 274, 1664-1672.

Esterlechner, J., Reichert, N., Iltzsche, F., Krause, M., Finkernagel, F., and Gaubatz, S. (2013). LIN9, a subunit of the DREAM complex, regulates mitotic gene expression and proliferation of embryonic stem cells. PloS one 8, e62882.

Fang, B. (2016). RAS signaling and anti-RAS therapy: lessons learned from genetically engineered mouse models, human cancer cells, and patient-related studies. Acta biochimica et biophysica Sinica 48, 27-38.

Feil, S., Valtcheva, N., and Feil, R. (2009). Inducible Cre mice. Methods in molecular biology (Clifton, NJ) 530, 343-363.

Feldser, D.M., Kostova, K.K., Winslow, M.M., Taylor, S.E., Cashman, C., Whittaker, C.A., Sanchez-Rivera, F.J., Resnick, R., Bronson, R., Hemann, M.T., et al. (2010). Stage-specific sensitivity to p53 restoration during lung cancer progression. Nature 468, 572-575.

Fischer, M., Grossmann, P., Padi, M., and DeCaprio, J.A. (2016). Integration of TP53, DREAM, MMB-FOXM1 and RB-E2F target gene analyses identifies cell cycle gene regulatory networks. Nucleic acids research 44, 6070-6086.

Foos, G., Grimm, S., and Klempnauer, K.H. (1992). Functional antagonism between members of the myb family: B-myb inhibits v-myb-induced gene activation. The EMBO journal 11, 4619-4629.

Forristal, C., Henley, S.A., MacDonald, J.I., Bush, J.R., Ort, C., Passos, D.T., Talluri, S., Ishak, C.A., Thwaites, M.J., Norley, C.J., et al. (2014). Loss of the mammalian DREAM complex deregulates chondrocyte proliferation. Molecular and cellular biology 34, 2221-2234.

Fowler, K.J., Saffery, R., Irvine, D.V., Trowell, H.E., and Choo, K.H. (1998). Mouse centromere protein F (Cenpf) gene maps to the distal region of chromosome 1 by interspecific backcross analysis. Cytogenetics and cell genetics 82, 180-181.

Francis, R.E., Myatt, S.S., Krol, J., Hartman, J., Peck, B., McGovern, U.B., Wang, J., Guest, S.K., Filipovic, A., Gojis, O., et al. (2009). FoxM1 is a downstream target and marker of HER2 overexpression in breast cancer. International journal of oncology 35, 57-68.

Fujii, K., Murase, T., Beppu, S., Saida, K., Takino, H., Masaki, A., Ijichi, K., Kusafuka, K., Iida, Y., Onitsuka, T., et al. (2017). MYB, MYBL1, MYBL2 and NFIB gene alterations and MYC overexpression in salivary gland adenoid cystic carcinoma. Histopathology 71, 823-834.

Fuster, O., Llop, M., Dolz, S., Garcia, P., Such, E., Ibanez, M., Luna, I., Gomez, I., Lopez, M., Cervera, J., et al. (2013). Adverse prognostic value of MYBL2 overexpression and association with microRNA-30 family in acute myeloid leukemia patients. Leukemia research 37, 1690-1696.

Garcia, P., Berlanga, O., Watson, R., and Frampton, J. (2005). Generation of a conditional allele of the B-myb gene. Genesis (New York, NY: 2000) 43, 189-195.

Garcia, P., and Frampton, J. (2006). The transcription factor B-Myb is essential for S-phase progression and genomic stability in diploid and polyploid megakaryocytes. Journal of cell science 119, 1483-1493.

Garg, H., Suri, P., Gupta, J.C., Talwar, G.P., and Dubey, S. (2016). Survivin: a unique target for tumor therapy. Cancer cell international 16, 49.

Gaubatz, S., Wood, J.G., and Livingston, D.M. (1998). Unusual proliferation arrest and transcriptional control properties of a newly discovered E2F family member, E2F-6. Proceedings of the National Academy of Sciences of the United States of America 95, 9190-9195.

Gautschi, O., Heighway, J., Mack, P.C., Purnell, P.R., Lara, P.N., Jr., and Gandara, D.R. (2008). Aurora kinases as anticancer drug targets. Clinical cancer research: an official journal of the American Association for Cancer Research 14, 1639-1648.

Giaccone, G., Zatloukal, P., Roubec, J., Floor, K., Musil, J., Kuta, M., van Klaveren, R.J., Chaudhary, S., Gunther, A., and Shamsili, S. (2009). Multicenter phase II trial of YM155, a small-molecule suppressor of survivin, in patients with advanced, refractory, non-small-cell lung cancer. Journal of clinical oncology: official journal of the American Society of Clinical Oncology 27, 4481-4486.

Ginsberg, D., Vairo, G., Chittenden, T., Xiao, Z.X., Xu, G., Wydner, K.L., DeCaprio, J.A., Lawrence, J.B., and Livingston, D.M. (1994). E2F-4, a new member of the E2F transcription factor family, interacts with p107. Genes & development 8, 2665-2679.

Gonda, T.J., Leo, P., and Ramsay, R.G. (2008). Estrogen and MYB in breast cancer: potential for new therapies. Expert opinion on biological therapy 8, 713-717.

Grant, G.D., Brooks, L., 3rd, Zhang, X., Mahoney, J.M., Martyanov, V., Wood, T.A., Sherlock, G., Cheng, C., and Whitfield, M.L. (2013). Identification of cell cycle-regulated genes periodically expressed in U2OS cells and their regulation by FOXM1 and E2F transcription factors. Molecular biology of the cell 24, 3634-3650.

Grassilli, E., Salomoni, P., Perrotti, D., Franceschi, C., and Calabretta, B. (1999). Resistance to apoptosis in CTLL-2 cells overexpressing B-Myb is associated with B-Myb-dependent bcl-2 induction. Cancer research 59, 2451-2456.

Gulzar, Z.G., McKenney, J.K., and Brooks, J.D. (2013). Increased expression of NuSAP in recurrent prostate cancer is mediated by E2F1. Oncogene 32, 70-77.

Hanahan, D., and Weinberg, R.A. (2011). Hallmarks of cancer: the next generation. Cell 144, 646-674.

Harbour, J.W., and Dean, D.C. (2000). The Rb/E2F pathway: expanding roles and emerging paradigms. Genes & development 14, 2393-2409.

Harper, J.W., and Elledge, S.J. (2007). The DNA damage response: ten years after. Molecular cell 28, 739-745.

Harrison, M.K., Adon, A.M., and Saavedra, H.I. (2011). The G1 phase Cdks regulate the centrosome cycle and mediate oncogene-dependent centrosome amplification. Cell division 6, 2.

Harrison, M.M., Ceol, C.J., Lu, X., and Horvitz, H.R. (2006). Some C. elegans class B synthetic multivulva proteins encode a conserved LIN-35 Rb-containing complex distinct from a NuRD-like complex. Proceedings of the National Academy of Sciences of the United States of America 103, 16782-16787.

Hartwell, L.H., and Kastan, M.B. (1994). Cell cycle control and cancer. Science (New York, NY) 266, 1821-1828.

Hauf, S. (2013). The spindle assembly checkpoint: progress and persistent puzzles. Biochemical Society transactions 41, 1755-1760.

Hauser, S., Ulrich, T., Wurster, S., Schmitt, K., Reichert, N., and Gaubatz, S. (2012). Loss of LIN9, a member of the DREAM complex, cooperates with SV40 large T antigen to induce genomic instability and anchorage-independent growth. Oncogene 31, 1859-1868.

Heinrichs, S., Conover, L.F., Bueso-Ramos, C.E., Kilpivaara, O., Stevenson, K., Neuberg, D., Loh, M.L., Wu, W.S., Rodig, S.J., Garcia-Manero, G., et al. (2013). MYBL2 is a sub-haploinsufficient tumor suppressor gene in myeloid malignancy. eLife 2, e00825.

Hennet, T., Hagen, F.K., Tabak, L.A., and Marth, J.D. (1995). T-cell-specific deletion of a polypeptide N-acetylgalactosaminyl-transferase gene by site-directed recombination. Proceedings of the National Academy of Sciences of the United States of America 92, 12070-12074.

Henrich, S.M., Usadel, C., Werwein, E., Burdova, K., Janscak, P., Ferrari, S., Hess, D., and Klempnauer, K.H. (2017). Interplay with the Mre11-Rad50-Nbs1 complex and phosphorylation by GSK3beta implicate human B-Myb in DNA-damage signaling. Scientific reports 7, 41663.

Hijmans, E.M., Voorhoeve, P.M., Beijersbergen, R.L., van 't Veer, L.J., and Bernards, R. (1995). E2F-5, a new E2F family member that interacts with p130 in vivo. Molecular and cellular biology 15, 3082-3089.

Hirsch, F.R., Scagliotti, G.V., Mulshine, J.L., Kwon, R., Curran, W.J., Jr., Wu, Y.L., and Paz-Ares, L. (2017). Lung cancer: current therapies and new targeted treatments. Lancet (London, England) 389, 299-311.

Hochegger, H., Takeda, S., and Hunt, T. (2008). Cyclin-dependent kinases and cell-cycle transitions: does one fit all? Nature reviews Molecular cell biology 9, 910-916.

Horvath, P., and Barrangou, R. (2010). CRISPR/Cas, the immune system of bacteria and archaea. Science (New York, NY) 327, 167-170.

Hsu, P.D., Lander, E.S., and Zhang, F. (2014). Development and applications of CRISPR-Cas9 for genome engineering. Cell 157, 1262-1278.

Iltzsche, F., Simon, K., Stopp, S., Pattschull, G., Francke, S., Wolter, P., Hauser, S., Murphy, D.J., Garcia, P., Rosenwald, A., et al. (2017). An important role for Myb-MuvB and its target gene KIF23 in a mouse model of lung adenocarcinoma. Oncogene 36, 110-121.

Inoue, A., and Nukiwa, T. (2005). Gene mutations in lung cancer: promising predictive factors for the success of molecular therapy. PLoS medicine 2, e13.

Islam, A., Kageyama, H., Takada, N., Kawamoto, T., Takayasu, H., Isogai, E., Ohira, M., Hashizume, K., Kobayashi, H., Kaneko, Y., et al. (2000). High expression of Survivin, mapped to 17q25, is significantly associated with poor prognostic factors and promotes cell survival in human neuroblastoma. Oncogene 19, 617-623.

Jackson, E.L., Willis, N., Mercer, K., Bronson, R.T., Crowley, D., Montoya, R., Jacks, T., and Tuveson, D.A. (2001). Analysis of lung tumor initiation and progression using conditional expression of oncogenic K-ras. Genes & development 15, 3243-3248.

Jin, Y., Zhu, H., Cai, W., Fan, X., Wang, Y., Niu, Y., Song, F., and Bu, Y. (2017). B-Myb Is Up-Regulated and Promotes Cell Growth and Motility in Non-Small Cell Lung Cancer. International journal of molecular sciences 18.

Junttila, M.R., Karnezis, A.N., Garcia, D., Madriles, F., Kortlever, R.M., Rostker, F., Brown Swigart, L., Pham, D.M., Seo, Y., Evan, G.I., et al. (2010). Selective activation of p53-mediated tumour suppression in high-grade tumours. Nature 468, 567-571.

Kastan, M.B., and Bartek, J. (2004). Cell-cycle checkpoints and cancer. Nature 432, 316-323.

Kim, I.M., Ackerson, T., Ramakrishna, S., Tretiakova, M., Wang, I.C., Kalin, T.V., Major, M.L., Gusarova, G.A., Yoder, H.M., Costa, R.H., et al. (2006). The Forkhead Box m1 transcription factor stimulates the proliferation of tumor cells during development of lung cancer. Cancer research 66, 2153-2161.

Kissil, J.L., Walmsley, M.J., Hanlon, L., Haigis, K.M., Bender Kim, C.F., Sweet-Cordero, A., Eckman, M.S., Tuveson, D.A., Capobianco, A.J., Tybulewicz, V.L., et al. (2007). Requirement for Rac1 in a K-ras induced lung cancer in the mouse. Cancer research 67, 8089-8094.

Kittler, R., Pelletier, L., Heninger, A.K., Slabicki, M., Theis, M., Miroslaw, L., Poser, I., Lawo, S., Grabner, H., Kozak, K., et al. (2007). Genome-scale RNAi profiling of cell division in human tissue culture cells. Nature cell biology 9, 1401-1412.

Klein, D.K., Hoffmann, S., Ahlskog, J.K., O'Hanlon, K., Quaas, M., Larsen, B.D., Rolland, B., Rosner, H.I., Walter, D., Kousholt, A.N., et al. (2015). Cyclin F suppresses B-Myb activity to promote cell cycle checkpoint control. Nature communications 6, 5800.

Knight, A.S., Notaridou, M., and Watson, R.J. (2009). A Lin-9 complex is recruited by B-Myb to activate transcription of G2/M genes in undifferentiated embryonal carcinoma cells. Oncogene 28, 1737-1747.

Kobayashi, K., Suzuki, T., Iwata, E., Nakamichi, N., Suzuki, T., Chen, P., Ohtani, M., Ishida, T., Hosoya, H., Muller, S., et al. (2015). Transcriptional repression by MYB3R proteins regulates plant organ growth. The EMBO journal 34, 1992-2007.

Korenjak, M., Kwon, E., Morris, R.T., Anderssen, E., Amzallag, A., Ramaswamy, S., and Dyson, N.J. (2014). dREAM co-operates with insulator-binding proteins and regulates expression at divergently paired genes. Nucleic acids research 42, 8939-8953.

Lamers, F., van der Ploeg, I., Schild, L., Ebus, M.E., Koster, J., Hansen, B.R., Koch, T., Versteeg, R., Caron, H.N., and Molenaar, J.J. (2011). Knockdown of survivin (BIRC5) causes apoptosis in neuroblastoma via mitotic catastrophe. Endocrine-related cancer 18, 657-668.

Lang, G., Gombert, W.M., and Gould, H.J. (2005). A transcriptional regulatory element in the coding sequence of the human Bcl-2 gene. Immunology 114, 25-36.

Lange-zu Dohna, C., Brandeis, M., Berr, F., Mossner, J., and Engeland, K. (2000). A CDE/CHR tandem element regulates cell cycle-dependent repression of cyclin B2 transcription. FEBS letters 484, 77-81.

Lania, L., Majello, B., and Napolitano, G. (1999). Transcriptional control by cell-cycle regulators: a review. Journal of cellular physiology 179, 134-141.

Laoukili, J., Kooistra, M.R., Bras, A., Kauw, J., Kerkhoven, R.M., Morrison, A., Clevers, H., and Medema, R.H. (2005). FoxM1 is required for execution of the mitotic programme and chromosome stability. Nature cell biology 7, 126-136.

Lara-Gonzalez, P., Westhorpe, F.G., and Taylor, S.S. (2012). The spindle assembly checkpoint. Current biology: CB 22, R966-980.

Lee, M.G., and Nurse, P. (1987). Complementation used to clone a human homologue of the fission yeast cell cycle control gene cdc2. Nature 327, 31-35.

Lefebvre, C., Rajbhandari, P., Alvarez, M.J., Bandaru, P., Lim, W.K., Sato, M., Wang, K., Sumazin, P., Kustagi, M., Bisikirska, B.C., et al. (2010). A human B-cell interactome identifies MYB and FOXM1 as master regulators of proliferation in germinal centers. Molecular systems biology 6, 377.

Li, C., and Wang, J. (2014). Landscape and flux reveal a new global view and physical quantification of mammalian cell cycle. Proceedings of the National Academy of Sciences of the United States of America 111, 14130-14135.

Li, J., Ran, C., Li, E., Gordon, F., Comstock, G., Siddiqui, H., Cleghorn, W., Chen, H.Z., Kornacker, K., Liu, C.G., et al. (2008). Synergistic function of E2F7 and E2F8 is essential for cell survival and embryonic development. Developmental cell 14, 62-75.

Liang, H.B., Cao, Y., Ma, Q., Shu, Y.J., Wang, Z., Zhang, F., Ye, Y.Y., Li, H.F., Xiang, S.S., Song, X.L., et al. (2017). MYBL2 is a Potential Prognostic Marker that Promotes Cell Proliferation in Gallbladder Cancer. Cellular physiology and biochemistry: international journal of experimental cellular physiology, biochemistry, and pharmacology 41, 2117-2131.

Lipsick, J.S., Manak, J., Mitiku, N., Chen, C.K., Fogarty, P., and Guthrie, E. (2001). Functional evolution of the Myb oncogene family. Blood cells, molecules & diseases 27, 456-458.

Litovchick, L., Sadasivam, S., Florens, L., Zhu, X., Swanson, S.K., Velmurugan, S., Chen, R., Washburn, M.P., Liu, X.S., and DeCaprio, J.A. (2007). Evolutionarily conserved multisubunit RBL2/p130 and E2F4 protein complex represses human cell cycle-dependent genes in quiescence. Molecular cell 26, 539-551.

Liu, D.X., Biswas, S.C., and Greene, L.A. (2004). B-myb and C-myb play required roles in neuronal apoptosis evoked by nerve growth factor deprivation and DNA damage. The Journal of neuroscience: the official journal of the Society for Neuroscience 24, 8720-8725.

Liu, M., Dai, B., Kang, S.H., Ban, K., Huang, F.J., Lang, F.F., Aldape, K.D., Xie, T.X., Pelloski, C.E., Xie, K., et al. (2006). FoxM1B is overexpressed in human glioblastomas and critically regulates the tumorigenicity of glioma cells. Cancer research 66, 3593-3602.

Lodish H, Berk A, Zipursky SL, et al. Molecular Cell Biology. 4th edition. New York: W. H. Freeman; 2000. Available from: https://www.ncbi.nlm.nih.gov/books/NBK21475/

Löbrich, M., and Jeggo, P.A. (2007). The impact of a negligent G2/M checkpoint on genomic instability and cancer induction. Nature reviews Cancer 7, 861-869.

Lok, G.T., Chan, D.W., Liu, V.W., Hui, W.W., Leung, T.H., Yao, K.M., and Ngan, H.Y. (2011). Aberrant activation of ERK/FOXM1 signaling cascade triggers the cell migration/invasion in ovarian cancer cells. PloS one 6, e23790.

Lorvellec, M., Dumon, S., Maya-Mendoza, A., Jackson, D., Frampton, J., and Garcia, P. (2010). B-Myb is critical for proper DNA duplication during an unperturbed S phase in mouse embryonic stem cells. Stem cells (Dayton, Ohio) 28, 1751-1759.

Luo, J., Emanuele, M.J., Li, D., Creighton, C.J., Schlabach, M.R., Westbrook, T.F., Wong, K.K., and Elledge, S.J. (2009). A genome-wide RNAi screen identifies multiple synthetic lethal interactions with the Ras oncogene. Cell 137, 835-848.

Maiti, B., Li, J., de Bruin, A., Gordon, F., Timmers, C., Opavsky, R., Patil, K., Tuttle, J., Cleghorn, W., and Leone, G. (2005). Cloning and characterization of mouse E2F8, a novel mammalian E2F family member capable of blocking cellular proliferation. The Journal of biological chemistry 280, 18211-18220.

Malumbres, M. (2014). Cyclin-dependent kinases. Genome biology 15, 122.

Malumbres, M., and Barbacid, M. (2009). Cell cycle, CDKs and cancer: a changing paradigm. Nature reviews Cancer 9, 153-166.

Malumbres, M., Sotillo, R., Santamaria, D., Galan, J., Cerezo, A., Ortega, S., Dubus, P., and Barbacid, M. (2004). Mammalian cells cycle without the D-type cyclin-dependent kinases Cdk4 and Cdk6. Cell 118, 493-504.

Mannefeld, M., Klassen, E., and Gaubatz, S. (2009). B-MYB is required for recovery from the DNA damage-induced G2 checkpoint in p53 mutant cells. Cancer research 69, 4073-4080.

Marino, S., Vooijs, M., van Der Gulden, H., Jonkers, J., and Berns, A. (2000). Induction of medulloblastomas in p53-null mutant mice by somatic inactivation of Rb in the external granular layer cells of the cerebellum. Genes & development 14, 994-1004.

Marth, J.D. (1996). Recent advances in gene mutagenesis by site-directed recombination. The Journal of clinical investigation 97, 1999-2002.

Martinez, I., and Dimaio, D. (2011). B-Myb, cancer, senescence, and microRNAs. Cancer research 71, 5370-5373.

Maruyama, H., Ishitsuka, Y., Fujisawa, Y., Furuta, J., Sekido, M., and Kawachi, Y. (2014). B-Myb enhances proliferation and suppresses differentiation of keratinocytes in three-dimensional cell culture. Archives of dermatological research 306, 375-384.

Masselink, H., Vastenhouw, N., and Bernards, R. (2001). B-myb rescues ras-induced premature senescence, which requires its transactivation domain. Cancer letters 171, 87-101.

Meerbrey, K.L., Hu, G., Kessler, J.D., Roarty, K., Li, M.Z., Fang, J.E., Herschkowitz, J.I., Burrows, A.E., Ciccia, A., Sun, T., et al. (2011). The pINDUCER lentiviral toolkit for inducible RNA interference in vitro and in vivo. Proceedings of the National Academy of Sciences of the United States of America 108, 3665-3670.

Maton A, Lahart D, Hopkins J, Warner MQ, Johnson S, Wright JD (1997). Cells: Building Blocks of Life. New Jersey: Prentice Hall. pp. 70–4. ISBN 0-13-423476-6

Mitchison, T.J., and Salmon, E.D. (2001). Mitosis: a history of division. Nature cell biology 3, E17-21.

Moberg, K., Starz, M.A., and Lees, J.A. (1996). E2F-4 switches from p130 to p107 and pRB in response to cell cycle reentry. Molecular and cellular biology 16, 1436-1449.

Moon, N.S., and Dyson, N. (2008). E2F7 and E2F8 keep the E2F family in balance. Developmental cell 14, 1-3.

Morgan, D.O. (1997). Cyclin-dependent kinases: engines, clocks, and microprocessors. Annual review of cell and developmental biology 13, 261-291.

Morkel, M., Wenkel, J., Bannister, A.J., Kouzarides, T., and Hagemeier, C. (1997). An E2F-like repressor of transcription. Nature 390, 567-568.

Mowla, S.N., Lam, E.W., and Jat, P.S. (2014). Cellular senescence and aging: the role of B-MYB. Aging cell 13, 773-779.

Müller, G.A., and Engeland, K. (2010). The central role of CDE/CHR promoter elements in the regulation of cell cycle-dependent gene transcription. The FEBS journal 277, 877-893.

Müller, G.A., Quaas, M., Schumann, M., Krause, E., Padi, M., Fischer, M., Litovchick, L., DeCaprio, J.A., and Engeland, K. (2012). The CHR promoter element controls cell cycle-dependent gene transcription and binds the DREAM and MMB complexes. Nucleic acids research 40, 1561-1578.

Müller GA, Stangner K, Schmitt T, Wintsche A, Engeland K. (2017). Timing of transcription during the cell cycle: protein complexes binding to E2F, E2F/CLE, CDE/CHR, or CHR promoter elements define early and late cell cycle gene expression. Oncotarget Vol. 8, (No. 58), 97736-97748.

Murray, A.W. (1992). Creative blocks: cell-cycle checkpoints and feedback controls. Nature 359, 599-604.

Musa, J., Aynaud, M.M., Mirabeau, O., Delattre, O., and Grunewald, T.G. (2017). MYBL2 (B-Myb): a central regulator of cell proliferation, cell survival and differentiation involved in tumorigenesis. Cell death & disease 8, e2895.

Musacchio, A. (2011). Spindle assembly checkpoint: the third decade. Philosophical transactions of the Royal Society of London Series B, Biological sciences 366, 3595-3604.

Musacchio, A., and Salmon, E.D. (2007). The spindle-assembly checkpoint in space and time. Nature reviews Molecular cell biology 8, 379-393.

Nebreda, A.R. (2006). CDK activation by non-cyclin proteins. Current opinion in cell biology 18, 192-198.

Nigg, E.A. (1995). Cyclin-dependent protein kinases: key regulators of the eukaryotic cell cycle. BioEssays: news and reviews in molecular, cellular and developmental biology 17, 471-480.

Nikitin, A.Y., Alcaraz, A., Anver, M.R., Bronson, R.T., Cardiff, R.D., Dixon, D., Fraire, A.E., Gabrielson, E.W., Gunning, W.T., Haines, D.C., et al. (2004). Classification of proliferative

pulmonary lesions of the mouse: recommendations of the mouse models of human cancers consortium. Cancer research 64, 2307-2316.

Nomura, N., Takahashi, M., Matsui, M., Ishii, S., Date, T., Sasamoto, S., and Ishizaki, R. (1988). Isolation of human cDNA clones of myb-related genes, A-myb and B-myb. Nucleic acids research 16, 11075-11089.

Nordhoff, V., Hubner, K., Bauer, A., Orlova, I., Malapetsa, A., and Scholer, H.R. (2001). Comparative analysis of human, bovine, and murine Oct-4 upstream promoter sequences. Mammalian genome: official journal of the International Mammalian Genome Society 12, 309-317.

Novak, A., Guo, C., Yang, W., Nagy, A., and Lobe, C.G. (2000). Z/EG, a double reporter mouse line that expresses enhanced green fluorescent protein upon Cre-mediated excision. Genesis (New York, NY: 2000) 28, 147-155.

Nurse, P. (2000). A long twentieth century of the cell cycle and beyond. Cell 100, 71-78.

Ogawa, H., Ishiguro, K., Gaubatz, S., Livingston, D.M., and Nakatani, Y. (2002). A complex with chromatin modifiers that occupies E2F- and Myc-responsive genes in G0 cells. Science (New York, NY) 296, 1132-1136.

Oh, I.H., and Reddy, E.P. (1998). The C-terminal domain of B-Myb acts as a positive regulator of transcription and modulates its biological functions. Molecular and cellular biology 18, 499-511.

Okamoto, A., Higo, M., Shiiba, M., Nakashima, D., Koyama, T., Miyamoto, I., Kasama, H., Kasamatsu, A., Ogawara, K., Yokoe, H., et al. (2015). Down-Regulation of Nucleolar and Spindle-Associated Protein 1 (NUSAP1) Expression Suppresses Tumor and Cell Proliferation and Enhances Anti-Tumor Effect of Paclitaxel in Oral Squamous Cell Carcinoma. PloS one 10, e0142252.

Osterloh, L., von Eyss, B., Schmit, F., Rein, L., Hubner, D., Samans, B., Hauser, S., and Gaubatz, S. (2007). The human synMuv-like protein LIN-9 is required for transcription of G2/M genes and for entry into mitosis. The EMBO journal 26, 144-157.

Paddison, P.J., Caudy, A.A., Bernstein, E., Hannon, G.J., and Conklin, D.S. (2002). Short hairpin RNAs (shRNAs) induce sequence-specific silencing in mammalian cells. Genes & development 16, 948-958.

Paggi, M.G., Baldi, A., Bonetto, F., and Giordano, A. (1996). Retinoblastoma protein family in cell cycle and cancer: a review. Journal of cellular biochemistry 62, 418-430.

Palomero, T., Lim, W.K., Odom, D.T., Sulis, M.L., Real, P.J., Margolin, A., Barnes, K.C., O'Neil, J., Neuberg, D., Weng, A.P., et al. (2006). NOTCH1 directly regulates c-MYC and activates a feed-forward-loop transcriptional network promoting leukemic cell growth. Proceedings of the National Academy of Sciences of the United States of America 103, 18261-18266.

Paweletz, N. (2001). Walther Flemming: pioneer of mitosis research. Nature reviews Molecular cell biology 2, 72-75.

Perou, C.M., Sorlie, T., Eisen, M.B., van de Rijn, M., Jeffrey, S.S., Rees, C.A., Pollack, J.R., Ross, D.T., Johnsen, H., Akslen, L.A., et al. (2000). Molecular portraits of human breast tumours. Nature 406, 747-752.

Pilkinton, M., Sandoval, R., and Colamonici, O.R. (2007). Mammalian Mip/LIN-9 interacts with either the p107, p130/E2F4 repressor complex or B-Myb in a cell cycle-phase-dependent context distinct from the Drosophila dREAM complex. Oncogene 26, 7535-7543.

Raemaekers, T., Ribbeck, K., Beaudouin, J., Annaert, W., Van Camp, M., Stockmans, I., Smets, N., Bouillon, R., Ellenberg, J., and Carmeliet, G. (2003). NuSAP, a novel microtubule-associated protein involved in mitotic spindle organization. The Journal of cell biology 162, 1017-1029.

Rao, D.D., Vorhies, J.S., Senzer, N., and Nemunaitis, J. (2009). siRNA vs. shRNA: similarities and differences. Advanced drug delivery reviews 61, 746-759.

Raschella, G., Cesi, V., Amendola, R., Negroni, A., Tanno, B., Altavista, P., Tonini, G.P., De Bernardi, B., and Calabretta, B. (1999). Expression of B-myb in neuroblastoma tumors is a poor prognostic factor independent from MYCN amplification. Cancer research 59, 3365-3368.

Raschella, G., Negroni, A., Sala, A., Pucci, S., Romeo, A., and Calabretta, B. (1995). Requirement of b-myb function for survival and differentiative potential of human neuroblastoma cells. The Journal of biological chemistry 270, 8540-8545.

Rattner, J.B., Rao, A., Fritzler, M.J., Valencia, D.W., and Yen, T.J. (1993). CENP-F is a .ca 400 kDa kinetochore protein that exhibits a cell-cycle dependent localization. Cell motility and the cytoskeleton 26, 214-226.

Reichert, N., Wurster, S., Ulrich, T., Schmitt, K., Hauser, S., Probst, L., Gotz, R., Ceteci, F., Moll, R., Rapp, U., et al. (2010). Lin9, a subunit of the mammalian DREAM complex, is essential for embryonic development, for survival of adult mice, and for tumor suppression. Molecular and cellular biology 30, 2896-2908.

Ren, B., Cam, H., Takahashi, Y., Volkert, T., Terragni, J., Young, R.A., and Dynlacht, B.D. (2002). E2F integrates cell cycle progression with DNA repair, replication, and G(2)/M checkpoints. Genes & development 16, 245-256.

Ren, F., Wang, L., Shen, X., Xiao, X., Liu, Z., Wei, P., Wang, Y., Qi, P., Shen, C., Sheng, W., et al. (2015). MYBL2 is an independent prognostic marker that has tumor-promoting functions in colorectal cancer. American journal of cancer research 5, 1542-1552.

Rhodes, D.R., Yu, J., Shanker, K., Deshpande, N., Varambally, R., Ghosh, D., Barrette, T., Pandey, A., and Chinnaiyan, A.M. (2004). Large-scale meta-analysis of cancer microarray data identifies common transcriptional profiles of neoplastic transformation and progression. Proceedings of the National Academy of Sciences of the United States of America 101, 9309-9314.

Ribbeck, K., Raemaekers, T., Carmeliet, G., and Mattaj, I.W. (2007). A role for NuSAP in linking microtubules to mitotic chromosomes. Current biology: CB 17, 230-236.

Robbins SL, Cotran RS (2004). Kumar V, Abbas AK, Fausto N, eds. Pathological Basis of Disease. Elsevier. ISBN 81-8147-528-3.

Sadasivam, S., and DeCaprio, J.A. (2013). The DREAM complex: master coordinator of cell cycle-dependent gene expression. Nature reviews Cancer 13, 585-595.

Sadasivam, S., Duan, S., and DeCaprio, J.A. (2012). The MuvB complex sequentially recruits B-Myb and FoxM1 to promote mitotic gene expression. Genes & development 26, 474-489.

Sahni, J.M., Gayle, S.S., Webb, B.M., Weber-Bonk, K.L., Seachrist, D.D., Singh, S., Sizemore, S.T., Restrepo, N.A., Bebek, G., Scacheri, P.C., et al. (2017). Mitotic Vulnerability in Triple-Negative Breast Cancer Associated with LIN9 Is Targetable with BET Inhibitors. Cancer research 77, 5395-5408.

Sakura, H., Kanei-Ishii, C., Nagase, T., Nakagoshi, H., Gonda, T.J., and Ishii, S. (1989). Delineation of three functional domains of the transcriptional activator encoded by the c-myb protooncogene. Proceedings of the National Academy of Sciences of the United States of America 86, 5758-5762.

Sala, A. (2005). B-MYB, a transcription factor implicated in regulating cell cycle, apoptosis and cancer. European journal of cancer (Oxford, England: 1990) 41, 2479-2484.

Santamaria, D., Barriere, C., Cerqueira, A., Hunt, S., Tardy, C., Newton, K., Caceres, J.F., Dubus, P., Malumbres, M., and Barbacid, M. (2007). Cdk1 is sufficient to drive the mammalian cell cycle. Nature 448, 811-815.

Satyanarayana, A., and Kaldis, P. (2009). Mammalian cell-cycle regulation: several Cdks, numerous cyclins and diverse compensatory mechanisms. Oncogene 28, 2925-2939.

Schafer, K.A. (1998). The cell cycle: a review. Veterinary pathology 35, 461-478.

Schmit, F., Cremer, S., and Gaubatz, S. (2009). LIN54 is an essential core subunit of the DREAM/LINC complex that binds to the cdc2 promoter in a sequence-specific manner. The FEBS journal 276, 5703-5716.

Schmit, F., Korenjak, M., Mannefeld, M., Schmitt, K., Franke, C., von Eyss, B., Gagrica, S., Hanel, F., Brehm, A., and Gaubatz, S. (2007). LINC, a human complex that is related to pRB-containing complexes in invertebrates regulates the expression of G2/M genes. Cell cycle (Georgetown, Tex) 6, 1903-1913.

Scholzen, T., and Gerdes, J. (2000). The Ki-67 protein: from the known and the unknown. Journal of cellular physiology 182, 311-322.

Shao, X., Somlo, S., and Igarashi, P. (2002). Epithelial-specific Cre/lox recombination in the developing kidney and genitourinary tract. Journal of the American Society of Nephrology: JASN 13, 1837-1846.

Shepard, J.L., Amatruda, J.F., Stern, H.M., Subramanian, A., Finkelstein, D., Ziai, J., Finley, K.R., Pfaff, K.L., Hersey, C., Zhou, Y., et al. (2005). A zebrafish bmyb mutation causes genome instability and increased cancer susceptibility. Proceedings of the National Academy of Sciences of the United States of America 102, 13194-13199.

Sherr, C.J., and Roberts, J.M. (1999). CDK inhibitors: positive and negative regulators of G1-phase progression. Genes & development 13, 1501-1512.

Shi, H., Bevier, M., Johansson, R., Enquist-Olsson, K., Henriksson, R., Hemminki, K., Lenner, P., and Forsti, A. (2012). Prognostic impact of polymorphisms in the MYBL2 interacting genes in breast cancer. Breast cancer research and treatment 131, 1039-1047.

Takashima, A., and Faller, D.V. (2013). Targeting the RAS oncogene. Expert opinion on therapeutic targets 17, 507-531.

Tanaka, Y., Patestos, N.P., Maekawa, T., and Ishii, S. (1999). B-myb is required for inner cell mass formation at an early stage of development. The Journal of biological chemistry 274, 28067-28070.

Tanner, M.M., Grenman, S., Koul, A., Johannsson, O., Meltzer, P., Pejovic, T., Borg, A., and Isola, J.J. (2000). Frequent amplification of chromosomal region 20q12-q13 in ovarian cancer. Clinical cancer research: an official journal of the American Association for Cancer Research 6, 1833-1839.

Tao, D., Pan, Y., Lu, H., Zheng, S., Lin, H., Fang, H., and Cao, F. (2014). B-myb is a gene implicated in cell cycle and proliferation of breast cancer. International journal of clinical and experimental pathology 7, 5819-5827.

Tarasov, K.V., Testa, G., Tarasova, Y.S., Kania, G., Riordon, D.R., Volkova, M., Anisimov, S.V., Wobus, A.M., and Boheler, K.R. (2008). Linkage of pluripotent stem cell-associated transcripts to regulatory gene networks. Cells, tissues, organs 188, 31-45.

Tashiro, S., Takemoto, Y., Handa, H., and Ishii, S. (1995). Cell type-specific trans-activation by the B-myb gene product: requirement of the putative cofactor binding to the C-terminal conserved domain. Oncogene 10, 1699-1707.

Testa, J.R., Zhou, J.Y., Bell, D.W., and Yen, T.J. (1994). Chromosomal localization of the genes encoding the kinetochore proteins CENPE and CENPF to human chromosomes 4q24-->q25 and 1q32-->q41, respectively, by fluorescence in situ hybridization. Genomics 23, 691-693.

Thalmeier, K., Synovzik, H., Mertz, R., Winnacker, E.L., and Lipp, M. (1989). Nuclear factor E2F mediates basic transcription and trans-activation by E1a of the human MYC promoter. Genes & development 3, 527-536.

Thorner, A.R., Hoadley, K.A., Parker, J.S., Winkel, S., Millikan, R.C., and Perou, C.M. (2009). In vitro and in vivo analysis of B-Myb in basal-like breast cancer. Oncogene 28, 742-751.

Tian, S., Roepman, P., Van't Veer, L.J., Bernards, R., de Snoo, F., and Glas, A.M. (2010). Biological functions of the genes in the mammaprint breast cancer profile reflect the hallmarks of cancer. Biomarker insights 5, 129-138.

Tiscornia, G., Singer, O., and Verma, I.M. (2006). Production and purification of lentiviral vectors. Nature protocols 1, 241-245.

Trimarchi, J.M., Fairchild, B., Wen, J., and Lees, J.A. (2001). The E2F6 transcription factor is a component of the mammalian Bmi1-containing polycomb complex. Proceedings of the National Academy of Sciences of the United States of America 98, 1519-1524.

Trimarchi, J.M., and Lees, J.A. (2002). Sibling rivalry in the E2F family. Nature reviews Molecular cell biology 3, 11-20.

Vanden Bosch, A., Raemaekers, T., Denayer, S., Torrekens, S., Smets, N., Moermans, K., Dewerchin, M., Carmeliet, P., and Carmeliet, G. (2010). NuSAP is essential for chromatin-induced spindle formation during early embryogenesis. Journal of cell science 123, 3244-3255.

Vogelstein, B., Lane, D., and Levine, A.J. (2000). Surfing the p53 network. Nature 408, 307-310.

Wang, I.C., Chen, Y.J., Hughes, D., Petrovic, V., Major, M.L., Park, H.J., Tan, Y., Ackerson, T., and Costa, R.H. (2005). Forkhead box M1 regulates the transcriptional network of genes essential for mitotic progression and genes encoding the SCF (Skp2-Cks1) ubiquitin ligase. Molecular and cellular biology 25, 10875-10894.

Weinberg, R.A. (1995). The retinoblastoma protein and cell cycle control. Cell 81, 323-330.

Werwein, E., Dzuganova, M., Usadel, C., and Klempnauer, K.H. (2013). B-Myb switches from Cyclin/Cdk-dependent to Jnk- and p38 kinase-dependent phosphorylation and associates with SC35 bodies after UV stress. Cell death & disease 4, e511.

Whitfield, M.L., George, L.K., Grant, G.D., and Perou, C.M. (2006). Common markers of proliferation. Nature reviews Cancer 6, 99-106.

Whyte, P., Buchkovich, K.J., Horowitz, J.M., Friend, S.H., Raybuck, M., Weinberg, R.A., and Harlow, E. (1988). Association between an oncogene and an anti-oncogene: the adenovirus E1A proteins bind to the retinoblastoma gene product. Nature 334, 124-129.

Wierstra, I., and Alves, J. (2007). FOXM1, a typical proliferation-associated transcription factor. Biological chemistry 388, 1257-1274.

Winslow, M.M., Dayton, T.L., Verhaak, R.G., Kim-Kiselak, C., Snyder, E.L., Feldser, D.M., Hubbard, D.D., DuPage, M.J., Whittaker, C.A., Hoersch, S., et al. (2011). Suppression of lung adenocarcinoma progression by Nkx2-1. Nature 473, 101-104.

Winter, G.E., Buckley, D.L., Paulk, J., Roberts, J.M., Souza, A., Dhe-Paganon, S., and Bradner, J.E. (2015). DRUG DEVELOPMENT. Phthalimide conjugation as a strategy for in vivo target protein degradation. Science (New York, NY) 348, 1376-1381.

Wiseman, E.F., Chen, X., Han, N., Webber, A., Ji, Z., Sharrocks, A.D., and Ang, Y.S. (2015). Deregulation of the FOXM1 target gene network and its coregulatory partners in oesophageal adenocarcinoma. Molecular cancer 14, 69.

Wolter, P., Hanselmann, S., Pattschull, G., Schruf, E., and Gaubatz, S. (2017). Central spindle proteins and mitotic kinesins are direct transcriptional targets of MuvB, B-MYB and FOXM1 in breast cancer cell lines and are potential targets for therapy. Oncotarget 8, 11160-11172.

Wu, Q.F., Liu, C., Tai, M.H., Liu, D., Lei, L., Wang, R.T., Tian, M., and Lu, Y. (2010). Knockdown of FoxM1 by siRNA interference decreases cell proliferation, induces cell cycle arrest and inhibits cell invasion in MHCC-97H cells in vitro. Acta pharmacologica Sinica 31, 361-366.

Yamauchi, T., Ishidao, T., Nomura, T., Shinagawa, T., Tanaka, Y., Yonemura, S., and Ishii, S. (2008). A B-Myb complex containing clathrin and filamin is required for mitotic spindle function. The EMBO journal 27, 1852-1862.

Yang, Z.Y., Guo, J., Li, N., Qian, M., Wang, S.N., and Zhu, X.L. (2003). Mitosin/CENP-F is a conserved kinetochore protein subjected to cytoplasmic dynein-mediated poleward transport. Cell research 13, 275-283.

Young, N.P., and Jacks, T. (2010). Tissue-specific p19Arf regulation dictates the response to oncogenic K-ras. Proceedings of the National Academy of Sciences of the United States of America 107, 10184-10189.

Yue, X., Zhao, Y., Xu, Y., Zheng, M., Feng, Z., and Hu, W. (2017). Mutant p53 in Cancer: Accumulation, Gain-of-Function, and Therapy. Journal of molecular biology 429, 1595-1606.

Zhang, X., Lv, Q.L., Huang, Y.T., Zhang, L.H., and Zhou, H.H. (2017). Akt/FoxM1 signaling pathway-mediated upregulation of MYBL2 promotes progression of human glioma. Journal of experimental & clinical cancer research: CR 36, 105.

Zhou, Z., Yin, Y., Chang, Q., Sun, G., Lin, J., and Dai, Y. (2017). Downregulation of B-myb promotes senescence via the ROS-mediated p53/p21 pathway, in vascular endothelial cells. Cell proliferation 50.

8. Appendix

8.1 List of figures

Figure 1: Simplified representation of the mammalian cell cycle 3

Figure 2: The mammalian DREAM/MMB complex…….....7

Figure 3: NSCLC mouse model to determine the requirement of B-MYB to lung tumorigenesis……...60

Figure 4: Requirement of B-MYB for tumorigenesis in an *in vivo* NSCLC mouse model…….62

Figure 5: Expression of B-MYB in lung adenocarcinoma 64

Figure 6: Expression of MMB target genes NUSAP1 and CENPF in lung tumors……....65

Figure 7: Correlation between expression of B-MYB and its target gene NUSAP1…….....66

Figure 8: p-ERK expression in murine lung adenocarcinomas.....67

Figure 9: KI-67 expression in murine lung adenocarcinomas…….....68

Figure 10: Incomplete recombination of B-Myb in primary lung tumors……..69

Figure 11: Incomplete recombination of B-Myb in lung cancer cell lines before and after multiple infection with a retrovirus encoding for CreERT2……....71

Figure 12: mRNA expression of B-Myb and MMB target genes in lung adenocarcinoma cell lines.....72

Figure 13: B-MYB is required for proliferation of lung cancer cells.....73

Figure 14: Cytokinesis defects in BC2 cell line after 4-OHT treatment compared to KR1 cell line ……74

Figure 15: Abnormal cell cycle profile in BC2 cell line after loss of B-Myb……..75

Figure 16: The knockdown efficiency of shRNAs against B-MYB was tested in the breast cancer cell line MDA-MB-231……76

Figure 17: Knockdown of B-MYB in the human lung cancer cell line H23……..77

Figure 18: B-Myb but not MMB targets were efficiently downregulated on transcriptional level…….....78

Figure 19: Impaired proliferation after loss of B-Myb in human lung cancer cell lines…….80

Figure 20: Cytokinesis defects in different lung cancer cell lines after loss of B-Myb……81

Figure 21: Cell cycle profile was largely unchanged after treatment with 1 µg/ml doxycycline……...83

Figure 22: Gene regulation in human lung cancer cell lines after RNAi mediated depletion of B-Myb or FoxM1……...85

Figure 23: B-MYB is required for normal mitosis of human lung cancer cells……....86

8.2. Abbreviations

AAH	Atypical adenomatous hyperplasia
ADP	Adenosine diphosphate
APC/C	Anaphase promoting complex/cylcosome
ARF	ADP ribosylation factors
ATM	Ataxia-telangiectasia mutated
ATP	Adenosine triphosphate
ATR	Ataxia-telangiectasia mutated RAD3-related
AurkB	Aurora B kinase
Birc5	Baculoviral inhibitor of apoptosis repeat-containing 5
B-Myb	v-Myb myeloblastosis viral oncogene homolog (avian)-like 2
CAF1	Chromatin assembly factor 1
CDE	Cell cycle-dependent element
CDK	Cyclin-dependent kinase
CDKi	CDK inhibitor
Cenpf	Centromere protein F
CIN	Chromosomal instability
cip/kip	CDK interacting protein/ Kinase inhibitory protein
Chk1	Checkpoint kinase 1
ChIP	Chromatin immunoprecipitation
CHR	Cell cycle genes homology
Co-IP	Co-immunopreciptation
Ctrl	Control
DAB	3,3'-Diaminobenzidine
DNA	Deoxyribonucleic acid

DNA-PK	DNA-dependent protein kinase
DP1/DP2	Differentiation-regulated transcription factor-1 and 2
DREAM	Drosophila RBF, dE2F2 and dMyb-interacting proteins
DRM	DP, Rb and MuvB
E2F	E2 factor
e.g.	Example
ESC	Embryonic stem cell
FACS	Fluorescence activated cell sorting
FBS	FoxM1 binding site
Fig	Figure
Fl	Floxed
GAPDH	Glyceraldehyde-3-phosphate dehydrogenase
G0, G1, G2	Gap phase
h	Hours
HDAC	Histone deacetylase
H&E	Haematoxylin and Eosin
HPRT	Hypoxanthine-guanine phosphoribosyltransferase
HPV	Human papillomavirus
ICM	Inner cell mass
IF	Immunofluorescence
IgG	Immunoglobulin G
IP	Immunoprecipitation
kda	kilodalton
Kif	Kinesin
lenti-Cre	Lentiviral Cre recombinase
LSL	LoxP-STOP-LoxP cassette
MAPK	Mitogen-activated protein kinase
MBS	Myb binding site
MEF	Mouse embryonic fibroblasts
Mip	Myb interacting proteins
MMB	Myb-MuvB
MMB-FoxM1	Myb-MuvB-FoxM1
M-phase	Mitosis

MYBL2	v-Myb myeloblastosis viral oncogene homolog (avian)-like 2
NSCLC	Non-small-cell lung carcinoma
Nusap1	Nucleolar spindle–associated protein
PCR	Polymerase chain reaction
Plk1	Polo-like kinase 1
pRB	product of the retinoblastoma tumor suppressor
qRT-PCR	Quantitative real-time PCR
RB	Retinoblastoma
RFP	Red fluorescent protein
RNA	Ribonucleic acid
RNAi	RNA interference
RT	Room temperature/Reverse transcriptase
SAC	Spindle assembly checkpoint
SCLC	Small-cell lung carcinoma
SDS-PAGE	SDS-polyacrylamide gel electrophoresis
shRNA	Short-hairpin RNA
siRNA	Small interfering RNA
S-phase	Synthesis phase
UV	ultraviolet
Wt	Wild type
+/+	Homozygous, wild type
+/-	Heterozygous
-/-	Homozygous, knock out
Δ	Delta/Deletion

8.3. Own publications and conference contributions

Iltzsche F.*, Simon K.*, Stopp S*., Pattschull G.*, Francke S., Wolter P., Hauser S., Murphy DJ., Garcia P., Rosenwald A., Gaubatz S. (2017) „An important role for Myb-MuvB and its target gene KIF23 in a mouse model of lung adenocarcinoma"; Oncogene; 36(1):110-121

*These authors contributed equally to this work.

Conference contributions (Talks and Posters)

10/2016	International GSLS Symposium. "Eureka" held at RVZ, Würzburg, Germany Poster: Identifying the role of Myb-MuvB in lung cancer
10/2015	International GSLS Symposium. "Eureka" held at RVZ, Würzburg, Germany Poster: Role of B-MYB and DREAM in the development and progression in lung cancer
09/2015	Retreat of the GSLS Oberelsbach, Germany Talk: Role of B-MYB and DREAM in the development and progression in lung cancer
10/2014	International GSLS Symposium. "Eureka" held at RVZ, Würzburg, Germany Poster: Role of B-MYB and DREAM in the development and progression in lung cancer
08/2014	Retreat of the GSLS Rothenburg, Germany Poster: Role of B-MYB and DREAM in the development and progression in lung cancer

8.4. Curriculum vitae

The Curriculum vitae will not be published for data protection reasons.

8.5. Acknowledgments

First and foremost, I convey my gratitude and sincere thanks to my supervisor Prof. Dr. Stefan Gaubatz for giving me the opportunity to work in his lab and for supervising my PhD thesis. I appreciate all the scientific support and guidance during my PhD project.

Besides my supervisor, I extend my gratitude and thanks to other members of my thesis committee: Dr. Peter Gallant and Prof. Dr. Svenja Meierjohann for their encouragement and valuable comments during our meetings.

I thank all former and current lab members for the cheerful atmosphere, their advice and support: Dr. Fabian Iltzsche, Dr. Patrick Wolter, Dr. Marc Fackler, Dr. Sabine Stopp, Dr. Geeta Kumari, Grit Pattschull, Steffen Hanselmann, Marco Gründl, Susanne Spahr and Adelgunde Wolpert

A special thanks goes to my mentor from the GSLS mentoring program Dr. Stefan Schlör for his support and advice

I thank all my friends here in Würzburg for the pleasant and unforgettable moments: Fabian, Kristina, Stephanie, Andrea, Pascal, Denise, Janna and Caro

Special thanks to my friends at home for their understanding and support: Julia, Meike, Susanne, Natalia, Laura and Petra

Most importantly I am grateful my family, specially my parents for their continuous unconditional love and support throughout my life.

8.6. Affidativ

I hereby confirm that my thesis entitled "Identifying the role of Myb-MuvB in gene expression and proliferation of lung cancer cells " is the result of my own work. I did not receive any help or support from commercial consultants. All sources and / or materials applied are listed and specified in the thesis.

Furthermore, I confirm that this thesis has not yet been submitted as part of another examination process neither in identical nor in similar form.

Place, Date Signature

Eidesstattliche Erklärung

Hiermit erkläre ich an Eides statt, die Dissertation “Identifizierung der Rolle des Myb-MuvB in der Genexpression und der Proliferation von Lungenkrebszellen” eigenständig, d.h. insbesondere selbständig und ohne Hilfe eines kommerziellen Promotionsberaters, angefertigt und keine anderen als die von mir angegebenen Quellen und Hilfsmittel verwendet zu haben.

Ich erkläre außerdem, dass die Dissertation weder in gleicher noch in ähnlicher Form bereits in einem anderen Prüfungsverfahren vorgelegen hat.

Ort, Datum Unterschrift